1986

Evaluation of a direct injection nebulizer interface for flow injection analysis and high performance liquid chromatography with inductively coupled plasma-atomic emission spectroscopic detection

Kimberly E. LaFreniere
Iowa State University

INFORMATION TO USERS

This reproduction was made from a copy of a manuscript sent to us for publication and microfilming. While the most advanced technology has been used to photograph and reproduce this manuscript, the quality of the reproduction is heavily dependent upon the quality of the material submitted. Pages in any manuscript may have indistinct print. In all cases the best available copy has been filmed.

The following explanation of techniques is provided to help clarify notations which may appear on this reproduction.

1. Manuscripts may not always be complete. When it is not possible to obtain missing pages, a note appears to indicate this.

2. When copyrighted materials are removed from the manuscript, a note appears to indicate this.

3. Oversize materials (maps, drawings, and charts) are photographed by sectioning the original, beginning at the upper left hand corner and continuing from left to right in equal sections with small overlaps. Each oversize page is also filmed as one exposure and is available, for an additional charge, as a standard 35mm slide or in black and white paper format.*

4. Most photographs reproduce acceptably on positive microfilm or microfiche but lack clarity on xerographic copies made from the microfilm. For an additional charge, all photographs are available in black and white standard 35mm slide format.*

***For more information about black and white slides or enlarged paper reproductions, please contact the Dissertations Customer Services Department.**

LaFreniere, Kimberly E.

EVALUATION OF A DIRECT INJECTION NEBULIZER INTERFACE FOR FLOW INJECTION ANALYSIS AND HIGH PERFORMANCE LIQUID CHROMATOGRAPHY WITH INDUCTIVELY COUPLED PLASMA-ATOMIC EMISSION SPECTROSCOPIC DETECTION

Iowa State University PH.D. 1986

Evaluation of a direct injection nebulizer interface for flow injection analysis and high performance liquid chromatography with inductively coupled plasma-atomic emission spectroscopic detection

by

Kimberly E. LaFreniere

A Dissertation Submitted to the
Graduate Faculty in Partial Fulfillment of the
Requirements for the Degree of
DOCTOR OF PHILOSOPHY

Department: Chemistry
Major: Analytical Chemistry

Approved:

Signature was redacted for privacy.
In Charge of Major Work

Signature was redacted for privacy.
For the Major Department

Signature was redacted for privacy.
For the Graduate College

Iowa State University
Ames, Iowa

1986

TABLE OF CONTENTS

DEDICATION

In loving memory of my parents, Dean and Billie Lawrence.

CHAPTER I. INTRODUCTION†

Review of the Literature

The toxicological impact of any given element on a biological system is greatly dependent upon the form in which that element exists (e.g., zerovalent, cationic, anionic, or bound to some organic counterpart). Typical cases in point are the biochemical effects of arsenic, for which arsenic(III), or arsenite, compounds are the most toxic. Inorganic arsenicals have been shown to coagulate proteins, to complex coenzymes, and to uncouple the energy-yielding process of phosphorylation (1). In the past 15 years, a heightened awareness regarding the toxic effects of certain elements in a wide variety of sample matrices has stimulated much interest in metal speciation. Metal speciation, or the separation and identification of the individual metallic forms that exist in a given matrix, has not been a trivial task, as documented in the many excellent reviews found in the literature (2-7).

Intuitively, the combination of some mode of species separation and an appropriate detector should provide the analyst with a powerful means of identifying metal-containing species. Gas chromatography (GC) or high performance liquid chromatography (HPLC) are the most widely accepted methods of separating compounds. Indeed, GC has been applied to the separation of many metal chelates and organometallic compounds, but its use is primarily limited to neutral, volatile, low molecular weight species of high thermal stability (8). Although the gas chromatographic

---

†Definitions of acronyms are given in Appendix A.

detection and determination of many involatile or thermally labile compounds can be made feasible by derivatization, this technique is often difficult to apply to "real world" sample matrices that contain mixtures of compounds of unknown structure (9). For these reasons, investigators have turned toward HPLC as the primary method of separating compounds for thermally unstable substances, such as biologically active materials, high molecular weight organic compounds, polymers, and organometallic compounds (8,10-13). The HPLC technique offers versatility in separation mechanisms, including liquid-liquid partition, liquid-solid adsorption, reverse-phase partition, ion exchange, and size exclusion, all of which have been employed for metal speciation studies. Although the technology required to perform the HPLC separation of metal-containing species is generally available, sensitive and specific detection of the metal of interest can best be achieved through the use of element-specific detectors. Conventional HPLC detectors, such as the refractive index (RI), ultraviolet (UV), fluorescence (FL), electrochemical (EC), flame ionization (FI), and infrared (IR) vary in degree of selectivity and applicability (14,15). Atomic spectroscopic detectors, on the other hand, are highly specific and are applicable to a variety of sample matrices. Among the various atomic spectroscopic detectors, flame atomic absorption spectroscopy (FAAS), graphite furnace atomic absorption spectroscopy (GFAAS), and flame or plasma atomic fluorescence spectroscopy (AFS), as well as microwave-induced plasma (MIP), direct-current plasma (DCP), and inductively-coupled plasma (ICP) atomic emission spectroscopy hold the most promise as element-specific detectors for HPLC. Indeed, 125 publications on atomic, element-specific detectors have appeared in the

literature in the last 10 to 15 years. Of the atomic spectroscopic detectors, emission sources are the most readily adapted to multielement monitoring, and many researchers agree that plasma emission spectroscopy will eventually be the method of choice for simultaneous, multielement, element-specific chromatographic detection (2-5). It should be noted, however, that non-specific, on-line HPLC detectors of molecular properties should not be discounted. Much valuable information can be extracted when conventional HPLC detectors are used in tandem with element-specific, atomic spectroscopic detectors.

On the following pages, a comprehensive tabulation and discussion is presented of papers concerned with element-specific, atomic spectroscopic detectors for high performance liquid chromatography. The intent of this review is not only to emphasize the significant accomplishments in element-specific detection for HPLC, but also illuminate the inadequacies of particular approaches or techniques. The review is divided into six major element-specific detection approaches that have been used, namely; 1) flame atomic absorption spectroscopy (FAAS), 2) graphite furnace atomic absorption spectroscopy (GFAAS), 3) atomic fluorescence spectroscopy (AFS), 4) microwave induced plasma-atomic emission spectroscopy (MIP-AES), direct current plasma-atomic emission spectroscopy (DCP-AES), and 6) inductively coupled plasma-atomic emission spectroscopy (ICP-AES) detectors. Specific applications of these approaches are summarized in Table I.

Flame atomic absorption spectroscopy (FAAS)

Flame atomic absorption spectroscopy (FAAS) provides a specific method for the analysis of trace metals in a variety of sample matrices.

Table I. Summary of applications for HPLC with atomic spectroscopic detection[a]

Species or compound of interest	Limit of detection (ng/mL)	Sample size (μL)	Column[b] type
Flame atomic absorption spectroscopic detectors			
K^+, Mg^{2+}	---	1000	Sephadex G-15 (10mm x 600mm)
Cu chelates of NTA and EDTA	---	100 to 500	"Chelex" ion exchange resin
Pb alkyls (TML,TEL)	---	0.1	Reverse phase: (2.6mm x 500mm)
Cu chelates of NTA and EDTA	100 to 200 (as Cu)	150	Anion exchange: 20 μm Aminex A-14 (2.1mm x 50mm)
Vitamin B_{12} and $Co(NO_3)_2$	---	500	Anion exchange: (Hitachi Ion Exchange Resin No. 2611)
Cr(III) and Cr(VI)	---	5000	Cation and anion exchange
Ca^{2+}, Mg^{2+}	---	250	Spherogel TSK-2000SW (7.5mm x 100mm)

[a]Definitions of acronyms are given in Appendix A.

[b]Column dimensions are (i.d. x length).

Mobile phase	Mobile phase flow rate (μL/min)	Interface design	Reference #
Flame atomic absorption spectroscopic detectors			
0.1 M NaCl w/ 0.001 M EDTA in water	---	Directly from column to nebulizer via polyethylene capillary tubing	(16)
EDTA or NTA in deionized water	---	Column effluent fed directly into aspirator of AA spectrometer	(17)
(3/2) water/MeOH	1000	From 0.1 mm i.d. stainless steel outlet tubing of UV detector to sample capillary of AA spectrometer	(18)
0.5 M $(NH_4)_2SO_4$ in water	2000	Directly from column to AAS aspirator inlet via 3 cm length of 0.6 mm i.d. polyethlene tubing	(19, 20)
2 M NH_4OAc in water	1000	---	(21)
Water	1000	Off-line	(22)
Aqueous buffer	400	Flow-injection sample manipulator (FISM): samples HPLC effluent, dilutes the aliquot, and delivers to FAA instrument	(23)

Table I. (Continued)

Species or compound of interest	Limit of detection (ng/mL)	Sample size (μL)	Column[b] type
Organotin	220 to 380 (as Sn)	50	Reverse phase: ODS Spherisorb SEW (3mm x 250mm)
Tetraalkylleads (TML, TMEL, DMDEL, METL, TEL)	500	20	Reverse phase: μ-Bondapak C_{18} (3.9mm x 300mm)
Organozinc (MW~6000) in rabbit aqueous humour	30 (as Zn)	100	Gel permeation: Two TSK G3000SW in series (7.5mm x 600mm)
Organomercurials	—	<50	Reverse phase: Whatman Partisil 10 (4.6mm x 250mm)
Organoleads	—	10	Reverse phase: Whatman Partisil 10 (4.6mm x 250mm)
Arsenite, arsenate, MMA, and DMA	10–20 (as As)	100	Ion exchange: BAX-10 (5mm x 100mm)
Inorganic and organoarsenicals, organotins	TBT: 2000	100	Ion exchange: Partisil 10 SCX (4.6mm x 250mm)
Atomic fluorescence spectroscopic detectors			
Cu-, Zn-, and Ni-glycines, -EDTAs, and Cu-trien complexes	—	25	Partisil-10 SCX 55°C

Mobile phase	Mobile phase flow rate (μL/min)	Interface design	Reference #
(3/2) acetone/pentane or (7/3) acetone/pentane	1000–1200	Column coupled directly to nebulizer with 50 mm length of 1 mm i.d. Teflon tubing	(24)
(70/30) AcN/water	3000	Short length of polyethylene tubing between column and AA nebulizer	(25)
50 mM Tris-HCl buffer, pH 7.4	1000	From refractive index detector to nebulizer of AA instrument	(26)
NaBr of NaCl in appropriate organic solvent, e.g., water/AcN	---	Short length of polyethylene tubing between column and Perkin-Elmer pneumatic concentric nebulizer	(27)
NaBr or NaCl in appropriate organic solvent, e.g., EtOH/water	---	Short length of polyethylene tubing between column and Perkin-Elmer pneumatic, concentric nebulizer	(28)
10^{-4}% H_2SO_4 followed by 0.1 M ammonium carbonate	4000	Hydride generator to flame-heated silica tube for atomic absorption	(29)
(80/20) MeOH/water and 0.1 M NH_4(OAc)	3000	Direct connection between column and nebulizer allowed for "Discrete Volume Nebulization"	(30, 31)
Atomic fluorescence spectroscopic detectors			
Pure water followed by a convex gradient to 100% 1 M NH_4NO_3	4000	Outlet of column connected directly to the nebulizer capillary tube	(32)

Table I. (Continued)

Species or compound of interest	Limit of detection (ng/mL)	Sample size (μL)	Column[b] type
Acetylation products of ferrocene	---	---	Chromasep S 10 μm silica gel (2mm x 500mm)
Graphite furnace atomic absorption spectroscopic detectors			
Organo-As, -Pb, -Hg, and -Sn	240-5000	20	Variable
Inorganic As and organoarsenicals in river water	2 (as As)	10	Cation exchange: AG 50W-X8, 100-200 mesh (10mm x 350mm)
Inorganic and organoarsenicals	<10	800	Dionex anion separator (3mm x 500mm)
Inorganic and organoarsenicals	10	10 to 100	Ion exchange: 90 mm of anion exchange resin followed by 260 mm of cation exchange resin
Organoarsenicals in a variety of energy-related materials	---	20	Variable
Organoleads in automotive oil	---	20	10 μm silica gel
Organotin polymers containing chemically bonded, biocidal organotin moieties and organosilicates	---	50 to 100	Size exclusion or reverse phase: LiChrosorb C_{18} (3.2mm x 250mm)

Mobile phase	Mobile phase flow rate (μL/min)	Interface design	Reference #
(40/1) diethyl ether/ MeOH	500-2000	A short length of vinyl heat-shrink tubing formed a union between exit of UV detector and aspirator tubing of acetylene-air capillary tube burner	(33)
Graphite furnace atomic absorption spectroscopic detectors			
Variable	Variable	Teflon, off-line "Well sampler"	(34)
0.2 M TCA followed by 1 M NH_4OAc	Gravity flow	Off-line	(35)
0.0024 M $NaHCO_3$/ 0.0019 M Na_2CO_3/ 0.001 M $Na_2B_4O_7$ in water	2600	Continuous arsine generation system followed by heated quartz furnace	(36)
1. 0.006 M TCA 2. 0.2 M TCA	5000-10,000	Off-line	(37)

Table I. (Continued)

Species or compound of interest	Limit of detection (ng/mL)	Sample size (μL)	Column[b] type
Copolymers of tributyltin methacrylate and methyl methacrylate	100-500 (as Sn)	50	Size exclusion: (7.8mm x 300mm)
cis-dichlorodiammeplatinum(II) in human blood plasma	—	50	Partisil 10 SAX (9.6mm x 250mm)
Organoselenium	—	20	Reverse phase: Partisil-PXS-ODS-10 μm
Cu-amino acid complexes in human serum	—	25	Silica gel (100-200 mesh)
Alkylleads	—	10	HitachiGel No.3010 (2.5mm x 500mm)
Arsenical pesticide residues	250 (as As)	20	Anion exchange: (3mm x 250mm)
Soil arsenical residues	500	10 to 20	Anion exchange: (20mm x 150mm)
Organophosphorus additives in lubricating oil	300	4	Reverse phase: ODS-H C Sil-X-1 (2.6mm x 250mm)

Mobile phase	Mobile phase flow rate (μL/min)	Interface design	Reference #
THF	1000	Teflon, off-line "Well sampler"	(45-47)
MeOH/acetate buffer (0.1 M, pH 3.8)	1000	Off-line	(48)
(2:1) MeOH/water	300	An eight-port, two-position sampling valve, a timing circuit, a co-analyte dispenser, and a sample dispenser	(49)
(40/60) water/acetone	400	Off-line	(50)
MeOH	670	High gas temperature furnace(HGT)	(51)
100% water/MeOH (80+20,v/v) to 100% $(NH_4)_2CO_3$/MeOH (85+15,v/v)	1200	Teflon flow through sampling cup and auto-sampler	(52)
100% water/MeOH (80+20,v/v) to 100% $(NH_4)_2CO_3$/MeOH (85+15,v/v)	1200	Teflon flow through sampling cup and auto-sampler	(53)
Gradient: 1. 50% MeOH to 100% MeOH; linear 2. 20% MeOH in an isochratic manner for 10 min, ramp to 100% MeOH within 30 min	1000	Off-line	(54)

Table I. (Continued)

Species or compound of interest	Limit of detection (ng/mL)	Sample size (μL)	Column[b] type
Vanadyl porphyrin and non-porphyrins in heavy crude oils	---	---	Size exclusion: 50/100 Å
Vanadyl and nickel compounds in heavy crude petroleums and asphaltenes	---	---	Size exclusion: series combination of 50/100/1000 Å μ-Spherogel (8mm x 300mm) Reverse phase: Altex C_{18} ODS (4.6mm x 250mm)
Microwave-induced plasma atomic emission spectroscopic detectors			
Deuterium oxide	---	---	Nucleosil 10 C_{18} or ODS-Hypersil
Organo-Cd, -Pb, -Zn	TEL: 40,300 TML: 6900	1	Reverse phase: C_2, 10 μm (1mm x 250mm) Normal phase: Cyano-Spherisorb (0.6mm x 250mm)

Mobile phase	Mobile phase flow rate (μL/min)	Interface design	Reference #
THF	500	Teflon, off-line "Well sampler"	(55)
SEC: CH_2Cl_2 RP: linear gradient 1. 100% MeOH/water (3:1,v/v) to 30% THF (1-3 min) 2. 30% THF to 70% THF (22-24 min) 3. Ramp to 100% THF (25-27 min)	SEC: 0.5 RP: 1500	Teflon, off-line "Well sampler"	(56)
Microwave-induced plasma atomic emission spectroscopic detectors			
Mixed from individually measured volumes of MeOH, AcN, THF, and water	1800	A short length of metal wire is welded to the column exit and positioned along the vertical axis of a 4-way piece of glass tubing. Column effluent is allowed to flow freely about the metal wire and a horizontal flow of heated He evaporates the effluent from the wire and transfers the vapor to a plasma sustained by original Beenakker TM_{010} cavity. (Incident power: 75 W)	(57)
MeOH (50/50) MeOH/water (90/10) cyclohexane/ CH_2Cl_2	100 100 120	Glass frit nebulizer to a plasma sustained by a modified Beenakker TM_{010} cavity (Incident power: 450 W)	(58)

Table I. (Continued)

Species or compound of interest	Limit of detection (ng/mL)	Sample size (μL)	Column[b] type
Direct current plasma atomic emission spectroscopic detectors			
Cr(VI) and Cr(III)	5 to 15	100	Reverse phase: variety of columns
Ni(II)-, Cu(II)-, and Co(III)-diethyl-dithiocarbamates	---	---	Spherisorb SGP (4mm x 250mm)
β-ketoamine complexes of Cu(II), Ni(II), Co(III); diethyldi-thiocarbamate complexes of Cu(II), Ni(II), Co(III), Hg(II), and Cr(III)	---	---	1. 10 μm Partisil ODS 2. Spherisorb SGP 8 μm
Geometrical isomers and mixed ligand forms of Co(II) and Cr(III) β-diketonates	10,000-100,000 (for Cr)	1-10	1. 10 μm Partisil silica (4mm x 300mm) 2. 5 μm Hypersil silica (4mm x 160mm)
Cd-sulfate, nitrate, and acetate	---	100	Sephadex G-10 (5mm x 500mm)
Protein bound Cu, Fe, and Zn in human serum and intravenous infusion fluids	Cu: 3.2 Fe: 3.9 Zn: 9.3	5000	Gel filtration: Sephacryl S-300 (26mm x 1000mm)
Copper hexafluoro-acetylacetonate	---	---	5.0 μm silica (4.5mm x 250mm)

Mobile phase	Mobile phase flow rate (μL/min)	Interface design	Reference #
Direct current plasma atomic emission spectroscopic detectors			
Variety of ion-pairing reagents	1000-2000	Short length(100mm) of 0.25 mm i.d. stainless steel tubing connected to a 190 mm section of flexible, plastic inlet tubing of nebulizer	(59)
5/15/80 AcN/diethyl-ether/Skellysolve B	2200	---	(60)
Aqueous, as well as hydrocarbon and halocarbon	500-4000	Jet impact nebulizer	(61)
1. 6% AcN in CH_2Cl_2	1500	Jet impact nebulizer	(62)
2. 3 to 20% concave gradient CH_2Cl_2 in hexane			
Deionized water	2000	A 10 cm length of 0.076 cm i.d. Tygon tubing from RI detector to cross-flow nebulizer	(63)
0.1 M Tris-HCl	---	---	(64)
100% CH_2Cl_2	1000	Nebulizer/spray chamber with mechanical efficiency of 20 to 95%	(65)

Table I. (Continued)

Species or compound of interest	Limit of detection (ng/mL)	Sample size (μL)	Column[b] type
Various inorganic polyphosphate oligomers in a neutralized polyphosphoric acid sample	10,000	---	Reverse phase: DuPont Zorbax ODS (4.6mm x 250mm) or Hamilton PRP-1 (4.1mm x 150mm)
1. cis- and facial trans isomers of Co(III)-iminodiacetate 2. Neutral N,N'-ethylenebis(acetylacetoneimine) chelates of Cu(II) and Ni(II) 3. Thermally labile isomers of aluminum trifluoroacetylacetonates	---	10	1. IBM Instruments: 5 μm methyl- and phenyl-bonded (4.6mm x 250mm) 2. Phenomenex: 5 μm nitrile bonded (5mm x 250mm) 3. Spherisorb nitrile (4.6mm x 150mm)
Inductively coupled plasma atomic emission spectroscopic detectors			
Organo-Cd, -Pb, -Zn	TEL: 5010 TML: 1920	1	Reverse phase: C_2, 10 μm (1mm x 250mm) Normal phase: Cyano-Spherisorb (0.6mm x 250mm)
Simulated HPLC peaks from 25 elements	e.g.: Cd 89 Co 21 Cr 20 Cu 6.8 Fe 28 Pb 230 P 290 Se 280	10	"Dummy" column that did not retain the analyte (Deactivated glass spheres)

Mobile phase	Mobile phase flow rate (μL/min)	Interface design	Reference #
Aqueous buffer	1500	A 1.6 mm o.d. x 0.23 mm i.d. Teflon tubing between column outlet and ceramic cross-flow nebulizer	(66)
1)Surfactants in water or water/MeOH 2)(90/10) CH_3Cl/hexane	1500	---	(67)
Inductively coupled plasma atomic emission spectroscopic detectors			
MeOH (50/50) MeOH/water (90/10) cyclohexane/ CH_2Cl_2	100 100 120	Glass frit nebulizer	(58)
Aqueous	1000	A 3 cm length of 1.6 mm o.d. narrow-bore Teflon capillary tubing between column and nebulizer	(68)

Table I. (Continued)

Species or compound of interest	Limit of detection (ng/mL)	Sample size (μL)	Column[b] type
Iron carbonyl and molybdenium carbonyl complexes and of ferrocene, organo-Hg, organoarsenic and organo-Pb	Mo: 0.3 Cu: 0.6 Fe: 1.0 Pb: 11 Sn: 11	15	Variable
Elemental composition of vitamin B_{12}; and protein mixtures	---	20	Gel permeation: TSK GEL 3000SW (2mm x 600mm)
C-21 Conoco organo-metallic standard and Pb, Sn, Si in synthetic organo-metallic mixtures	---	50	Size exclusion: Bio-Beads SX-2 or μ-Styragel (100 Å)
Synthetic mixtures and organically bound metals in coal-derived materials	---	50 or 200	Size exclusion: 100 Å μ-Styragel
Inorganic and organic arsenicals	---	---	Anion exchange: μ-Bondapak-NH_2, Nucleosil-$N(CH_3)_3$ -10, or Nucleosil-SO_3H-10
Ortho-, di-, and tri-phosphate; AMP, ADP, and ATP	PO_4^{3-}: 10,000 $P_2O_7^{4-}$: 20,000 $P_3O_{10}^{5-}$: 60,000	50	Anion exchange: μ-Bondapak-NH_2
NTA and EDTA chelates of Cu, Zn, Ca, and Mg	---	20	Anion exchange: AGI X4; sub 400 mesh (1.6mm x 250mm)

Mobile phase	Mobile phase flow rate (μL/min)	Interface design	Reference #
Variable	Variable	A 10 cm length of Teflon capillary tubing(0.3 mm i.d.) between the column and inlet side of the burner	(69)
0.9% NaCl in water	1000	Conventional cross-flow nebulizer	(70)
Toluene	1000	Length of stainless steel tubing between nebulizer and column; thermostated spray chamber	(71)
Pyridine	500 or 1000	Length of stainless steel tubing between nebulizer and column; thermostated spray chamber(20°C)	(72, 73)
Phosphate, borate, tris-HCl, tributyl-ammonium phosphate, and aqueous NaCl	1000	Teflon tubing(1.6 mm x 130 mm) between outlet of liquid chromatograph and cross-flow nebulizer	(74)
Aqueous buffer	1000	Teflon tubing(1.6 mm x 130 mm) between outlet of liquid chromatograph and cross-flow nebulizer	(75)
0.05 M $(NH_4)_2SO_4$	1000	From UV absorbance detector to nebulizer by means of a minimum length of PTFE tubing	(76)

Table I. (Continued)

Species or compound of interest	Limit of detection (ng/mL)	Sample size (μL)	Column[b] type
Nucleotides; AMP, CMP, UMP, and inorganic phosphate	7500	100	Anion exchange
Mg	---	Variable	Anion exchange: (4.1mm x 50mm)
Mg and Ca metal forms in natural waters	---	500	Size exclusion: TSK 3000SW (7.5mm x 600mm) or TSK 2000SW (7.5mm x 500mm)
Inorganic and organic forms of As, Se, and P	130	100	Reverse phase: Hamilton PRP-1
Organo-Cu, -Co, -Cr, -Fe	---	1.5	Reverse phase: Jasco SC-01 (ODS-silica,5 μm) (0.5mm x 120mm) Normal phase: Jasco FineSil-5 (0.5mm x 150mm)
Amino acids	30,000-50,000 (as C) 1000-3000 (as S)	100	Cation exchange: 50°C, IEX-210 SC (4mm x 300mm)
Inorganic forms of As and Se	As(III) 2600 As(V) 2850 Se(IV) 7000 Se(VI) 4550	20	Anion exchange: Nucleosil-$NH(CH_3)_2$

Mobile phase	Mobile phase flow rate (μL/min)	Interface design	Reference #
0.3 M NaOAc	1500	Babington-type nebulizer	(77)
Deionized water	Variable	Meintrard concentric or fixed cross-flow nebulizer	(78)
Deionized water	1000 or 1500	Small diameter Tygon tubing to cross-flow nebulizer	(79)
Aqueous; a ion-pairing reagent	1500	A 0.65 m length of 0.12 mm i.d. PTFE tubing to a Meinhard concentric nebulizer	(80)
RP: MeOH or MeOH/water NP: toluene	~500	T-type connection of two types of stainless steel tubes; one the size of the micro-HPLC column, the other a little larger; between outlet of column and cross-flow nebulizer	(81)
Stepped gradient: 0.2 M NaH_2PO_4, pH 3.2 (0-10 min) 0.2 M NH_2PO_4, pH 4.3 (10-20 min)	1400	A 0.5 mm i.d. by 300 mm length of Teflon tubing between outlet of column and cross-flow nebulizer	(82)
0.08 M ammonium dihydrogen phosphate pH 6.9	1400	Short length of 0.25 mm i.d. Teflon tubing from column to adjustable cross-flow nebulizer	(83)

Table I. (Continued)

Species or compound of interest	Limit of detection (ng/mL)	Sample size (μL)	Column[b] type
Tetraalkyllead components in commercial gasoline	TML: 42 (as Pb) TEL: 212 (as Pb)	50	10 μm LiChrosorb RP-2
Metal cations and anions as a function of oxidation state; organoarsenials	---	---	Reverse phase: variety, 25°C
Divalent cations of Cd, Zn, and Hg	---	20	Reverse phase: variety
Cr(III) and Cr(VI)	Cr(III): 220,000 Cr(VI): 450,000	20	Reverse phase: Ultrasphere ODS (4.6mm x 150mm) 25°C
Inorganic and organic arsenic anions	As(III): 50 As(V): 50 DMA: 105	200	Reverse phase: variety
Saccharides	---	1.6	SC-220 gel (1mm x 200mm) 80°C
Arsenite, arsenate; Cd-EDTA, Cd-NTA	Arsenite: 3100 Arsenate: 1500 Cd-EDTA: 350 Cd-NTA: 120	50	Reverse phase: Spherisorb ODS C_{18} or LiChrosorb 10 μm C_2 (4.6mm x 120mm)

Mobile phase	Mobile phase flow rate (μL/min)	Interface design	Reference #
(15/35/50) butanol/ EtOH/water	1000	Narrow-bore Teflon capillary(1.6 mm x 130 mm) between column and concentric nebulizer	(84)
Ion-pairing: 0.005 M sodium 1-pentanesulfonate and others in water	2000 to 3000	Approx. 50:50 effluent split ratio between column and nebulizer	(85)
Variety of ion-pairing reagents in MeOH/water	1000	Approx. 50:50 effluent split ratio between column and nebulizer	(86)
Ion-pairing: 0.005 M sodium 1-pentanesulfonate in water	1000	Approx. 50:50 effluent split ratio between column and nebulizer	(87)
Ion-pairing: 5 mM tetrabutyl-ammonium phosphate in water	1000	Hydride generator between column and cross-flow nebulizer	(88)
Water	16	T-type connection of two types of stainless steel tubing; one the same size as the micro-HPLC column, the other slightly larger, between outlet of column and cross-flow nebulizer	(89)
(90/10) water/MeOH saturated with tetrabutylammonium phosphate, pH 7.3	1000	A 0.16 mm x 130 mm narrow-bore(0.5 mm) Teflon capillary tubing between column and Meinhard concentric nebulizer	(90)

Table I. (Continued)

Species or compound of interest	Limit of detection (ng/mL)	Sample size (μL)	Column[b] type
Organics as C at 247.9 nm line	---	---	Cation exchange: Jasco SC-220 (1.0mm x 200mm) or Showa Denko KC-811 (0.5mm x 300mm)
Separation of 15 rare earth elements	1 to 300	100	Cation exchange: IEX-210SC Toya Soda Co. (4mm x 250mm) 50°C
Molecular size distribution of sulfur- and vandium-containing compounds in petroleum crudes and 650+ residua	---	100	Size exclusion: Ultragel MXL (mixed bed)
Alkyllead compounds (TML and TEL)	TML: 1346 TEL: 1919	20 and 50	Reverse phase: 1. C_{18}-ODS Spherisorb, 10 μm (4.6mm x 250mm) 2. Spherisorb C_{18}-ODS, 10 μm (4.6mm x 120mm) 3. LiChrosorb RP-2, 10 μm C_2 (4.6mm x 120mm)
Yttrium and selected rare earth elements from major, minor, and other trace elements	---	200	8PSCX 10 μm Radial Pak

Mobile phase	Mobile phase flow rate (μL/min)	Interface design	Reference #
Water	<10	Micro column is inserted into one arm of a cross-flow nebulizer	(91)
Linear gradient: 0.4 to 1.0 M ammonium lactate, pH 4.2	1400	Small diameter Teflon tubing(0.5 mm x 300 mm) between column and cross-flow nebulizer	(92)
Xylenes	1000	---	(93)
Variety of water, MeOH, AcN, EtOH mixtures	1000	A 1.6 mm o.d. x 100 mm narrow-bore Teflon capillary tubing between column and 1. glass frit nebulizer 2. C-1 Meinhard concentric glass nebulizer	(94)
0.1 M $NaNO_3$ or or 0.02 M $MgCl_2$ or deionized water	3000	Plastic tubing(0.076 mm x 35 mm) between column concentric glass nebulizer	(95)

Table I. (Continued)

Species or compound of interest	Limit of detection (ng/mL)	Sample size (μL)	Column[b] type
Organics as C at 247.9 nm line; NBS SRM-1580 shale oil	C: 33300 Cu: 3300	0.3	Cation exchange: Shodex KC-811 fused silica (0.35mm x 400mm) Gel permeation: TSK Gel 1000-H fused silica (0.5mm x 600mm)

Mobile phase	Mobile phase flow rate (μL/min)	Interface design	Reference #
Water	4	1. Modified cross-flow nebulizer with "no-spray chamber"	(96)
		2. Modified cross-flow nebulizer with spray chamber volume of 62 mL	
CH_2Cl_2	8	3. Modified cross-flow nebulizer with spray chamber volume of 124 mL	

Historically, two types of burners have been used to support the flame. The first type was called the total consumption burner, because the sample was aspirated at the burner tip, directly into the flame by the Venturi effect that drew the sample up the capillary (97). It will become apparent in Chapter II, that the direct injection nebulizer (DIN) is similar to the total consumption burner, as in both cases, all of the sample solution is directly introduced into the flame (plasma). The second burner type, the premix or laminar flow burner, has superseded the total consumption burner for most applications. With the premix burner, the aspirated sample, fuel, and oxidant are intimately mixed before introduction to the flame (97).

The earliest element-specific detector utilized for metal speciation studies was based on FAAS (16,17). In addition to providing a low cost, highly specific method for trace metal detection, FAAS detectors were usually free of spectral interferences and offered continuous, on-line, real-time monitoring of HPLC effluents. Despite initial excitement, the HPLC-FAAS approach to trace metal speciation has enjoyed only limited success because of one fundamental shortcoming, the limits of detection obtained by the HPLC-FAAS approach have generally been inadequate for many elemental studies. As shown in Table I, the reported values for the application of conventional HPLC-FAAS range from 30 ng/mL (26) to 500 ng/mL (25). In interpreting the unsatisfactory LODs shown in Table I, it should be recalled that 5 to 200 μL of sample are initially injected into the liquid chromatograph. During the liquid chromatographic separation and subsequent FAAS analysis of the effluent, a number of processes occur that drastically limit the powers of detection achieved. First, the

analyte species pass through the detector system in diluted form, as a result of intracolumn and extracolumn band broadening, thus leading to a reduced signal-to-noise ratio. By far, the greatest loss in detectability occurs in the FAAS analytical process. In conventional FAAS, the liquid sample, in our case the liquid chromatographic effluent, is transformed into an aerosol by pneumatic nebulizers (Figure 1), and is subsequently passed through a mixing chamber and then injected into the flame where atomization occurs. The operation of cross-flow or concentric pneumatic nebulizers is based on the Venturi principle, i.e., the small negative pressure developed as the flow of a carrier gas passes around or across a small capillary causes liquid to be drawn into and through the capillary tube, where an aerosol is formed with the carrier gas as the liquid leaves the capillary tube. Unfortunately, the overall nebulization, aerosol transport, and injection efficiency into the flame is inefficient. Typically, only 10 to 20% (97,98) of the original, very limited sample volume (5 to 200 μL) is injected as an aerosol into the flame and participates in the analysis. The remaining 80 to 90% of the liquid chromatographic effluent goes to waste. As a result of the very low analyte mass participation in the analysis, the limits of detection are inadequate for most applications of interest.

Although the limits of detection reported for the HPLC-FAAS method have been inadequate, in general, Tye et al. (29) reported limits of detection for As species of 10 to 20 ng/mL, however, a preconcentration column was required in series with the analytical column. Furthermore, the hydride generation technique was utilized to effect a more efficient transfer of the analyte to the flame. Although hydride generation

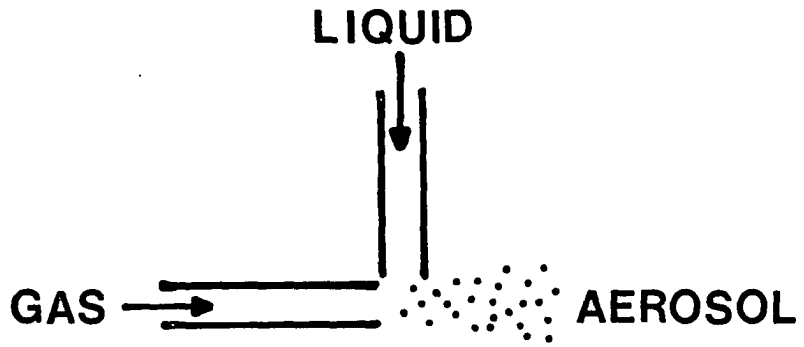

A

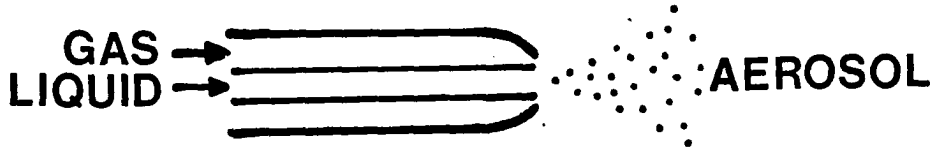

B

Figure 1. Simple schematic of two pneumatic nebulizers [A] cross-flow; [B] concentric

techniques offer improved detectability, the reader should be cautioned that the technique limits the analyst to the determination of only the hydride-forming elements (As, Se, Sb, Bi, Te, Ge, Pb, and Sn).

Atomic fluorescence spectroscopy (AFS)

Little use has been made of atomic fluorescence spectroscopy (AFS) as an element specific detector for HPLC, primarily because commercial instrumentation has not been available until recently. The development of the Plasma/AFS instrument by the Baird Corporation has greatly expanded the availability of the AFS technique, however, this instrument has not, to date, been successfully interfaced with HPLC. As with FAAS, the major deficiency of AFS has been the limited analyte mass participation in the overall analytical process. Only two applications in which AFS has been utilized for the detection of HPLC effluents have been reported (32,33). No detection limit data were given.

Graphite furnace atomic absorption spectroscopy (GFAAS)

The realization that FAAS or AFS do not generally provide practical limits of detection for the HPLC analysis of most actual sample matrices, led researchers to turn toward graphite furnace atomic absorption spectroscopy (GFAAS) detection to achieve improvements in the limits of detection by 2 to 3 orders of magnitude (34). Unfortunately, conventional GFAAS requires that the analytical process be executed "off-line" in a batch mode, as the sample atomization normally involves a three step drying (evaporation of solvent), ashing, and volatilization cycle before absorption measurements can be made. The HPLC effluent samples have been collected continuously, but in a segmented, batch mode followed by deposition of the individual batches in the graphite furnace. The 3-step

atomization cycle was then performed for each sample batch collected. As illustrated in Figure 2 (56), the resulting chromatograms appeared as bar graphs, hence much of the chromatographic resolution was lost. This loss of resolution has rendered GFAAS unsuitable for high resolution, liquid chromatography. Another problem associated with GFAAS is the loss of volatile analyte species during the ashing step (99,100). For example, alkyllead species were not readily detected in the conventional graphite furnace, because the alkyllead was volatilized from the cuvette before atomization. Despite these apparent limitations, HPLC-GFAAS has yielded some of the most impressive limits of detection for metal speciation, as demonstrated by several researchers (35-37). For low resolution, chromatographic studies that involve relatively involatile analyte species, the GFAAS approach has been particularly useful.

Microwave induced plasma atomic emission detectors

Historically, two types of microwave plasmas have been utilized as spectrochemical excitation sources. In the first version, microwaves radiated by a magnetron were conducted through a coaxial wave guide to the tip of a coaxial (single) electrode (101-103). These single electrode plasmas (SEP) were generated at the tip of the coaxial electrode and assumed a "flame-like" configuration. The SEP version has not been applied to the analysis of HPLC effluents. The microwave induced, capillary plasma (MIP) has superseded the first version for most analytical applications and is pictured in Figure 3a. The MIP is generated when microwave energy is coupled to a gas stream (typically He or Ar) that flows through a capillary discharge tube (electrodeless) that is contained in a resonant cavity.

Figure 2. Comparison of GFAAS and UV absorption detectors for HPLC Porphyrin standards [A]; Boscan asphaltene extract [B]; and Cerro Negro crude extract [C], monitored for vanadium and nickel (Reprinted with permission from Fish et al. 56, p.2454)

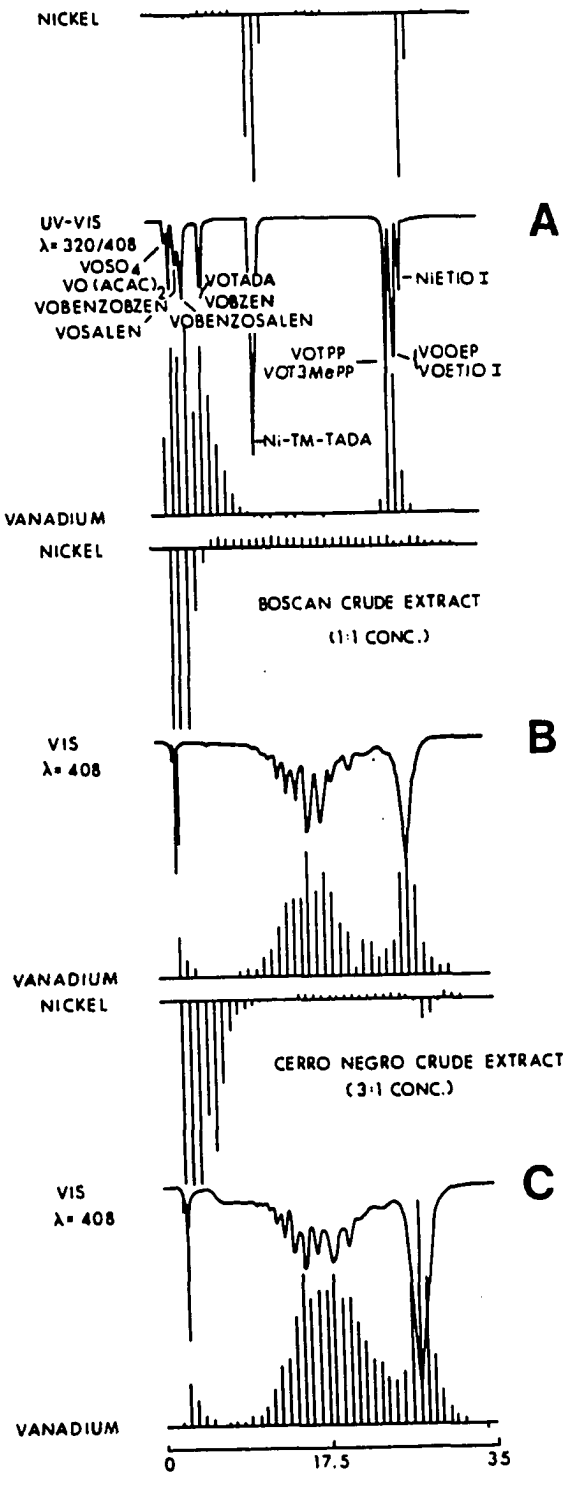
NICKEL
UV-VIS
λ= 320/408
VOSO4
VO(ACAC)2
VOBENZOBZEN
VOSALEN
VOTADA
VOBZEN
VOBENZOSALEN
NIETIO I
VOTPP
VOT3MePP
VOOEP
VOETIO I
Ni-TM-TADA
A
VANADIUM
NICKEL
BOSCAN CRUDE EXTRACT
(1:1 CONC.)
VIS
λ= 408
B
VANADIUM
NICKEL
CERRO NEGRO CRUDE EXTRACT
(3:1 CONC.)
VIS
λ= 408
C
VANADIUM
0
17.5
35

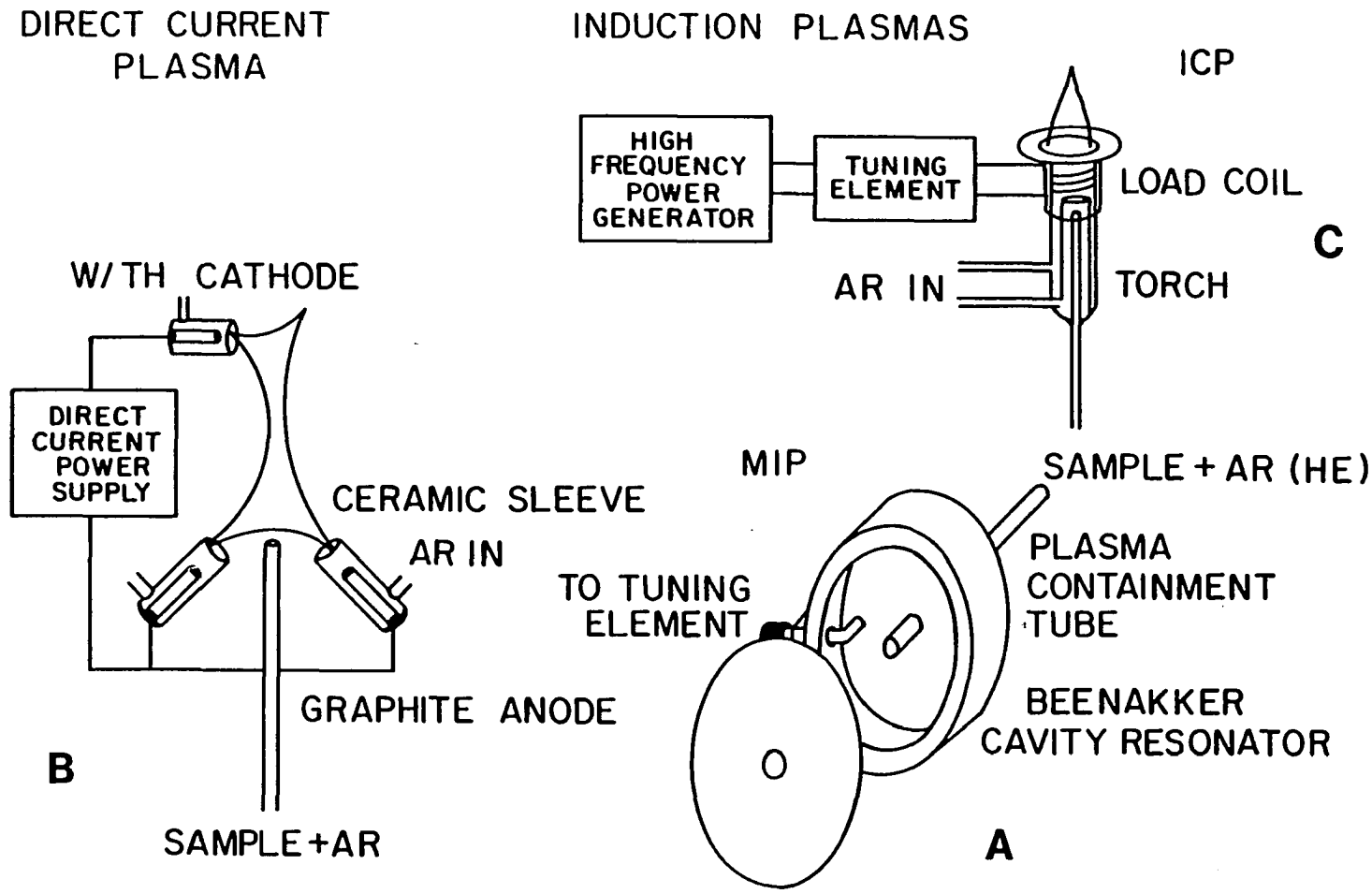

Figure 3. Plasma sources for elemental emission spectroscopy [A] microwave-induced plasma, MIP; [B] direct current plasma, DCP; and [C] inductively coupled plasma, ICP (Reprinted with permission from Carnahan et al. 5, p.228)

Although the capillary MIP has been used extensively for the analysis of gas chromatographic (GC) effluents (104-107), there have been but two references to the use of the MIP as a detector for HPLC (57,58). The absence of more HPLC-MIP applications in the literature may be attributed to the instability of the low power (<200 W) MIP upon the introduction of effluent aerosols into the plasma. Lichte and Skogerboe (108) and Skogerboe and Coleman (109) have shown that the analysis of aqueous solutions was possible with a low power MIP, but only if analyte desolvation occurred prior to introduction into the MIP. Unfortunately, desolvation techniques will not be generally applicable for the conditioning of aerosols generated from HPLC effluents!

In 1976, Beenakker (110) utilized the cylindrical, TM_{010} cavity as a means to sustain either an Ar or He, low power MIP at atmospheric pressure. Aqueous samples were nebulized pneumatically at liquid uptake rates of 1.7 mL/min. However, the overall efficiency for aerosol formation, transport, and injection into the MIP was only about 2%; therefore, aqueous aerosol was introduced at a rate of 34 μL of H_2O/min. Although stable MIP operation was maintained, stable analyte signals were not produced. Beenakker and coworkers (111) later concluded the MIP detection limits were satisfactory for solution analysis, although inferior to those obtained by inductively coupled plasma atomic emission spectroscopy (ICP-AES) for elements that have sensitive ion lines. In addition, matrix interferences were far more prominent in the MIP as compared to the ICP. Billiet et al. (57) utilized the low power, Beenakker TM_{010} cavity to sustain a MIP for the detection of HPLC

effluents after volatilization from a metal wire with subsequent introduction of vapor into the capillary discharge.

The higher power (200 to 500 W) MIP reported by Haas et al. (112) represented a modification of the Beenakker TM_{010} cavity. Direct solution nebulization with a typical ICP nebulizer-spray chamber arrangement resulted in a detection limit for Cu (4 ng/mL) that was comparable to that obtained by ICP-AES (113) with linearity of response over 3 orders on magnitude. Ibrahim et al. (58) utilized this version of the capillary MIP with aerosol introduction of the HPLC effluent. The relative limits of detection reported for tetramethyllead (6900 ng/mL) and tetraethyllead (40,300 ng/mL) were very poor.

Perhaps the most significant advances toward direct liquid sample introduction into a MIP was by Bollo-Kamara and Coding (114), in which a toroidal MIP was generated. Later, Kollotzek et al. (115,116) demonstrated that the low power (110 W), toroidal-MIP was suitable for the determination of trace elements in aqueous solution, in which the limits of detection observed were comparable to those obtained by ICP-AES. Aqueous samples were pneumatically nebulized at liquid uptake rates of 0.36 mL/min, however, up to 5 mL/min uptake rates were tolerated if the aerosol droplet size was small and uniform. The overall efficiency for aerosol formation, transport, and injection into the toroidal-MIP was about 3%; therefore, water was introduced at a rate of 10.8 μL/min (and up to 150 μl/min). The toroidal-MIP, however, was extinguished in the presence of μg-amounts of organic solvents, such as acetone, trichloromethane, or methyl alcohol. An inability to maintain plasma stability in the presence of organic aerosol severely limits the potential

chromatographic applications that might be pursued with a HPLC-toroidal-MIP facility. The toroidal-MIP has not been utilized as a detector for HPLC effluents.

Direct current plasma atomic emission detectors

Despite the apparent lack of interest in the direct current plasma (DCP) as an element-specific detector for HPLC effluents, recent publications have demonstrated the potential of the HPLC-DCP approach (59,64,117-118). The most popular DCP detector for HPLC has been the SpectraMetrics SpectraSpan IV (Smith Kline-Beckman Corp.) that incorporates two graphite anodes and a tungsten cathode as illustrated in Figure 3b. The plasma is maintained directly by an electrical discharge through the argon support gas. Sample aerosol is directed toward the fork in the inverted "Y"-shaped plasma by an argon stream. The DCP is stable to aqueous mobile phases, as well as a variety of organic mobile phases, including hydrocarbon and halocarbon solvents. Although the limits of detection attainable by DCP under unlimited sample volume conditions are comparable to those obtained by ICP-AES for most elements, there is confusion in the literature as to the utility of the DCP as an element-selective detector for HPLC. Gardiner et al. (64) reported good relative limits of detection for Cu (3.2 ng/mL), Fe (3.9 ng/mL), and Zn (9.3 ng/mL); however, the results are not for analytical HPLC, but for preparatory-scale column chromatography, for which 5.0 mL of sample was injected on column. It will become apparent in Chapter IV that the absolute detection limits reported by Gardiner et al. (64) for Cu (16 ng), Fe (20 ng), and Zn (47 ng) are approximately 1 to 1.5 orders of magnitude

inferior to those obtained by HPLC-ICP-AES with the direct injection nebulizer.

Krull et al. (59) have demonstrated the utilization of the HPLC-DCP-AES approach for the speciation of Cr(III) and Cr(VI) at trace levels. The limits of detection for the chromium species were found to be on the order of 5 to 15 ng/mL. The improved detection limits were likely attributable to the use of larger sample injection volumes (100 μL) in conjunction with a more efficient nebulizer-spray chamber arrangement (25% efficiency for aerosol formation and transport). Although Krull et al. (59) have achieved the best reported limits of detection for Cr by any plasma technique, this was the only instance in which "practical" limits of detection have been documented.

The DCP has shown potential as an element-specific detector for HPLC and more research is warranted. Recently, however, the ICP appears to have captured the limelight and most efforts have been directed toward the development of the still elusive, successful HPLC-ICP interface arrangement.

Inductively coupled plasma-atomic emission detectors

The inductively coupled plasma (ICP) has become the "work-horse" of analytical spectroscopy for the determination of metals, metalloids, and the non-metals at the major, minor, trace, and ultratrace concentration levels in a variety of sample matrices. An ICP is maintained at atmospheric pressure by a high frequency (usually 27.12 MHz) generator that supplies power to an induction coil. The high frequency currents that flow in the induction coil generate oscillating magnetic fields whose lines of flux are axially oriented inside the coil. The plasma is

sustained within the confines of a specially designed torch by eddy currents induced by the axial magnetic fields. The ICP assumes a toroidal, "flame-like" configuration that is readily developed through the proper choices of frequency and current provided by the generator, and argon support gas flow rates (Figure 3c). The base of the plasma is punctured by an aerosol carrier gas and gives the plasma its characteristic "doughnut" shape when viewed axially. Sample aerosols are injected, axially into the center of the base of the plasma (the "doughnut hole") and are subsequently vaporized, atomized, and finally excited as they pass the eddy current region. Analyte emission (from free atoms or ions) is viewed at 15 to 20 mm above the induction coil (119-121).

Presently, the ICP holds great potential as a multielement, element-specific detector for HPLC. Indeed, 30 publications concerned with HPLC-ICP interfaces can be found in the literature since November of 1979 (Table I). Unfortunately, most of the limits of detection that have been reported for HPLC-ICP-AES are not acceptable or useful for many "real world" sample matrices.

The earliest reference to the use of ICP as a multielement, element-specific detector for HPLC was that of Fraley et al. (68). In this particular study, a "dummy" column packed with deactivated glass spheres was utilized, hence peak broadening was due to diffusion and not to retention of the analyte species by the column material. The limits of detection (LODs) obtained for elements introduced as chromatographic peaks were, in general, inferior to those obtained by continuous nebulization, although the results were inconsistent. In addition, the LODs reported by

continuous nebulization were noticeably inferior to those reported by Winge et al. (113).

Gast et al. (69) have evaluated the on-line, element-specific ICP-AES detection of HPLC effluents. The impact of flow rate and the nature of the mobile phase on the stability of the plasma source, peak broadening, sensitivity, linearity, and limits of detection were studied. Most polar HPLC solvents were well-tolerated by the plasma, but non-polar solvents such as those employed in normal-phase HPLC separations caused plasma instability or extinguishment. The LODs reported for Fe (1 ng/mL), Mo (0.3 ng/mL), Cu (0.6 ng/mL), Sn (11 ng/mL), and Pb (11 ng/mL) as chromatographic peaks were significantly better than those reported by Winge et al. (113) for continuous nebulization. From a purely theoretical viewpoint, the LOD obtained for a species detected as a transient should be, at best, comparable to that of the same species detected on a continuous basis, simply due to dispersion caused by column retention and extracolumn void volumes. Indeed this has been the experience of all other authors. The results of this particular study are, therefore, especially unsettling and it is unfortunate that comparisons were not drawn between LODs obtained under continuous flow and HPLC conditions.

In sharp contrast, the authors of HPLC-ICP-AES publications that have followed that of Gast et al. (69) have reported inferior detection limits (often by 1 to 3 orders of magnitude) as compared to continuous flow ICP-AES analysis of unlimited sample volumes. A notable exception was that of Irgolic et al. (80) in which detection limits for several As species were found to be 130 ng/mL (13 ng). However, Irgolic et al. (80) employed a vacuum polychromator system, in which the more intense, 189.0 nm line of

As could be monitored. Furthermore, the LOD reported for As by continuous sample introduction of unlimited sample volume was 15 ng/mL. This means that the LOD reported for HPLC-ICP-AES (130 ng/mL) was inferior by a factor of 8.7 as compared to continuous sample introduction. Similar experiences have been reported by all other authors.

Researchers generally agree that there are two limiting factors to the widespread acceptance of the ICP as an element-specific detector for HPLC effluents. These are the not so simple matter of sample nebulization and transport, and the low tolerance of the ICP to common HPLC solvents. As sample nebulization and transport represents an integral part of the HPLC-ICP interface, the success of the approach is dependent on the presentation of analyte to the plasma. Present methods of sample introduction have long been a limiting factor in atomic spectroscopic analysis. Indeed, only very recently has this problem been addressed with vigor, as evidenced by the publication trends in atomic spectroscopy (122). The coupling of HPLC to the ICP has been accomplished most frequently by the utilization of cross-flow and concentric pneumatic, or Babington-type nebulizers (68,69,71,77,80). The operation of cross-flow and concentric pneumatic nebulizers (Figure 1) has been described earlier. With Babington-type nebulizers, the liquid sample is delivered with a force fed pump to a glass or metal surface that contains a small gas orifice. A thin film of liquid flows over the gas orifice and is ruptured into small droplets as the high velocity gas stream passes through the orifice and shears the film. For situations when the sample volume is limited, conventional cross-flow, concentric, and Babington nebulizers are known to limit drastically the analyte participation in the analytical

process (122-124). For example, for continuous, steady-state nebulization at a typical nebulizer uptake rate of one to two milliliters per minute and assuming 1 to 2% nebulizer-transport efficiency, the actual analyte solution flow rate through the plasma is only 10 to 40 μL/min. If a typical signal observation time of about 6 s is assumed, the integrated signal is representative of the passage of only 1 to 4 μL of the original sample solution through the plasma. For typical HPLC applications, the original analyte solution volumes introduced into the flowing carrier stream have been in the 5 to 200 μL range (107,108,114). If the same one to two percent nebulization-transport efficiencies are assumed, then again only a small fraction (0.5 to 4 μL) of the original sample injected into the flowing carrier stream participates in the analysis. Thus, for both transient and continuous introduction of sample to the aerosol generation device, the ultimate relative limits of detection are severely constrained by the inefficient participation of the original sample in the total analytical process. For HPLC effluent analysis, intracolumn band broadening (59,87) can cause further deterioration in powers of detection. As a consequence, detection limits observed under HPLC introduction are often reported inferior to continuous flow nebulization (75,77,82,83,87,90,94,96) and the ICP-AES detector approach has not been found useful for many, if not most, applications (59,87,122). In fact, Krull et al. (87) stated:

> "... the nature of the interface and nebulizer arrangement in any HPLC-ICP arrangement can affect the final MDLs (minimum detection limits),...there is a distinct possibility that conventional cross-flow or concentric nebulizers for direct-ICP operations

> are just not operationally compatible, in terms of MDLs, for HPLC-ICP operations."

This indeed, appears to be the case.

In addition to inadequate overall efficiencies for aerosol formation, transport, and injection, the conventional sample introduction methods for ICP-AES are not suitable for the introduction of common HPLC solvents (methanol, acetonitrile) into the plasma at flow rates greater than about 0.2 mL/min (125). Nisamaneepong et al. (126) reported that solutions of greater than 30% methanol or acetonitrile extinguished the plasma at a 1.0 mL/min uptake rate (3 to 6 μL/min to plasma). Indeed, if HPLC-ICP is to gain widespread acceptance, its scope of application must also include separations that require organic modifiers in the mobile phase, e.g., organometallics in crude oils.

The thermospray technique has proven to be a useful interface between the liquid chromatograph and mass spectrometer (127-129). Concurrent with the preparation of this dissertation, Meyer et al. (130) evaluated a thermospray nebulizer as a means of liquid sample introduction for ICP-AES. The principles that govern the operation of the thermospray nebulizer (Figure 4) are based upon the thermal heating and adiabatic expansion of a liquid stream pumped under pressure through a capillary tube. Reported limits of detection were improved by factors of 1.7 to 6 with this nebulizer as compared to a conventional, concentric pneumatic nebulizer. Although only preliminary work has been completed, the thermospray nebulizer appears to hold promise as an alternative method of sample introduction for ICP-AES.

Despite notable efforts toward the improvement of sample introduction methods for HPLC-ICP-AES (62,94,126,130-135), no dramatic improvements

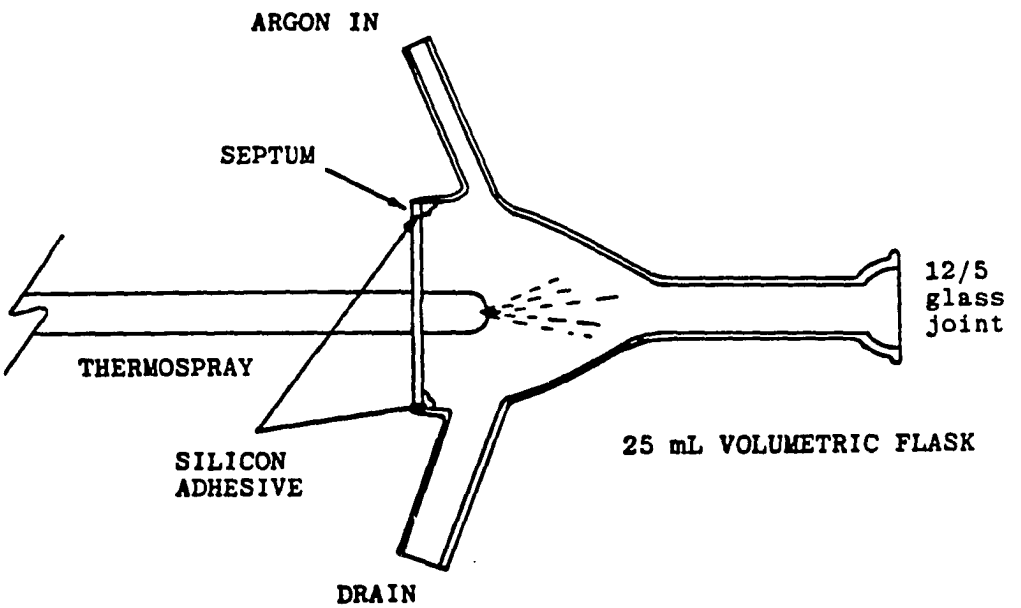

Figure 4. Thermospray nebulizer (Reprinted with permission from Meyer et al. 130, p.957)

have been reported. Browner and Boorn (122) have best summarized the present situation:

> "... the future growth of "speciation" measurement using atomic spectroscopy may be curtailed. In speciation studies, the sample introduction system acts as the interface between the chromatograph and the spectrometer. Developments in the interface may hold the key to the success of failure of the whole approach. Without some major improvements in interface performance, it is unlikely that LC/ICP interfacing will achieve widespread use. Speciation studies may then remain restricted to the few volatile compounds suitable for gas chromatographic separation."

Statement of Problem

The analysis of HPLC effluents is not the only important situation in which the analyst is routinely confronted with very limited sample volumes. Another prominent situation is flow injection analysis (FIA)--a form of sample presentation to the analytical device that is destined to come into common use. The FIA technique utilizes a continuously flowing carrier stream, into which highly reproducible volumes of sample are injected. Analyte species are detected as a transient signal, at a point downstream using an appropriate detector. Several advantages of FIA over continuous flow methods for sample introduction into the ICP have been discussed by Greenfield (136,137), and are summarized in Table II.

The ideal characteristics of an element-specific detector for chromatography are summarized in Table III. Clearly, points 2 and 6 have proven to be the most difficult. As documented earlier, all element-specific, atomic spectroscopic detectors, except for the batch mode GFAAS version, are based on the on-line atomization and excitation of limited effluent sample volumes, typically 5 to 200 μL. These limited sample

Table II. Advantages of flow injection analysis

1.	Provides a means of sample introduction with reproducible timing and controlled dispersion.
2.	Provides a rapid, precise, and accurate means of presenting sample solutions to the nebulizer.
3.	A continuous flow of the analyte carrier stream yields improved plasma stability.
4.	The nebulizer is continuously washed, therefore, reducing the possibility of blockage or build-up at the injector tip.
5.	Provides a continuous background that can be used to rapidly optimize signal-to-background values.

Table III. Element specific detectors for GC, LC, and IC: Idealized characteristics

1.	Applicable to the direct, on-line detection and determination of all elements
2.	Part-per-billion detection limits (based on content of sample injected into chromatograph)
3.	Capable of determining empirical formulae (no chemical structure or matrix effect)
4.	Linear response over 3 to 4 orders of magnitude of concentration changes
5.	Directly adaptable to collecting "n" element selective chromatograms simultaneously
6.	Compatible to various mobile phases and associated flow rates
7.	Minimum dead volumes
8.	Simplicity of operation and construction
9.	Low cost

volumes are converted into an aerosol that is subsequently introduced into the atomization-excitation cell. The powers of detection obtained in this manner have generally been inadequate for most real elemental speciation studies. The major contributing factor to the inadequate powers of detection is the ineffective participation of the very limited sample available in the analytical process. This is because the present technologies for converting the effluent flow into an aerosol and its transport leads to losses of 80 to 99% of the limited sample. Thus, only 1 to 20%, at best, of the original sample participates in the analytical process. Two general solutions to this problem can be suggested; 1) devise an atomization-excitation cell that is more effective in generating element-specific signals from the limited sample that is introduced, or 2) improve the efficiency of the nebulization and transport process, up to 100%. A 100% nebulization and transport efficiency should lead, in principle, to 1 to 2 orders of magnitude improvement in powers of detection.

The development and evaluation of a 100% efficient nebulizer-transport device constitutes a major part of this thesis investigation. A direct injection nebulizer (DIN) was evaluated to determine its potential utilization as an effective interface for FIA and HPLC coupled with ICP-AES. The analytical figures of merit observed under FIA conditions for the DIN were critically compared with conventional pneumatic and ultrasonic nebulizer performance. Simultaneous, multielement, element-specific HPLC-DIN-ICP-AES analysis of synthetic and actual samples was demonstrated. Finally, analytical excitation temperatures in the ICP were

measured and compared for the DIN, conventional pneumatic, and ultrasonic nebulizers.

CHAPTER II. EXPERIMENTAL FACILITIES AND OPERATING CONDITIONS

Plasma Operating Conditions

The plasma operating conditions employed for this study are summarized in Table IV.

Methods of Sample Introduction

Direct injection nebulizer interface

Construction A schematic diagram of the nebulizer and torch assembly used in this study is shown in Figure 5. Both the torch and nebulizer were fabricated at the Ames Laboratory. A magnified view of the direct injection nebulizer tip is shown in Figure 6. The liquid samples [A] were introduced through a 0.19 mm o.d. by 0.05 mm i.d. fused-silica, inner capillary tube [B] (Spectran Corporation, Sturbridge, MA 01566). The argon nebulizer gas flow [C] was directed through a 0.70 mm o.d. by 0.50 mm i.d. fused-silica, outer capillary tube [D] that sheathed the inner capillary tube [B]. The tip of the nebulizer gas capillary tube was tapered down to a 0.25 mm orifice as shown in Figure 6. The 0.03 mm annular spacing between the tubes at the nebulizer tip created a high-velocity nebulizing gas flow capable of producing an aerosol for direct introduction into the axial channel of the plasma. A 1.6 mm o.d. by 0.8 mm i.d. ceramic insulating tube [E] (Ventron Corporation, Alfa Products, Beverly, MA 01915) was inserted over the outer capillary tube to straighten and hold the nebulizer rigid. The gap between the outer capillary tube and ceramic was sealed with an epoxy resin. Auxiliary

Table IV. Plasma operating conditions and detection facilities

Plasma (General):	Plasma-Therm, Inc., Kresson, NJ
HF Generator:	Model HFS-5000D; 27.12 MHz
Power (Forward):	1.8 kW
Plasma Ar flow rate:	17 L/min
Auxiliary plasma Ar flow rate:	0.5 L/min
Monochromator:	McPherson Model 2051
Focal length:	1 m
Grating:	1800 grooves/mm, holographic
Slit widths:	20 μm
Polychromator:	Modified Model QVAC-127 Applied Research Laboratories, Sunland, CA
10 channel A/D converter:	Ames Laboratory Design (138)
Computer facility:	Digital PDP 11/34A Digital Equipment Corp., Maynard, MA
Graphics terminal:	HP 2648A, Hewlett Packard
Printer:	HP 2631G, Hewlett Packard
Plotter:	HP 9872S, Hewlett Packard
Amplifier:	Model 417, Keithley Instruments, Inc., Cleveland, OH.
Pneumatic Nebulizer:	Kniseley-type, cross-flow (139)
Spray chamber:	Scott-type (140)
Nebulizer Ar flow rate:	1 L/min
Ultrasonic Nebulizer:	Ames Laboratory Design (141,142)
Nebulizer Ar flow rate:	1 L/min
Desolvation chamber temperature:	124°C
Power(forward):	45W
Direct Injection Nebulizer:	Ames Laboratory Design (herein, p. 51)
Nebulizer Ar flow rate[a]:	0.2 L/min
Auxiliary nebulizer Ar flow rate[b]:	0.6 L/min

[a]Defined as the argon flow in the DIN.

[b]Defined as the argon flow in the annular space between the DIN and the normal sample introduction tube.

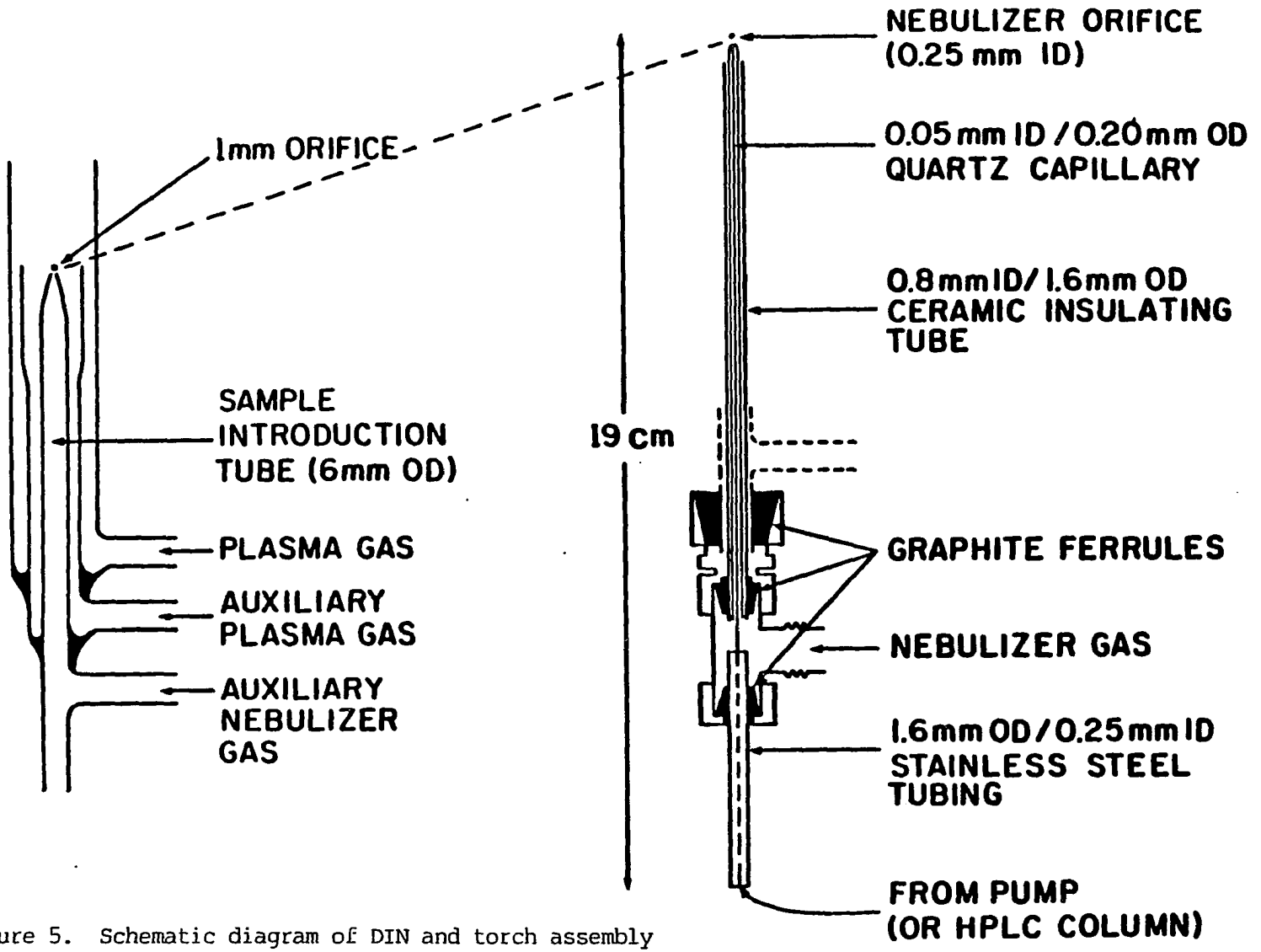

Figure 5. Schematic diagram of DIN and torch assembly

Figure 6. A magnified view of the direct injection nebulizer tip [A] liquid sample; [B] fused-silica, inner capillary tube; [C] nebulizer argon gas flow; [D] fused-silica, outer capillary tube; [E] ceramic insulating tube; [F] auxiliary nebulizer argon gas; [G] normal sample introduction tube (All dimensions are in mm)

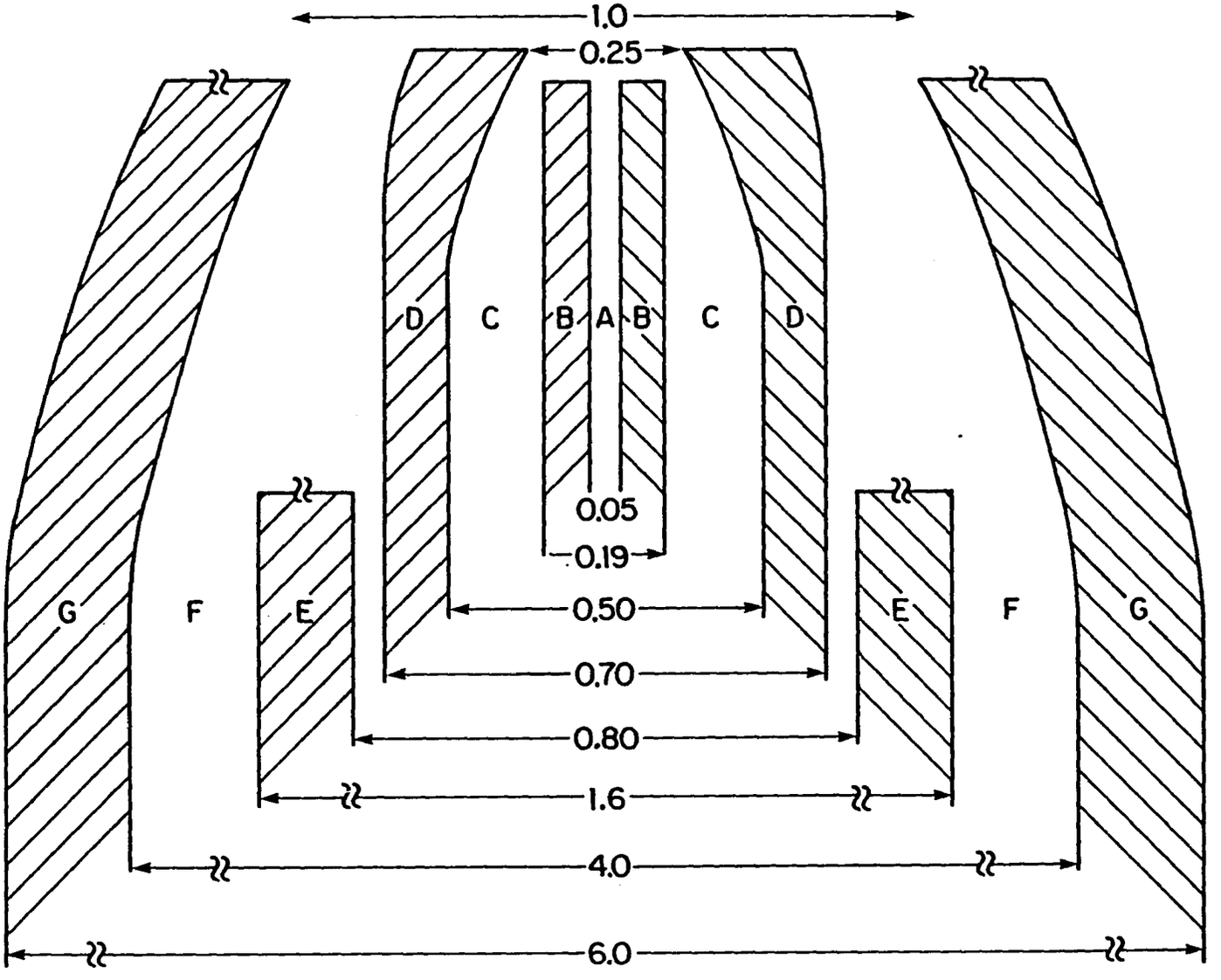
1.0
0.25
D
C
B
A
B
C
D
0.05
0.19
G
F
E
0.50
E
F
G
0.70
0.80
1.6
4.0
6.0

nebulizer argon flow [F] was carried between the normal sample introduction tube [G] and the ceramic insulating tube.

Optimization of aerosol plume The procedure used for the optimization of the aerosol plume produced by the DIN is as follows:

1. Adjust the inner capillary tube so that it protrudes from the outer capillary tube by about 0.5 mm.
2. Support the nebulizer in a suitable manner, e.g., a three-pronged clamp.
3. Connect the nebulizer gas tubing to the nebulizer.
4. Initiate nebulizer gas flow. Use a high flow rate initially (~0.5 L/min) so as not to flood the nebulizer.
5. Connect the 1.6 mm o.d. stainless steel tubing from the HPLC pump to the liquid inlet tube of the nebulizer.
6. Initiate liquid flow rate (~500 μL/min).
7. To optimize visually the shape of the aerosol plume, gradually pull down the liquid inlet tube until the aerosol plume takes on a symmetric, conical form. (If liquid droplets form on the nebulizer tip, the optimum position has been passed.)
8. After the overall shape and production of the aerosol has been optimized, reduce the liquid flow rate to about 120 μL/min (the standard liquid flow rate).
9. Now reduce the nebulizer gas flow rate to as great a degree as possible, while still maintaining efficient aerosol production.
10. This optimum nebulizer gas flow rate should be noted and used subsequently.

FIA/HPLC-DIN-ICP system Standard FIA and HPLC techniques and equipment were used throughout this study. As illustrated in Figure 7, solutions were drawn continuously from a solvent reservoir [A] through a high pressure, single piston pump [B] (Model 112, Beckman Instruments, Inc., Berkeley, CA 94710) into a syringe loading sample loop injector [C]

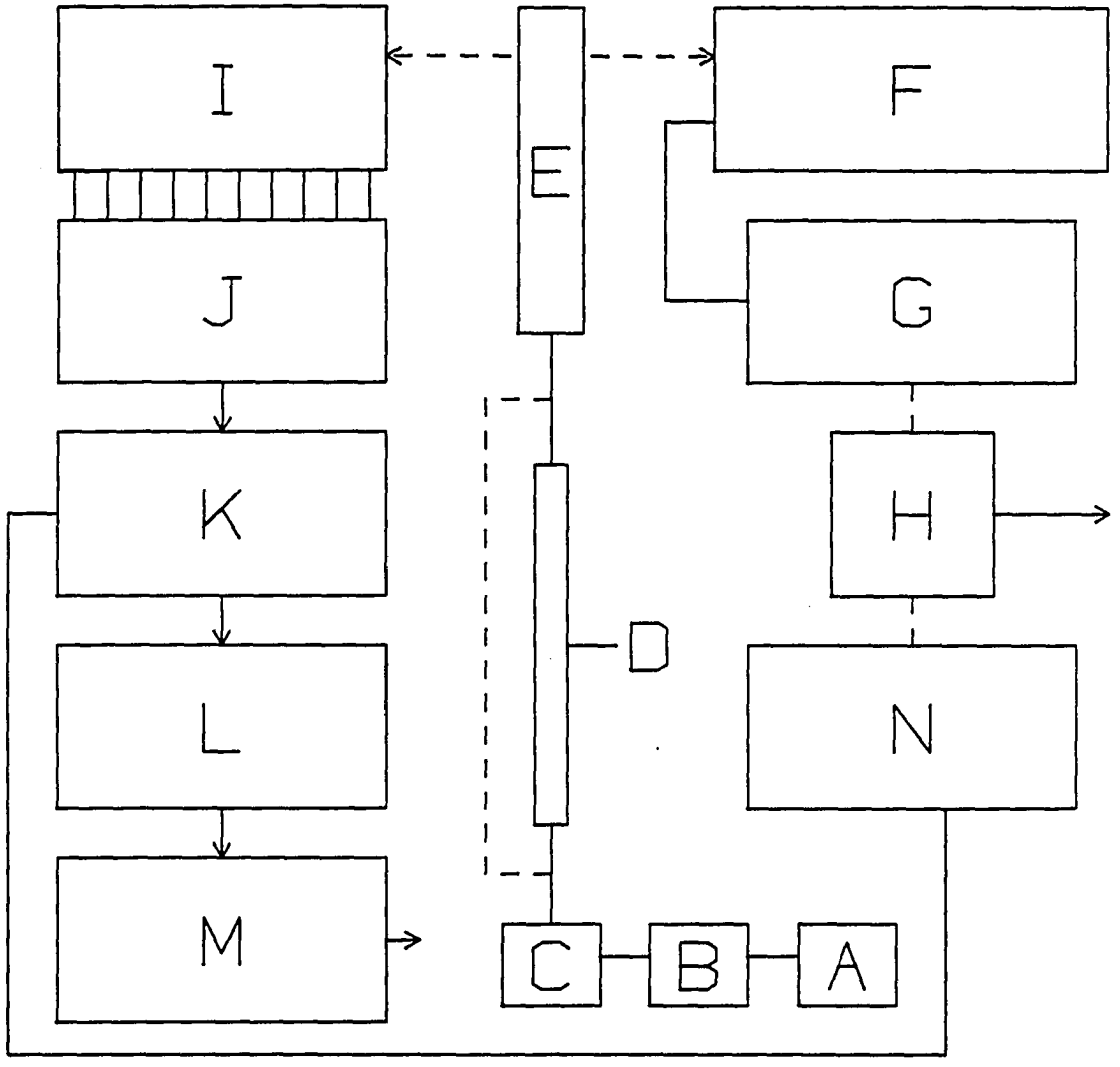

Figure 7. Schematic of instrumentation and computer facilities [A] solvent reservoir; [B] Beckman Model 112 Solvent Delivery Module; [C] sample injector, Rheodyne Model 7125 or Beckman Model 210; [D] HPLC column; [E] nebulizer/torch assembly; [F] McPherson Model 2051, 1-meter scanning monochromator; [G] Keithley Model 417 electrometer amplifier; [H] Curken Model #250-1 strip chart recorder; [I] ARL polychromator; [J] current-to-frequency converters; [K] Digital PDP 11/34A computer system; [L] HP 2648A graphics terminal; [M] HP 2631G printer plotter or HP 9872S pen plotter; [N] single channel analog output device

(Model 7125, Rheodyne, Inc., Cotati, CA 94928 or Model 210, Beckman Instruments, Inc., Berkeley, CA 94710). Sample volumes of 30 μL were used for the FIA mode, and 100 or 200 μL volumes for the HPLC mode. Analyte solutions injected into the sample loops were transported by the solvent stream through a 12 cm length of 100 μm i.d. stainless steel tubing for FIA, or through a 4.6 mm i.d. x 250 mm C_{18} reverse phase column [D] (Partisil 5 ODS-3, Whatman Chemical Separation, Inc., Clifton, NJ 07014) for HPLC. For the HPLC analysis of the energy-related materials, a pre-column (CO:PELL ODS, Whatman Chemical Separation, Inc., Clifton, NJ 07014) was inserted between the sample loop injector and analytical column. Effluent from the columns passed directly into the inner capillary tube of the nebulizer assembly to the base of the plasma where direct nebulization into the plasma occurred. The dead volume between the ends of the FIA transfer tubing or HPLC columns to the nebulizer tip was approximately 1.5 μL. For HPLC studies with UV absorption detection, a Tracor variable wavelength detector (Tracor Model 970A Austin, TX) was employed.

Pneumatic nebulizer interface

Pneumatic nebulization was employed in both the flow injection analysis and continuous sample introduction modes. The analyte solutions or flow injection carrier streams were drawn continuously from a reservoir [A] through a high pressure, single-piston pump [B] (Model 112, Beckman Instruments, Inc., Berkeley, CA 94710) into a syringe loaded, sample-loop injector [C] (Model 7125 Rheodyne, Inc., Cotati, CA 94928). Analyte solutions injected into the sample loop were transported by the flow injection carrier stream through an 18.5 cm length of 0.19 mm o.d. by 0.10 mm i.d. fused-silica, capillary tubing (Spectran Corp., Sturbridge, MA

01566) that was cemented into a 5 cm length of 1.6 mm o.d. by 0.25 mm i.d. stainless steel tubing. The fused-silica, capillary tubing was connected to a conventional Kniseley-type, cross-flow nebulizer (139) so that the capillary tubing protruded approximately 0.1 mm from the normal liquid uptake capillary tube. The transport volume from the sample loop to the point of nebulization was restricted to about 1.5 μL. The generated aerosol was swept through a Scott spray chamber (140), and directly to the base of a conventional ICP torch.

Ultrasonic nebulizer interface

Ultrasonic nebulization was employed in both the flow injection analysis and continuous sample introduction modes. The ultrasonic nebulization system developed at the Ames Laboratory was used with and without desolvation of the aerosol (141,142). The analyte solutions or flow injection carrier streams were drawn continually from a reservoir through a peristaltic pump (Model Minipuls 2, Gilson Medical Electronics, Inc., Middleton, WI 53562) into a 4-way Teflon rotary valve (Type 50, Rheodyne, Inc., Cotati, CA 94928). Analyte solutions injected into the sample loop were transported by the flow injection stream through an 8 cm length of 0.5 mm i.d. by 1.0 mm o.d. Teflon tubing that was inserted into a 5 cm length of 1 mm i.d. by 3 mm o.d. glass tubing. The aerosol generated at the transducer plate was swept through a conical spray chamber containing a Teflon baffle and then into the desolvation apparatus (141,142). When aerosol desolvation was not desired, the aerosol was swept from the spray chamber and transported directly to the base of a conventional ICP torch.

Detection Facilities

Single element detection

As illustrated in Figure 7, the plasma was imaged onto the slit of a 1 meter scanning monochromator [F] (McPherson Model 2051, GCA Corporation, Acton, MA 01720). The monochromator was fitted with a 1800 grooves/mm, holographic grating. A photomultiplier tube (EMI, 9781A) was used as the detector. The photocurrents produced were amplified by an electrometer amplifier [G] (Model 417, Keithley Instruments, Inc., Cleveland, OH 44139) and the spectral information recorded on a strip chart recorder [H] (Model #250-1, Curken Scientific, Inc., Danbury, CT 06810).

Simultaneous, multielement detection

As illustrated in Figure 7, the plasma was imaged onto the slit of a modified ARL polychromator [I] (Model QVAC-127, Applied Research Laboratories, Sunland, CA). The spectral lines used for this study are listed in Table V. These lines were preprogramed, thus, the detection of other lines was restricted. When sulfur-specific detection at 182.0 nm was desirable, the argon purge tube illustrated in Figure 8 was inserted between the CaF_2 lens of the polychromator and torch assembly as shown. The tube was purged with argon gas (1 L/min) and served to eliminate oxygen from the optical path, as oxygen absorbs radiation below 190 nm. A sapphire window positioned inside the argon purge tube filtered out second order oxygen atom emission (130.22 nm, 130.49 nm, and 130.60 nm) that interfered with the detection of Fe at the 261.19 nm wavelength. Note that when organic solvents were utilized as carrier streams (mobile phases), the formation and optical emission of the CO fourth positive molecular band system imposed a serious limitation on the detection of

Table V. QVAC line array

Element[a]	Wavelength (nm)
S I	182.04[b]
As I	193.76[b]
Se I	196.09[b]
Hg I	184.95[b]
Cr II	205.55
Zn I	213.86
Ni II	231.60
Fe II	261.19
V I	292.40
Cu I	324.75
Ti II	334.94
Co II	228.62
Cd II	226.50

[a] I: Spectral line originates from neutral atom state; II: spectral line originates from singly ionized state.

[b] Vacuum wavelengths.

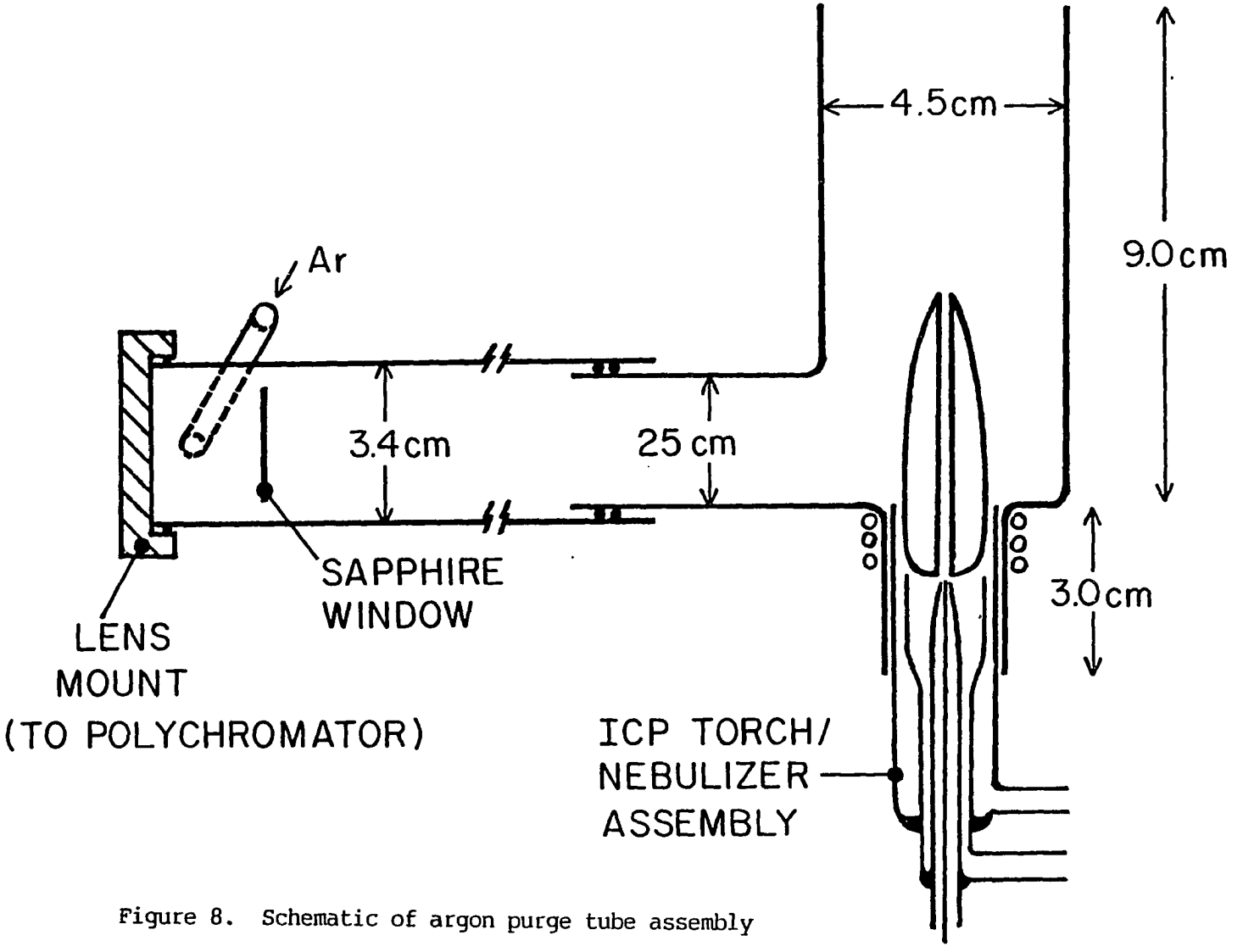

Figure 8. Schematic of argon purge tube assembly

sulfur atom emission at the 182.0 nm wavelength. From considerations of spectral interferences, the sulfur atom line at 182.0 nm was not the logical choice (see Chapter IV). The detectability of sulfur would have improved if the 180.7 nm sulfur atom line was used, as this line falls between the CO fourth positive molecular bands at 179.2 nm and 181.1 nm.

As the software associated with the original ICP-AES facility was not capable of the analysis of transient signals, a new data aquisition facility was designed and constructed (138). This facility was capable of the aquisition of ten, simultaneous chromatograms at sampling rates up to 20 data points per second, per channel. For liquid chromatographic applications in which peak widths are typically on the order of 15 to 60 seconds, a sampling rate of 5 data points per second, per channel more than adequately defined the peak shape. The electronic circuits associated with the data aquisition facility consisted of ten, current-to-frequency converters [J], one converter for each spectral channel or photomultiplier tube that was used. Data collection was under control of the Digital PDP 11/34A computer system [K] (Digital Equipment Corp., Maynard, MA).

The chromatography software for the ICP polychromator system was command driven from a graphics terminal [L] (HP 2648A, Hewlett Packard, Palo Alto, CA). The RECORD command was used to record the multichannel chromatogram, while simultaneously providing an analog output of a single channel [N] for monitoring purposes on a strip chart recorder [H] (Model #250-1, Curken Scientific, Inc., Danbury, CT 06810). The FILTER command allowed the user to filter (smooth) the chromatographic data employing a digital Butterworth filter (143,144) of either first, second, or third

order. The INTEGRATE command provided the user with the capability of integrating a user specified region of a chromatogram. The user also specified the two background correction points to be employed for the integration of the user specified region. A straight line was drawn between the two background correction points. The PLOT command allowed the user to plot one or more channels on either a printer plotter [M] (HP 2631G, Hewlett Packard, Palo Alto, CA) or pen plotter [M] (HP 9872S, Hewlett Packard, Palo Alto, CA).

Analytical Figures of Merit Studies

Because the acceptance of any new analytical method is greatly dependent on performance, it was important to evaluate the analytical figures of merit for the DIN before applying the nebulizer to actual analytical studies, be it limited volume solution analysis via FIA or HPLC effluent analysis. As the DIN is best suited to the flow injection mode of sample presentation, the FIA method was used to evaluate the analytical figures of merit. The figures of merit investigated include detection limits, reproducibility, linear dynamic range, interelement effects, and minimal sample volumes required to achieve powers of detection equal to continuous, or steady-state sample introduction.

Preparation of reference solutions

For detection limit, reproducibility, and linear dynamic range evaluations, reference solutions containing As, Se, Hg, Pb, Cr, Zn, Cd, Fe, Mn, and Ba were prepared, via serial dilutions, from 1000 μg/mL stock solutions (Fisher Scientific Co., Fair Lawn, NJ 07410) and used immediately.

For the interelement effect studies, a 20 μg/mL (0.5 μmol/mL) Ca reference solution was prepared by dissolving reagent grade $CaCO_3$ in 10 mL of concentrated HCl and diluting to 100 mL in a volumetric flask. Phosphorus was added as reagent grade H_3PO_4 (85%) in the Ca-PO_4 system. The Na and Al concomitant solutions were prepared from NaCl and $Al(NO_3)_3 \cdot 6H_2O$, respectively, in the Ca-Al and Ca-Na systems.

Interelement effects

The extent to which several interelement effects occur with flow injection into the DIN interface were investigated in a manner similar to experiments previously described (145). Emission intensity measurements were made at 15, 20, and 25 mm observation heights above the load coil. Triplicate, 20 μL sample volumes containing a fixed concentration of Ca (20 μg/mL or 0.5 μmol/mL) and known amounts of interferents were injected into an aqueous FIA solvent stream, flowing at a rate of 120 μL/min. The emission intensities were monitored at the Ca I 422.7 nm and Ca II 393.4 nm lines.

Applications to Synthetic and Real Samples

Detailed experimental procedures for the analysis of real samples are given in Chapter IV. Synthetic mixtures containing Cr(III) and Cr(VI) were prepared from chromium(III) chloride and sodium chromate, respectively (J.T. Baker, Phillipsburg, NJ or Alfa Products, Danvers, MA), or chromium(III) acetate (Alfa Products) for speciation studies. Synthetic mixtures containing sodium arsenate and sodium arsenite (Fisher), benzenearsonic acid (Eastman Kodak Co., Rochester, NY), methanearsonic acid (Sigma, St. Louis, MO), and dimethylarsinic acid (EPA, Research Triangle Park, NC) were prepared for As speciation studies.

were prepared for Se speciation studies. Sodium 1-pentanesulfonate (PIC B-5) and tetrabutylammonium phosphate (PIC A), respectively, (Waters Associates, Milford, MA) were used as ion pair reagents for the Cr, Se, and As chromatographic separations at a concentration of 5mM in both the HPLC mobile phase and analyte solutions. All of the chemicals listed above were used without further purification and all solvents used were of HPLC quality (Burdick and Jackson, Muskegon, MI).

CHAPTER III. ANALYTICAL FIGURES OF MERIT

General

A stable argon plasma has been maintained when the direct injection nebulizer (DIN) was employed for the direct introduction of aqueous aerosol at uptake rates up to 200 μL/min, and methanol, acetonitrile, methyl isobutyl ketone, or pyridine uptake rates up to 150 μL/min. The analytical figures of merit observed under flow injection analysis (FIA) conditions for the DIN interfaced to an inductively coupled plasma-atomic emission spectroscopy (ICP-AES) facility were found to be comparable to or better than conventional pneumatic nebulization in terms of limits of detection, reproducibility, and interelement effects. The results of these studies are summarized in the following sections.

Results and Discussion

Detection limit comparisons

For the flow injection or HPLC introduction of limited sample volumes into a nebulizer for subsequent ICP detection, the quantitative analytical information is primarily derived from peak area or height measurements. The initial concentration of the analyte, C_0, in the injected sample can be related to the concentration of the analyte in that volume element of fluid which corresponds to the maximum of the peak, C_{max}, after dispersion. Thus:

$$D = \frac{C_0}{C_{max}} \qquad [1]$$

where D is the dispersion factor (146). This means that when the analyte emissions peak height from a flow injected sample is equivalent to the steady-state analyte emission signal produced from a continuously flowing sample, no dispersion has occurred (D=1). This is the criterion used in the determination of the optimum sample injection volumes and carrier stream flow rates for each of the nebulizers studied.

In this study, the transport volume from the sample loop injector to the point of nebulization was constrained to as low a value as possible. For each type of nebulizer, the injected sample volumes and carrier stream flow rates were optimized by alternating between loop injected and continuously flowing analyte solutions until the intensity of the two signals was approximately equal, D then being very close to one. A typical pattern of peaks obtained from sample volume additions of a 10 μg/mL As reference solution to the flow injection carrier stream is illustrated in Figure 9 for the DIN. It is seen that equivalent intensities were obtained when the flow injected volumes were 30 μL or greater. The optimum sample volumes and carrier stream flow rates determined for each type of nebulizer are summarized in Table VI.

Limits of detection

The estimated ICP-AES limits of detection for flow injected and continuous introduction of the analyte into the nebulizers studied are given in Table VII. For the flow injected analyte, limits of detection were based on peak height measurements that gave a signal to background scatter ratio of three. In the case of continuous analyte introduction, the limits of detection represent the analyte concentration required to produce extended time recordings having a signal to background scatter

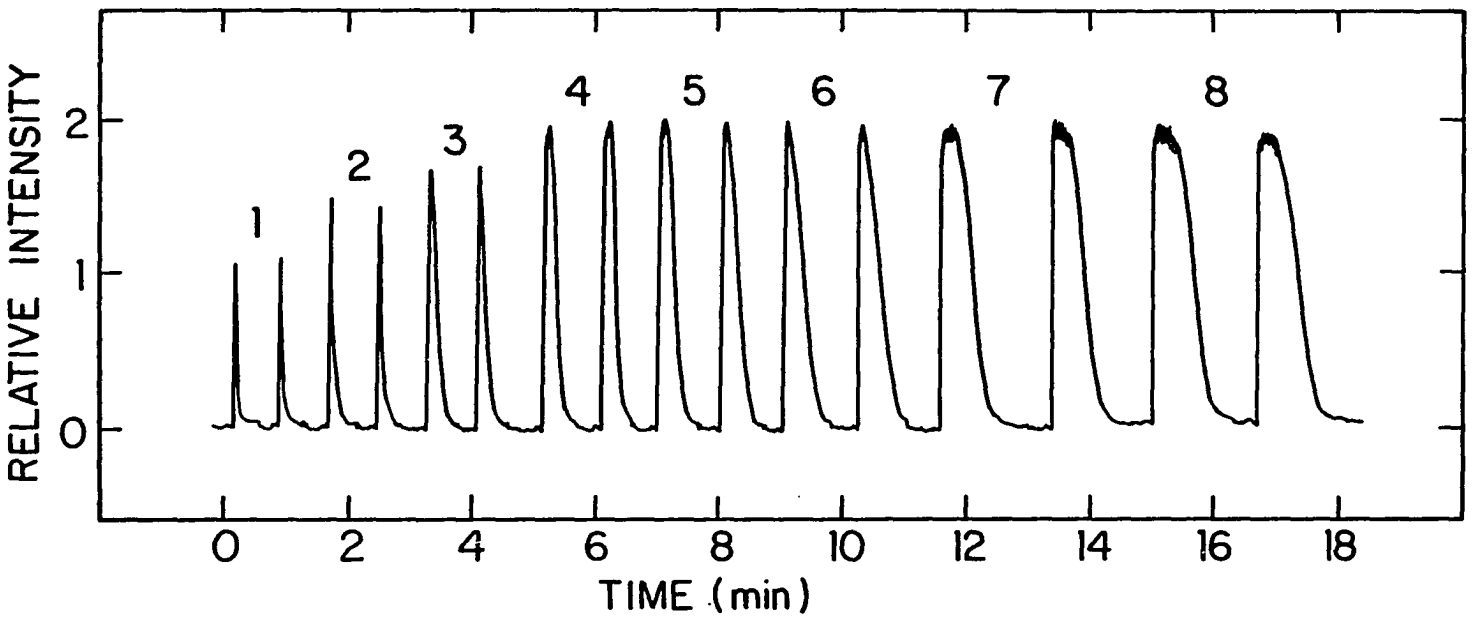

Figure 9. Signals produced from incremented volumes of a 10 μg/mL As reference solution (1) 5 μL, (2) 10 μL, (3) 20 μL, (4) 30 μL, (5) 40 μL, (6) 50 μL, (7) 80 μL, (8) 100 μL; Carrier stream flow rate: 120 μL/min

Table VI. Optimum sample volumes and flow rates for the flow injection systems described

Nebulizer	Sample Volume (μL)	Carrier Stream flow rate (mL/min)
Direct injection	30	0.120
Pneumatic	200	2.5
Ultrasonic		
(w/aerosol desolvation)	500	2.5
(w/o aerosol desolvation)	500	2.5

Table VII. Estimated limits of detection by both FIA- and continuous Flow-ICP for three types of nebulizers

Element	Analytical Wavelength (nm)	Relative Limits of Detection (ng/mL)							
		Direct Injection		Pneumatic		Ultrasonic[a]		Ultrasonic[b]	
		FIA	Continuous	FIA	Continuous	FIA	Continuous	FIA	Continuous
As	193.7	41	40	91	80	42	41	6	7
Se	196.0	37	52	94	81	64	66	6	8
Hg	194.2	20	22	27	16	34	45	10	11
Pb	220.4	28	28	31	27	36	35	4	4
Cr	205.6	12	12	13	12	5	5	0.8	0.9
Zn	213.9	2	2	4	4	4	4	0.1	0.1
Fe	238.2	1	4	3	3	2	2	2	2
Cd	214.4	4	1	5	4	7	8	0.4	0.4
Mn	257.6	1	1	1	1	0.5	0.5	0.07	0.06
Ba	455.4	1	2	3	2	—	—	—	—

[a]Without aerosol desolvation.
[b]With aerosol desolvation.

ratio of three. The following general conclusions can be drawn from the data in Table VII. First, within the limits of uncertainty (factor of two to three) inherent in detection limit determinations, the DIN required only 30 μL of analyte solution by flow injection to achieve powers of detection equivalent to those for: (a) continuous sample introduction into the DIN; (b) either FIA introduction of 200 μL or continuous sample introduction into a cross-flow pneumatic nebulizer; and (c) either FIA introduction of 500 μL or continuous sample introduction into the Ames Laboratory ultrasonic nebulizer, without subsequent aerosol desolvation. Second, with the exception of Fe, the best powers of detection were observed for ultrasonic nebulization with aerosol desolvation, for either FIA (500 μL) or continuous introduction. Obviously, for situations where analyte solution volumes are severely limited, e.g., 20 to 30 μL, the FIA-DIN combination offers an attractive means for achieving detection limits comparable to those obtained by pneumatic nebulization for unlimited sample volumes.

Comparison of detection limits for other microliter solution volume introduction methods to the FIA-DIN approach

The absolute and relative limits of detection for FIA-DIN-ICP for 30 μL sample volumes are summarized in Tables VIII and IX, respectively, and compared to FIA-ICP-AES with conventional pneumatic nebulizers (147-150), graphite furnace vaporization-ICP-AES (151-158), graphite yarn thermal atomization-ICP-AES (159), tantalum filament vaporization-ICP-AES (160), tantalum boat vaporization-ICP-AES (161), graphite cup direct insertion-ICP-AES (162), graphite rod insertion-ICP-AES (163,164), and wire loop direct sample insertion-ICP-AES (165). Overall, the absolute and relative

Table VIII. Comparison of absolute detection limits (ng)

Element	FIA-DIN-ICP-AES (30 μL)	FIA-ICP-AES[a] (20 to 500 μL)	Graphite Furnace Vaporization ICP-AES[b] (10 to 50 μL)	Graphite Yarn Thermal Atomization ICP-AES[c] (25 μL)
As	1.2	—	0.2 to 20	0.5
Se	1.1	—	—	—
Hg	0.60	—	0.004 to 0.6	1
Pb	0.84	6.8	0.005 to 6.5	0.08
Cr	0.36	1.7[i] to 14	0.1 to 0.20	0.13
Ni	0.45	1.8[i] to 100	0.4 to 9	0.35
Co	0.21	12	0.3 to 3	—
Cu	0.18	0.3[i] to 4.5	0.002 to 2	0.05
Zn	0.06	0.5[i] to 75	0.003 to 0.30	0.18
Fe	0.03	1.1[i] to 3.5	0.03 to 0.70	0.28
Cd	0.10	150	0.01 to 0.50	0.15
Mn	0.03	2.3 to 28	0.001 to 0.02	0.008

[a]Reference 147-150.
[b]Reference 151-158.
[c]Reference 159.
[d]Reference 160.
[e]Reference 161.
[f]Reference 162.
[g]References 163, 164.
[h]Reference 165.
[i]20% HCl matrix.

Tantalum Filament Vaporization ICP-AES[d] (100 μL)	Tantalum Boat Vaporization ICP-AES[e] (5 μL)	Graphite Cup Direct Insertion ICP-AES[f] (10 μL)	Graphite Rod Insertion ICP-AES[g] (5 μL)	Wire Loop Direct Sample Insertion[h] (10 μL)
1	—	—	—	—
0.6	—	—	—	—
0.2	—	—	—	—
0.3	—	0.06	0.03	—
—	0.02	0.07	0.02	—
—	—	—	0.07	—
—	—	—	0.02	—
—	0.005	—	0.02	0.002
—	—	0.12	0.004	0.001
—	—	0.81	0.04	—
0.6	—	0.10	0.02	—
0.003	0.005	0.04	0.006	—

Table IX. Comparison of relative detection limits (ng/mL)

Element	FIA-DIN-ICP-AES (30 μL)	FIA-ICP-AES[a] (20 to 500 μL)	Graphite Furnace Vaporization ICP-AES[b] (10 to 50 μL)	Graphite Yarn Thermal Atomization ICP-AES[c] (25 μL)
As	41	—	20 to 200	20
Se	37	—	—	—
Hg	20	—	0.8 to 6	40
Pb	28	340	1 to 30	3
Cr	12	17[i] to 70	0.7 to 20	5
Ni	15	18[i] to 200	4 to 90	14
Co	7	62	3 to 30	—
Cu	6	3[i] to 90	0.1 to 20	2
Zn	2	5[i] to 150	0.2 to 10	7
Fe	1	11[i] to 70	2 to 70	11
Cd	4	300	1 to 50	6
Mn	1	16 to 55	0.1 to 2	0.3

[a]Reference 147-150.
[b]Reference 151-158.
[c]Reference 159.
[d]Reference 160.
[e]Reference 161.
[f]Reference 162.
[g]References 163, 164.
[h]Reference 165.
[i]20% HCl matrix.

Tantalum Filament Vaporization ICP-AES[d] (100 μL)	Tantalum Boat Vaporization ICP-AES[e] (5 μL)	Graphite Cup Direct Insertion ICP-AES[f] (10 μL)	Graphite Rod Insertion ICP-AES[g] (5 μL)	Wire Loop Direct Sample Insertion[h] (10 μL)
10	—	—	—	—
6	—	—	—	—
2	—	—	—	—
3	—	6	7	—
—	4.4	7	4	—
—	—	—	13	—
—	—	—	4	—
—	1	—	4	0.2
—	—	12	0.8	0.08
—	—	81	8	—
6	—	10	4	—
0.03	1	4	1	—

LODs obtained by the DIN-ICP-AES approach are 1) comparable to or within the range of values reported for graphite furnace vaporization-ICP-AES, and graphite yarn thermal atomization-ICP-AES; and 2) comparable or superior to those values reported for FIA-ICP-AES with conventional pneumatic nebulization and graphite cup direct insertion-ICP-AES. For FIA-DIN sample introduction, the absolute LODs are generally inferior to those values reported for tantalum boat vaporization-ICP-AES and graphite rod insertion-ICP-AES. However, because the tantalum boat vaporization and graphite rod insertion values were based on 5 μL sample volumes, the relative LODs for these techniques are still comparable to those obtained by FIA-DIN introduction of 30 μL sample volumes. For FIA-DIN sample introduction, the relative LODs are somewhat inferior to those values reported for tantalum filament vaporization. As the tantalum filament vaporization values were based on 100 μL sample volumes, the absolute LODs for this technique are still comparable to those obtained by FIA-DIN introduction of 30 μL sample volumes. Both the relative and absolute limits of detection obtained by the DIN-ICP-AES approach are inferior to those reported for the wire loop direct sample insertion method.

The overall comparability of the limits of detection found for the FIA-DIN aerosol introduction method and those reported for electrothermal vaporization introduction methods (with the exception of wire loop insertion) poses the question of the ultimate utility of these alternative procedures for the analysis of liquid samples of limited volume. In addition to the fact that the FIA-DIN-ICP approach is not burdened with the interelement effects that may occur during the thermal vaporization cycle, it has distinctive advantages with reference to the simplicity,

accuracy, precision, and rapidity of the overall sample presentation process. Moreover, the FIA-DIN form of sample presentation is readily automated whereas the thermal vaporization processes are less adaptable to automation. In view of these considerations, it appears unlikely that the thermal vaporization modes of sample introduction will find extensive applications for the analysis of liquids when at least 30 μL of samples are available. Although the wire loop direct sample insertion-ICP-AES method has shown considerable promise for the analysis of solutions of limited volume, it is less adaptable to automation and the lifetime of the tungsten wire loop is limited (100 insertions).

The limits of detection reported for FIA-DIN-ICP-AES were generally superior to those values reported for FIA-ICP-AES with conventional pneumatic nebulization. The question is now posed as to why the LODs obtained with the DIN were not far superior to those for FIA-ICP-AES with conventional pneumatic nebulization in view of the 100% aerosol injection efficiency achieved by the DIN. The DIN solvent loading of the plasma is approximately an order of magnitude greater than for conventional pneumatic nebulization. This increased loading causes some changes in the plasma characteristics, particularly a reduction in the excitation temperatures attained in the axial channel. The impact of these changes will be considered in Appendix B.

Reproducibility

The precision evaluations were based on the pattern of relative average deviations from the mean of triplicate flow injections of sample solution volumes giving a dispersion of one (see equation 1). These volumes were 30 μL, 200 μL, and 500 μL, respectively, for the DIN,

pneumatic, and ultrasonic nebulizers. For the latter, analyte concentrations were adjusted downward so that line/background ratios were similar to the ratios for pneumatic nebulizers. Data were collected for nine analyte elements. An examination of these data (Table X) shows that the direct nebulization of 30 μL sample volumes provided overall reproducibility values comparable to those measured for the conventional cross-flow pneumatic nebulization of 200 μL sample volumes, and for the ultrasonic nebulization of 500 μL volumes.

Linear dynamic range

The analytical calibration curves illustrated in Figures 10 and 11 were obtained from peak height and peak area measurements, respectively, for the FIA-DIN introduction of varying concentrations of the elements indicated. Linear dynamic ranges of at least three orders of magnitude were obtained for the elements studied. In the case of peak height measurements, slopes ranged from 0.98 (Cr) to 1.09 (Se) and yielded correlation coefficients greater than or equal to 0.9991. For peak area measurements, the slopes ranged from 0.95 (Se) to 1.04 (Fe) and yielded correlation coefficients greater than or equal to 0.9992.

Interelement effect studies

The ultimate success or failure of a new analytical approach will greatly depend on its degree of freedom from interelement interactions or interferences. The extent to which several interelement effects occurred under FIA introduction of aqueous solutions into the DIN interface with subsequent ICP-AES quantitation was investigated in a manner similar to experiments described previously (145). In particular, two classic solute vaporization interferences often observed in flame atomization-excitation

Table X. Reproducibility of measured peak heights obtained by FIA-ICP with three types of nebulizers

Element	Analytical Wavelength (nm)	Concentration (ng/mL)	Relative Average Deviation from the Mean (%) Type of Nebulizer			
			Direct Injection	Pneumatic	Ultrasonic[a]	Ultrasonic[b]
As	193.7	1000	0.3	2.4	6.0	—
		100	—	—	—	1.8
Se	196.0	1000	2.1	2.3	1.0	—
		100	—	—	—	2.4
Hg	194.2	1000	1.7	1.2	4.6	—
		100	—	—	—	1.6
Pb	220.4	1000	1.9	2.0	0.7	—
		100	—	—	—	0.5
Cr	205.6	1000	0.7	3.0	—	—
		100	—	—	4.2	—
		10	—	—	—	2.0
Zn	213.9	100	1.5	1.8	2.9	—
		10	—	—	—	0.4
Fe	238.2	100	5.2	4.1	4.6	—
		10	—	—	—	2.0
Cd	214.4	100	0.8	0.3	3.1	—
		10	—	—	—	2.2

Mn	251.6	100	2.3	—	—	—
		10	—	3.2	0.3	—
		1	—	—	—	3.7
Ba	455.4	100	6.9	5.3	—	—

[a]Without aerosol desolvation.

[b]With aerosol desolvation.

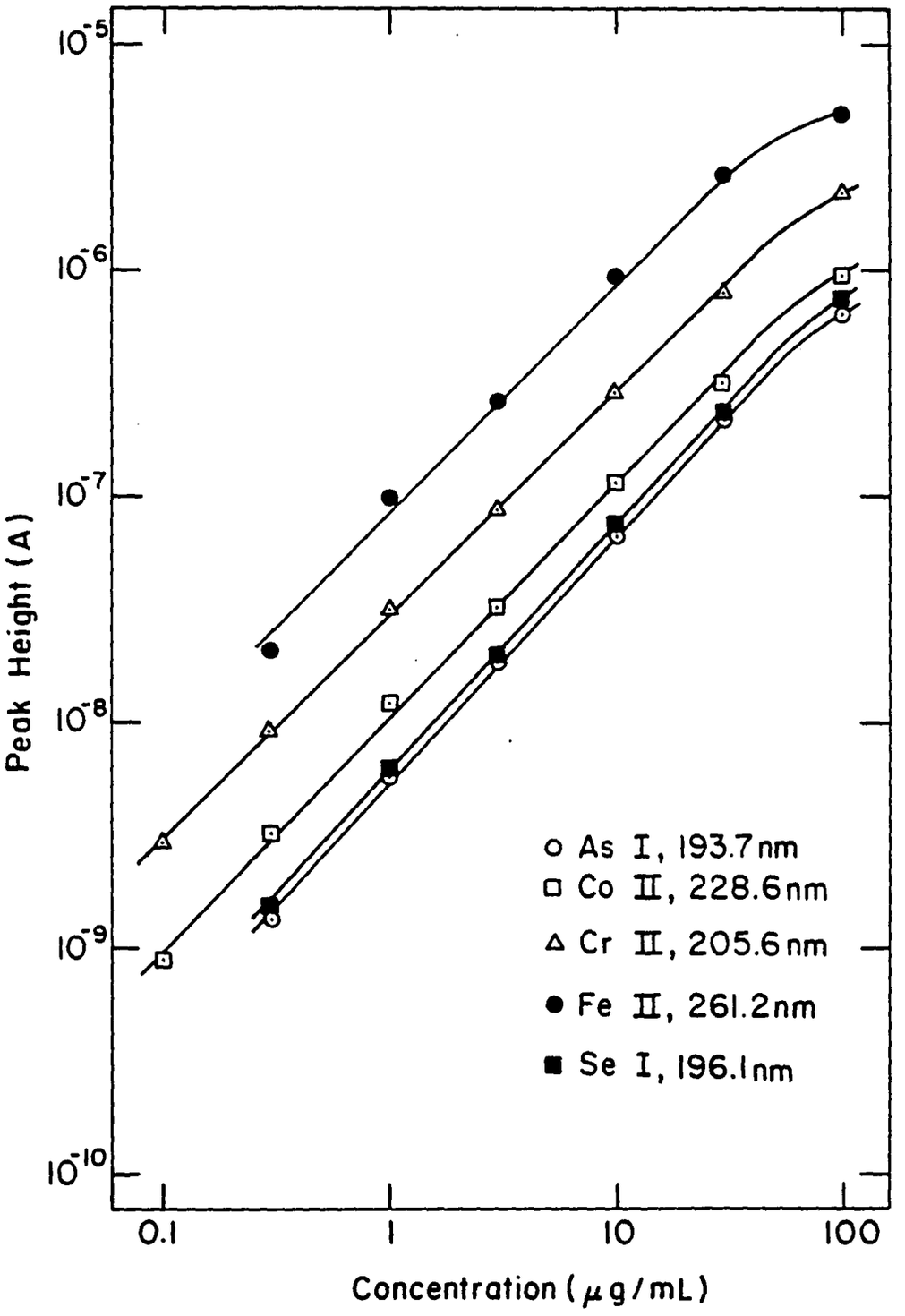

Figure 10. Linear dynamic range: peak height vs. concentration

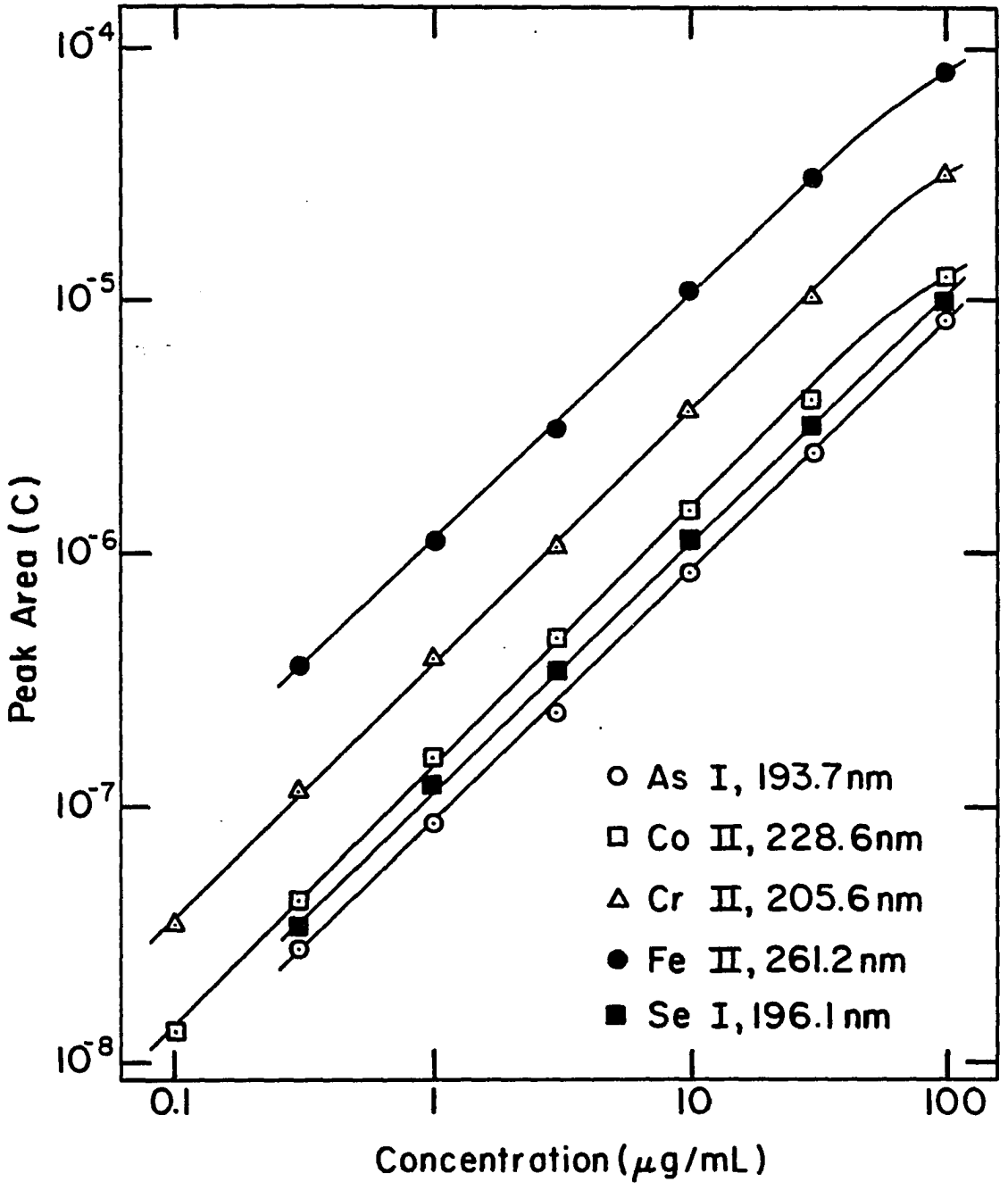

Figure 11. Linear dynamic range: peak area vs. concentration

sources and the interference effects produced by an easily ionizable element were evaluated.

The two most commonly studied solute vaporization interferences are the depression of calcium free-atom emission or absorption by increasing concentrations of PO_4^{3-} or Al^{3+} ions. The Ca-PO_4 solute vaporization interference has been attributed to the formation of a refractory compound, e.g., $Ca_2P_2O_7$ or $Ca_3(PO_4)_2$, whose greater thermal stability leads to a reduced efficiency of free-atom formation (166-168). The suppression of Ca free-atom formation in the presence of increasing concentrations of Al has also been attributed to the formation of refractory compounds ($CaAl_2O_4$, $Ca_3Al_2O_6$, etc.) and to the occlusion of Ca in a refractory aluminum oxide matrix (166,169). The effects of increasing phosphate and aluminum concentrations on Ca emission from a 20 μg/mL (0.5 μmole/mL) Ca reference solution injected into the ICP from the DIN are shown in Figures 12 and 13, respectively. In these and the subsequent figure, the net emission intensities of calcium in the absence of an interferent are normalized to 100 arbitrary units at each observation height. For the DIN, the solute vaporization interferences, to the extent that they are observable are comparable in magnitude to those reported by Larson et al. (145) for conventional cross-flow nebulization. Moreover, the magnitude of the interference effects are small or insignificant for analytically realistic changes in the concentration of concomitants.

The extent to which effects produced by an easily ionizable element (Na) occur under FIA introduction into the DIN interface with subsequent ICP detection were also considered. In particular, the interference

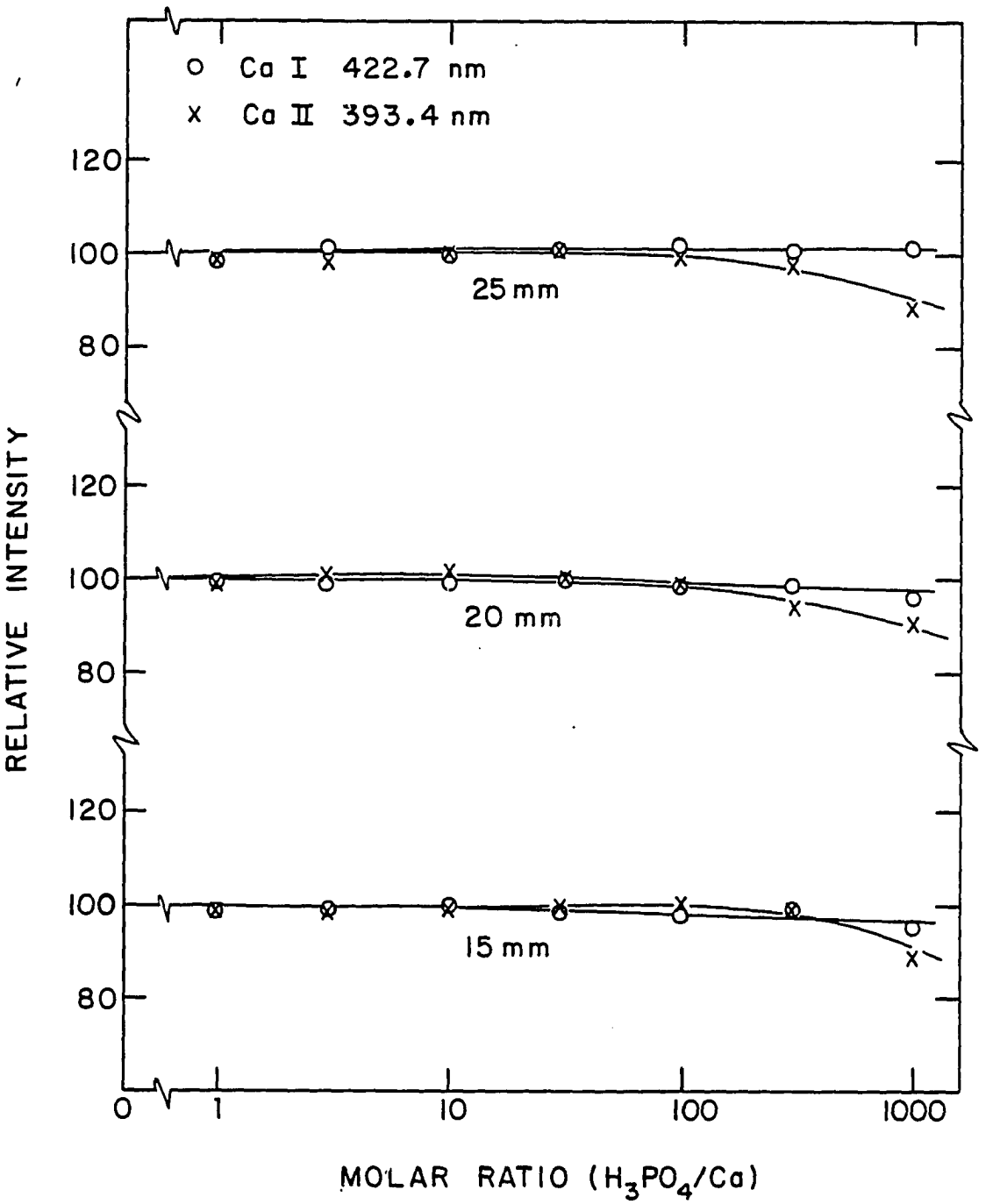

Figure 12. Effect of H_3PO_4 on Ca emission intensity at three heights of observation above load coil (0.5 μmol/mL Ca, 20 μg/mL)

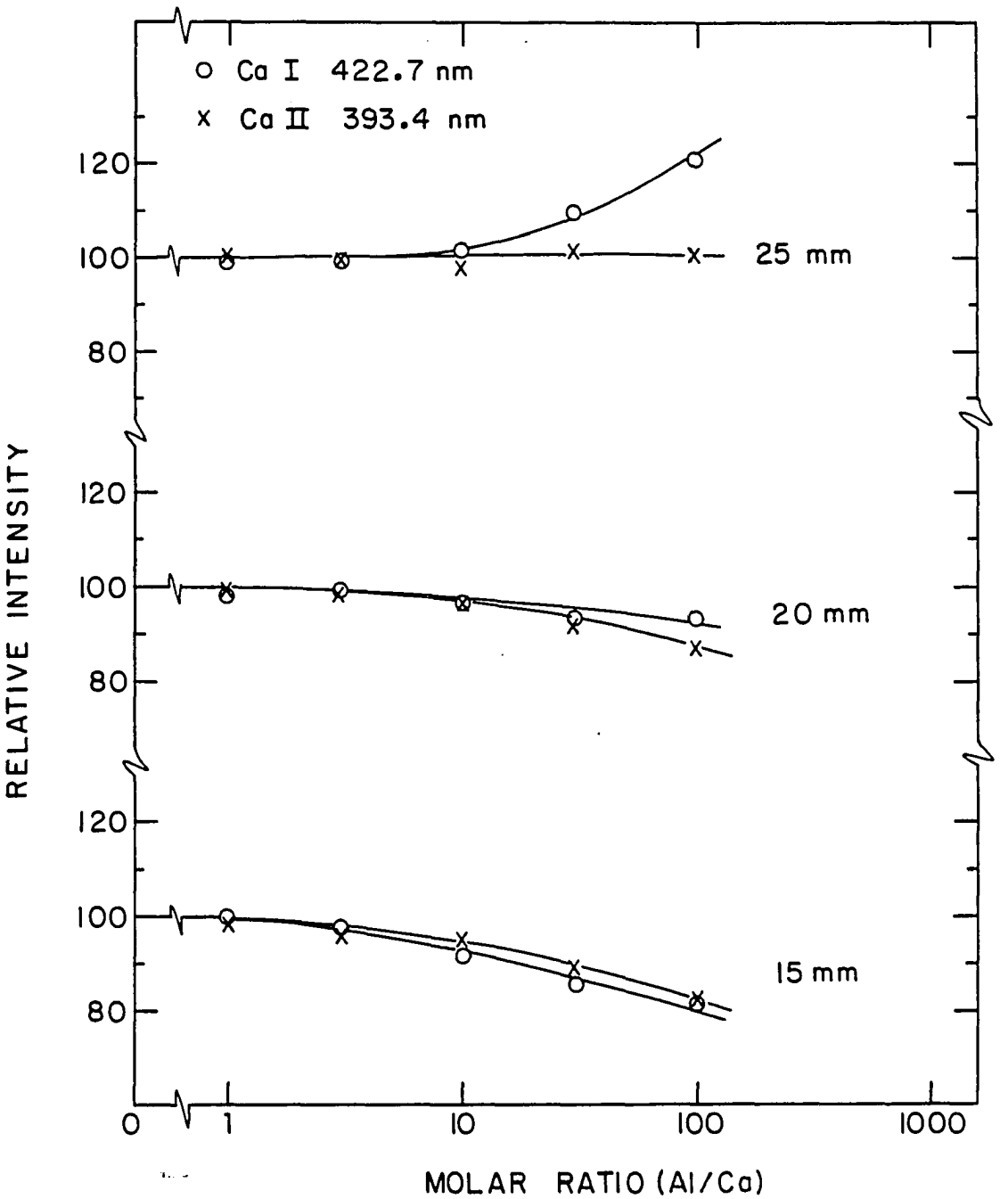

Figure 13. Effect of Al on Ca emission intensity at three heights of observation above load coil (0.5 μmol/mL Ca, 20 μg/mL)

effects produced by concentrations of Na up to 6900 μg/mL (300 μmole/mL) in 20 μg/mL (0.5 μmole/mL) Ca reference solutions on the emission intensities of Ca I and Ca II are shown in Figure 14. The interferences produced by increasing concentrations of Na on both Ca I and Ca II emissions are comparable in magnitude to those reported by Larson et al. (145) for conventional cross-flow nebulization, except for a slight enhancement of Ca free-atom emission at a 15 mm observation height.

Fundamental considerations

Effects of fused-silica, inner capillary tube inside diameter The development of the direct injection nebulizer (DIN) has paralleled advances in gas chromatographic column technology, in that these advances have led to the availability of fused-silica, microbore capillary tubing. The DIN has undergone many stages of development since its initial conception, however, it is worthwhile to summarize only the last four stages, i.e., those involving the variation of the inside diameter (i.d.) of the fused-silica, inner capillary tube. As shown in Table XI, the i.d. of the fused-silica, inner capillary tube dramatically affects the limits of detection obtained with the DIN. The 0.19 mm o.d. x 0.05 mm i.d. fused-silica, inner capillary tube provided the best overall limits of detection. Although a 0.19 mm o.d. x 0.025 mm i.d. fused-silica, inner capillary tube has also been evaluated, the injection of aqueous aerosol into the plasma resulted in unstable plasma operation. If a 120 μL/min liquid carrier stream flow rate is assumed, the linear velocity of the carrier stream as it exits the 0.025 mm i.d. fused-silica, inner capillary tube is increased by a factor of 4 over the 0.05 mm i.d. capillary tube.

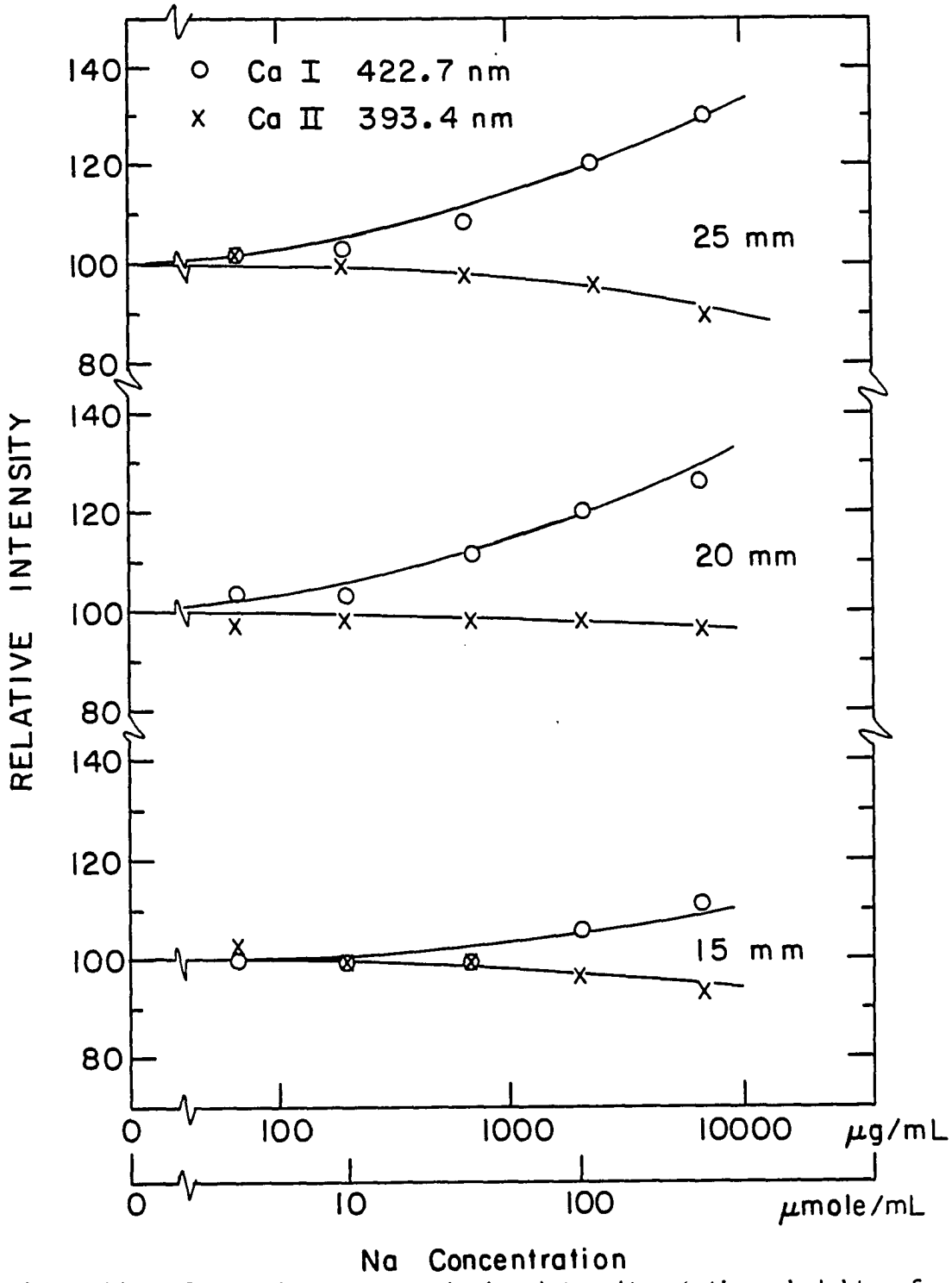

Figure 14. Effect of Na on Ca emission intensity at three heights of observation above load coil (0.5 μmol/mL Ca, 20 μg/mL)

Table XI. Limits of detection (ng/mL) for the DIN with varying inside diameters of the fused-silica, inner capillary tube

Element	Wavelength (nm)	Inner capillary tube inside diameter(μm)		
		150	100	50
As	193.7	240	153	41
Se	196.0	—	203	37
Hg	194.2	—	290	20
Pb	220.4	380	158	28
Cr	205.6	200	18	12
Zn	213.9	—	5	2
Fe	238.2	—	11	1
Cd	214.4	18	8	4
Mn	257.6	2	1	1
Co	238.9	—	19	7

Thus, plasma instability may have resulted because the liquid carrier stream was ineffectively sheared by the argon nebulizer gas.

Aerosol size distribution The physical characteristics of an aerosol droplet are known to influence dramatically both atomization and excitation characteristics in an ICP (86,170). One of the parameters that dictate the efficiency of free-atom formation is the aerosol droplet size distribution (86). In general, small aerosol droplet sizes and narrow aerosol droplet size distributions yield more favorable free-atom formation and subsequent excitation. In this study, the aerosol droplet size produced by the DIN was calculated and determined experimentally using accepted methods.

An established method for the estimation of the Sauter median (volume to surface area ratio) droplet diameter (SMDD) for an aerosol generated from water by concentric, pneumatic nebulization is the equation developed by Nukiyama and Tanasawa (171):

$$d_s = \frac{585}{V}\left(\frac{\sigma}{\rho}\right)^{0.5} + 597\left[\frac{\eta}{(\sigma\rho)^{0.5}}\right]^{0.45}\left[\frac{10^3 Q_l}{Q_g}\right]^{1.5} \qquad [2]$$

where d_s is the Sauter median diameter (μm), V is the velocity difference between the gas and liquid flows to the nebulizer (m/s), σ is the surface tension of the liquid (dyn/cm), ρ is the liquid density (g/cm^3), η is the liquid viscosity (P), and Q_l and Q_g are the volume flow rate of liquid and gas (cm^3/s), respectively (170).

In atomic spectroscopy, the mass median droplet diameter (MMDD) is of most direct relevance to the analytical signal (170). For water, the SMDD and MMDD are nearly equal because the aerosol is composed of spherical particles of unit density. The MMDD for water nebulized using the DIN at

an Ar nebulizer gas flow rate of 0.2 mL/min and a liquid uptake rate of 120 μL/min was calculated to be 50 μm.

The experimental measurement of the aerosol droplet diameter produced by the DIN under identical flow conditions was accomplished using the MgO impression method (172). The merit of this method was later confirmed by Hieftje (173) for the measurement of droplet sizes in a flame.

For the DIN, aerosol droplet impressions were collected on microscope slides that were coated with MgO from burning magnesium ribbon. The microscope slide was passed over the tip of the nebulizer at a position corresponding to an observation height of 18 mm above the load coil. Photomicrographs were made of the aerosol droplet impressions using reflected light, so as to provide more accurate results (173). An average aerosol droplet diameter of 8 μm (±3 μm) was obtained from 5 randomly chosen sets, each set containing more than 15 measurements.

Neither the Nukiyama and Tanasawa equation nor the MgO impression methods are completely adequate for the estimation of the aerosol sizes produced by the DIN. The Nukiyama and Tanasawa equation was developed for a specific concentric nebulizer design and begins to fail as sonic nebulizer gas velocities are approached. The DIN operates at an approximately 10-fold greater nebulizer gas velocity (120 m/s) as compared to conventional pneumatic nebulizers. The MgO method yields reasonable accuracy down to about 10 μm. Below 10 μm, the MgO method is of little value for measurement purposes due to the increased effect of grain size, although droplets down to less than 5 μm can be detected sufficiently at high impact velocities. Because the DIN yields high impact velocities and limits of detection that are comparable to those obtained by pneumatic

nebulizers (where preatomization aerosol sizes are about 1 to 3 μm), it seems logical that the 8 μm ($\pm$3 μm) aerosol droplet size is not too unreasonable.

CHAPTER IV. ANALYTICAL PERFORMANCE ON SAMPLES

The direct injection nebulizer (DIN) was used to analyze a variety of samples materials, not just synthetic mixtures, but also complex sample matrices, such as natural Bourbon vanilla extracts, shale oil process waters, coal extracts, crude oil, coal liquids, and shale oil. The simultaneous, multielement capability of the HPLC-DIN-ICP-AES system for the detection and speciation of inorganic and organometallic compounds is illustrated in the following sections.

Synthetic Mixtures

Arsenic species

Figure 15 shows the As-specific chromatogram resulting from the reverse phase (RP), ion-pairing (IP) separation of an aqueous solution containing 10 μg/mL each of arsenite (AsO_2^-), monomethylarsonic acid (MMAA), dimethylarsinic acid (DMAA), and arsenate ($HAsO_4^{2-}$). The chromatography was performed on a Whatman Partisil 5 ODS 3 column. The aqueous mobile phase contained 5 mM tetrabutylammonium phosphate (TBAP). Peak area measurements indicated that the ICP detector response was approximately equivalent for each of the species studied, in which arsenite constituted 23.2% of the total area; MMAA, 24.9%; DMAA, 26.4%; and arsenate, 25.5%. The signal levels shown in Figure 15 yielded relative limits of detection that ranged from 60 ng/mL (12 ng) as As for MMAA to 100 ng/mL (20 ng) as As for arsenite. These detection limits were based on peak height measurements that gave a signal-to-background scatter ratio of three. The limits of detection obtained by HPLC-DIN-ICP-AES were slightly superior to those of Irgolic (80) in which a detection limit

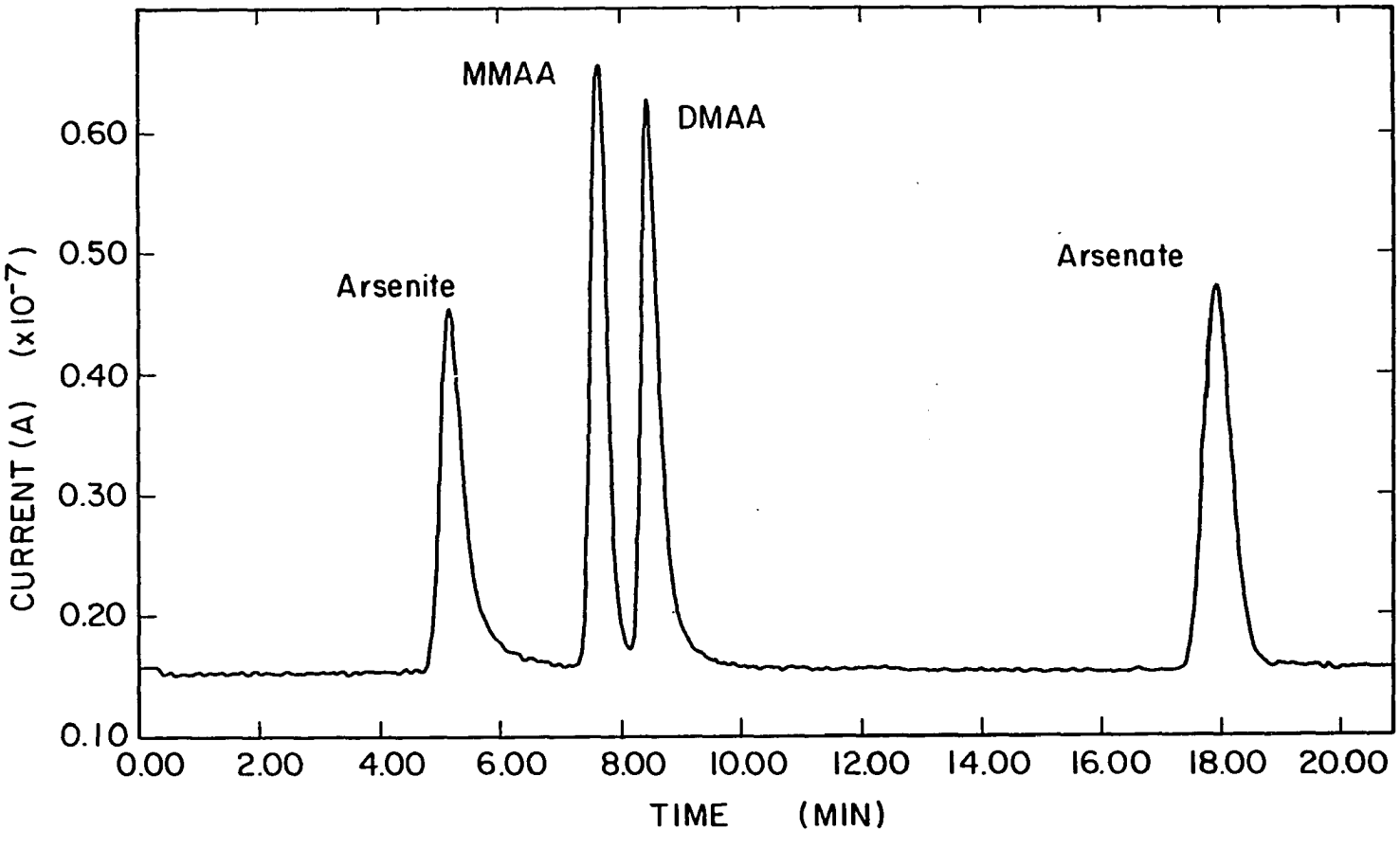

Figure 15. Ion-pairing, reverse-phase separation of 2000 ng each (10 μg/μL) as As of (1) arsenite, (2) monomethylarsonic acid, (3) dimethylarsinic acid, and (4) arsenate Mobile phase: 5mM tetrabutylammonium phosphate in water; column: Whatman Partisil 5 ODS-3 (4.2mm i.d. x 250 mm L); flow rate: 0.75 mL/min (~15% to plasma); sample size: 200 μL; wavelength: 193.7 nm

of 130 ng/mL (13 ng) was estimated, based on a signal-to-background scatter ratio of two from peak area measurements. Three reasons may be cited on why As LODs reported for the DIN were not significantly better, when compared with the HPLC-ICP result reported for conventional pneumatic nebulization. First, as indicated in Chapter III, increased solvent loading of the plasma with the DIN causes some changes in plasma characteristics, particularly a reduction in the excitation temperature attained in the axial channel. The impact of these changes will be considered in Appendix B. Second, the statistical basis for detection limit calculations has a small influence on the LODs reported (Irgolic, 2σ; this work, 3σ). More importantly, however, Irgolic employed a vacuum polychromator system, in which the more intense, 189.0 nm line of As could be monitored. Furthermore, the LOD reported by Irgolic (80) for As employing continuous sample introduction was 15 ng/mL. This means that the LOD reported for HPLC-ICP-AES (130 ng/mL) was inferior by a factor of 8.7 as compared to continuous nebulization. With the DIN, the LODs obtained by HPLC-ICP-AES (60 to 100 ng/mL) are comparable to (within a factor of 2 to 3) the value obtained by continuous nebulization (40 ng/mL). Thus, the DIN interface provided a more highly efficient interface for HPLC coupled to ICP-AES at an easily accessible wavelength (193.7 nm).

Selenium species

The Se-specific chromatogram resulting from the RP, IP separation of a solution containing 3 μg/mL each as Se of selenite (SeO_3^{2-}) and selenate (SeO_4^{2-}) is shown in Figure 16. The chromatography was performed on a Whatman Partisil 5 ODS-3 column. The mobile phase

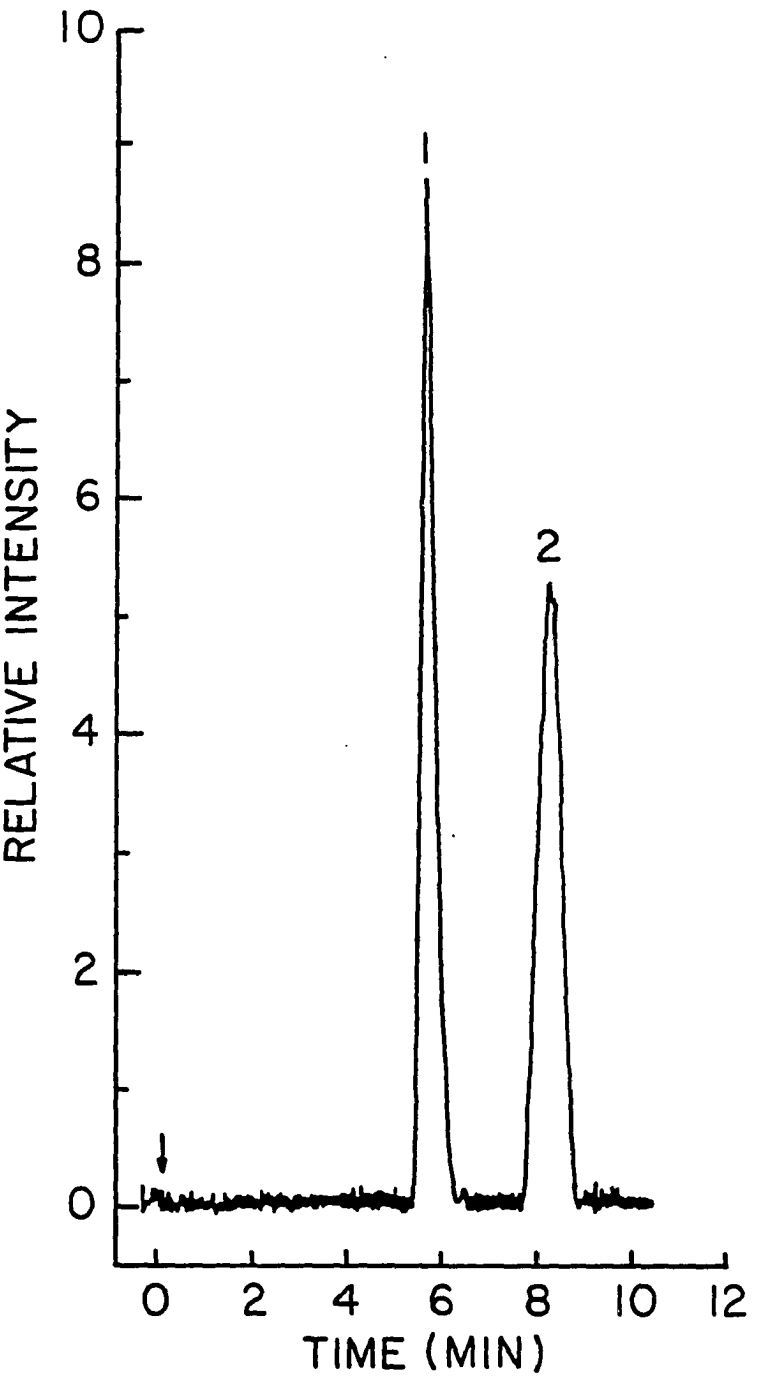

Figure 16. Ion-pairing, reverse-phase separation of 600 ng each (3 $\mu g/\mu L$) as Se of (1) selenite and (2) selenate
Mobile phase: 5mM tetrabutylammonium phosphate in (90/10) water/methanol; column: Whatman Partisil 5 ODS-3 (4.2 mm i.d. x 250 mm L); flow rate: 0.75 mL/min (~15% to plasma); sample size: 200 μL; wavelength: 196.1 nm

consisted of (90/10) water/methanol and contained 5 mM TBAP. The relative limits of detection, based on the same criteria that were used for As speciation studies were determined to be 42 ng/mL (8 ng) and 71 ng/mL (14 ng) for selenite and selenate, respectively. The HPLC-DIN-ICP-AES results are superior by factors of 64 to 167 over the best conventional HPLC-ICP-AES results so far reported for selenite (7000 ng/mL) and selenate (4550 ng/mL) (83). Again, peak area measurements indicated that the ICP detector response was approximately equivalent for each of the species studied, in which selenite constituted 52.7% of the total area and selenate 47.3%.

Chromium species

The Cr-specific chromatogram resulting from the RP, IP separation of a solution containing 1 μg/mL each as Cr of chromate (CrO_4^{2-}) and chromium(III) is shown in Figure 17. The chromatography was performed on a Whatman Partisil 5 ODS-3 column. The mobile phase consisted of (80/20) water/methanol and contained 5 mM sodium n-pentanesulfonate. As it has been difficult to obtain Cr^{3+} in a highly pure form, a limit of detection for chromium of 20 ng/mL (4 ng) was calculated based on Cr^{6+}. Again, the detection limit was calculated from peak height measurements that gave a signal-to-background scatter ratio of three. The HPLC-DIN-ICP-AES result was comparable to the best DCP emission investigations for which the limit of detection for Cr^{6+} was estimated to be 5 to 15 ng/mL (0.5 to 1.5 ng) (59), but markedly superior to the best ICP emission investigations for which the limit of detection for Cr^{6+} was estimated to be 450,000 ng/mL! The competitive LOD reported for Cr^{6+} by HPLC-DCP was attributed to a more efficient nebulizer-interface arrangement for the DCP (59),

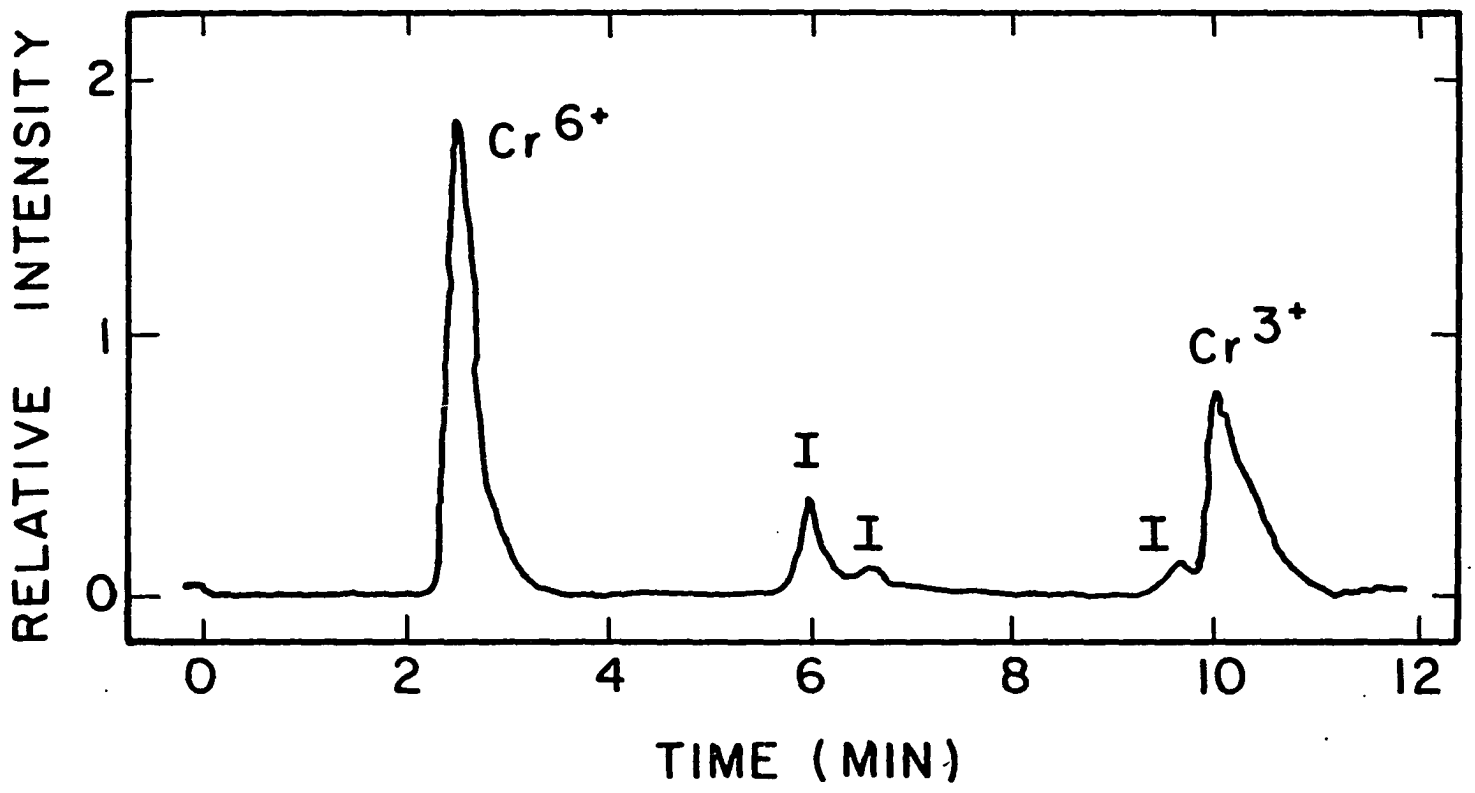

Figure 17. Ion-pairing, reverse phase separation of 200 ng each (1 μg/μL) as Cr of (1) Cr(VI) and (2) Cr(III)
Mobile phase: 5 mM sodium n-pentanesulfonate in (80/20) water/methanol; column: Whatman Partisil 5 ODS-3 (4.2 mm i.d. x 250 mm L); flow rate: 1 mL/min (~15% to plasma); sample size: 200 μL; wavelength: 205.6 nm; I = impurity peak

however, this is the only case in which the LODs obtained by HPLC-DCP-AES were comparable to those obtained by HPLC-DIN-ICP-AES.

Cr species in "pure" Cr salts

Element specific detection is also useful for the determination of species purity in "pure" materials. The Cr-specific chromatogram illustrated in Figure 18 revealed the impurities contained in four sources of chromium(III). Even an ultrapure source of chromium(III) chloride (99.998%, metals basis) exhibited two very distinct species impurity peaks. To date, the detection limit for chromium(III) has not been determined as it has been difficult to obtain chromium(III) in a highly pure form.

Sulfur species

The S-specific chromatogram resulting from the RP, IP separation of a solution containing 10 μg/mL each as S of sulfite, sulfate, and thiosulfate is shown in Figure 19. The chromatography was performed on a Whatman Partisil 5 ODS-3 column. The mobile phase consisted of (95/5) water/methanol and contained 5 mM TBAP. Sulfite was rapidly converted to sulfate as verified from peak area measurements in which sulfite constitutes 9.5% of the total area; sulfite + sulfate, 57.9%; and thiosulfate, 32.6%. The sum of the peak areas contributed by the sulfite peak and sulfite + sulfate peak represent 67.4% (~two-thirds) of the total area. The broad "peak" observed early in the chromatogram was baseline drift that resulted from a matrix mismatch between the mobile phase and injected sample. A limit of detection for sulfur was determined to be 164 ng/mL (16.4 ng) based on the thiosulfate peak and multiple (3) injections of a solution containing 10 ng/mL as S of sulfate only. Again, the HPLC-

Figure 18. Ion-pairing, reverse-phase separation of the impurities contained in four sources of chromium(III) [A] $CrCl_3 \cdot 6H_2O$, Source #1 (Lot #1); [B] $CrCl_3 \cdot 6H_2O$, Source #1 (Lot#2); [C] $Cr(OAc)_3 \cdot H_2O$; and [D] $CrCl_3 \cdot 6H_2O$, "Ultrapure" Mobile phase: 5mM sodium n-pentanesulfonate in (80/20) water/methanol; column: Whatman Partisil 5 ODS-3 (4.2 mm i.d. x 250 mm L); flow rate: 0.70 mL/min (~15% to plasma); sample size: 200 μL; wavelength: 205.6 nm

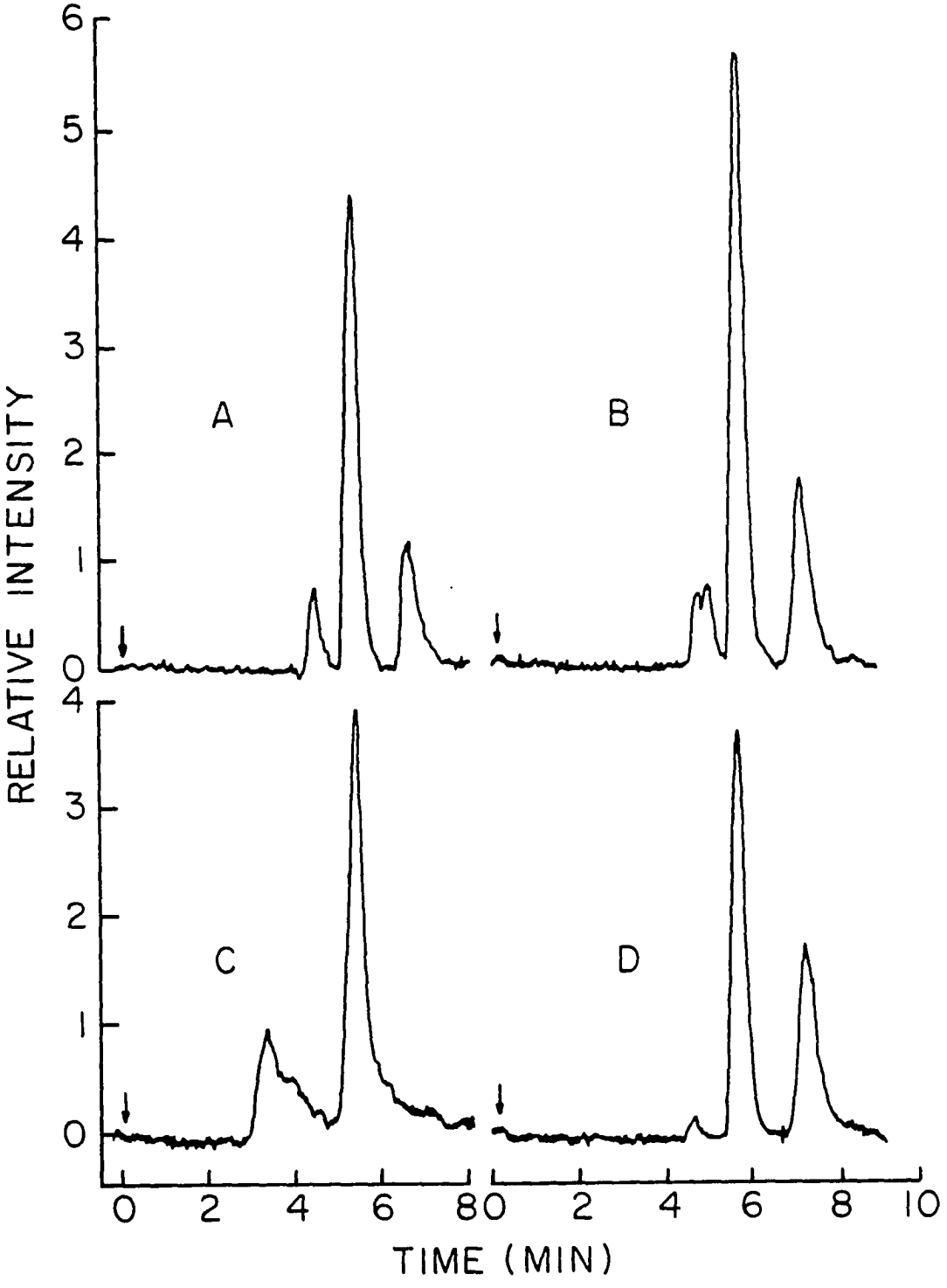
RELATIVE INTENSITY
A
B
C
D
TIME (MIN)

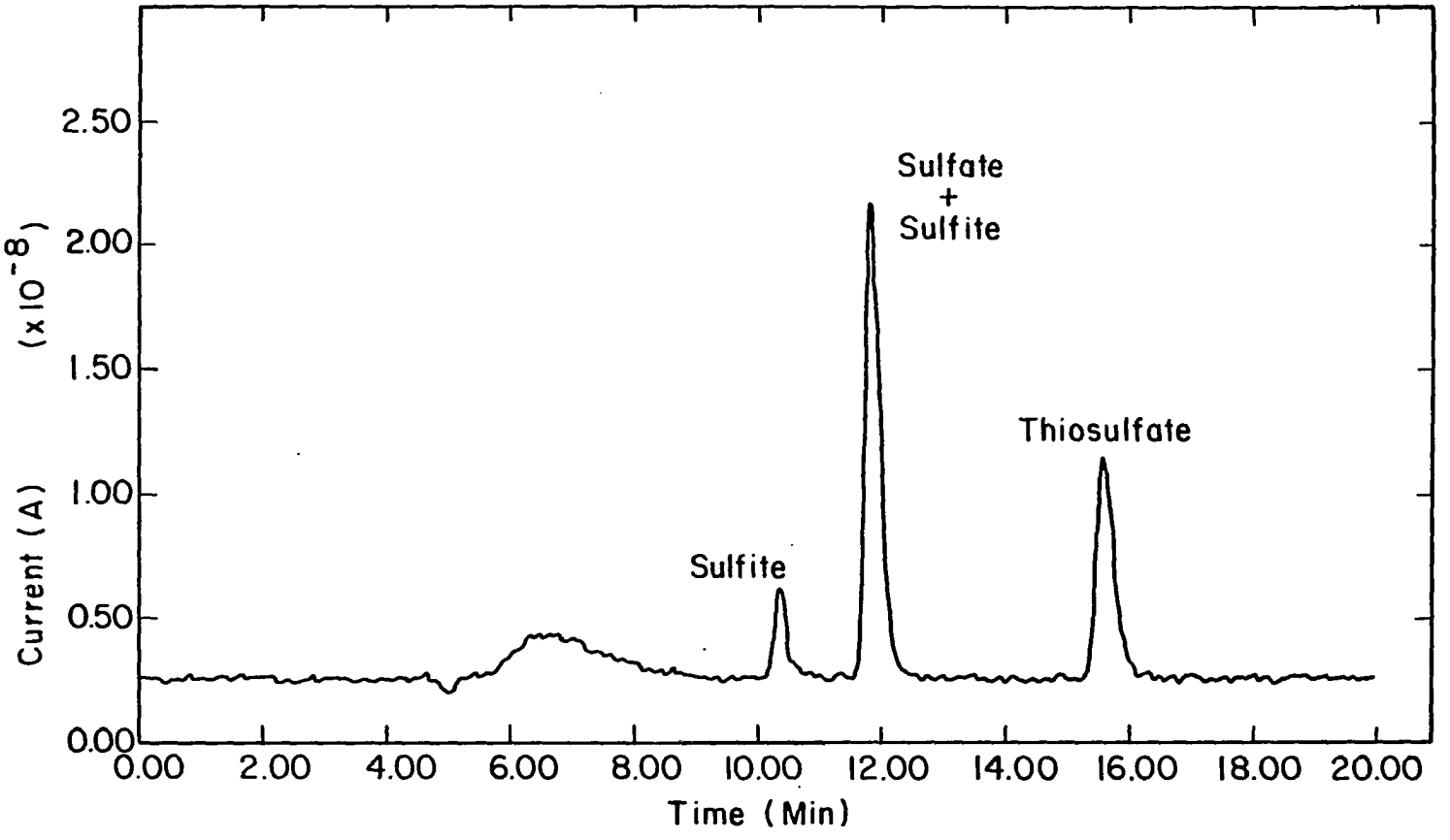

Figure 19. Ion-pairing, reverse-phase, chromatogram of several S containing anions at 10 μg/mL each as S
Mobile phase: 5 mM tetrabutylammonium phosphate in (95/5) water/methanol; column: Whatman Partisil 5 ODS-3 (4.2 mm i.d. x 250 mm L); flow rate: 0.7 mL/min (~15% to plasma); sample size: 100 μL; wavelength: 182.0 nm (Ar purge)

DIN-ICP-AES result was markedly superior to the best ICP emission investigations for which the LOD for S was reported to be 1000 to 3000 ng/mL (82).

Simultaneous multielement detection

An example of the chromatographic output from the simultaneous, multielement, data-aquisition system is illustrated in Figure 20 for the separation of a solution containing As, Se, and Cr ions. The concentration of each elemental species in solution was 10 μg/mL. The chromatography was performed on a Whatman Partisil 5 ODS-3 column. The mobile phase consisted of (95/5) water/methanol and contained 5 mM TBAP. For the As-specific chromatogram, relative limits of detection ranged from 56 ng/ml (11.2 ng) as As for MMAA to 98 ng/mL (19.6 ng) as As for arsenite. Peak area measurements indicated that the ICP detector response was approximately equivalent for each of the species studied, in which arsenite constituted 23.8% of the total area; MMAA, 25.3%; DMAA, 25.7%; and arsenate, 25.2%. For the Se-specific chromatogram, relative limits of detection were 23 ng/mL (4.6 ng) as Se for selenite and 42 ng/mL (8.4 ng) as Se for selenate. Again, peak area measurements indicated that the ICP detector response was approximately equivalent for selenite (47.1%) and selenate (50.7%). The impurity peak constituted 2.2% of the total peak area and was only present in the solution containing selenite. Detection limits were not calculated for Cr, as the separation of the Cr species is more effectively carried out using the sodium n-pentanesulfonate, ion-pairing reagent (Figure 17). The LODs obtained for As and Se species with simultaneous multielement detection were comparable to those obtained in the single channel mode.

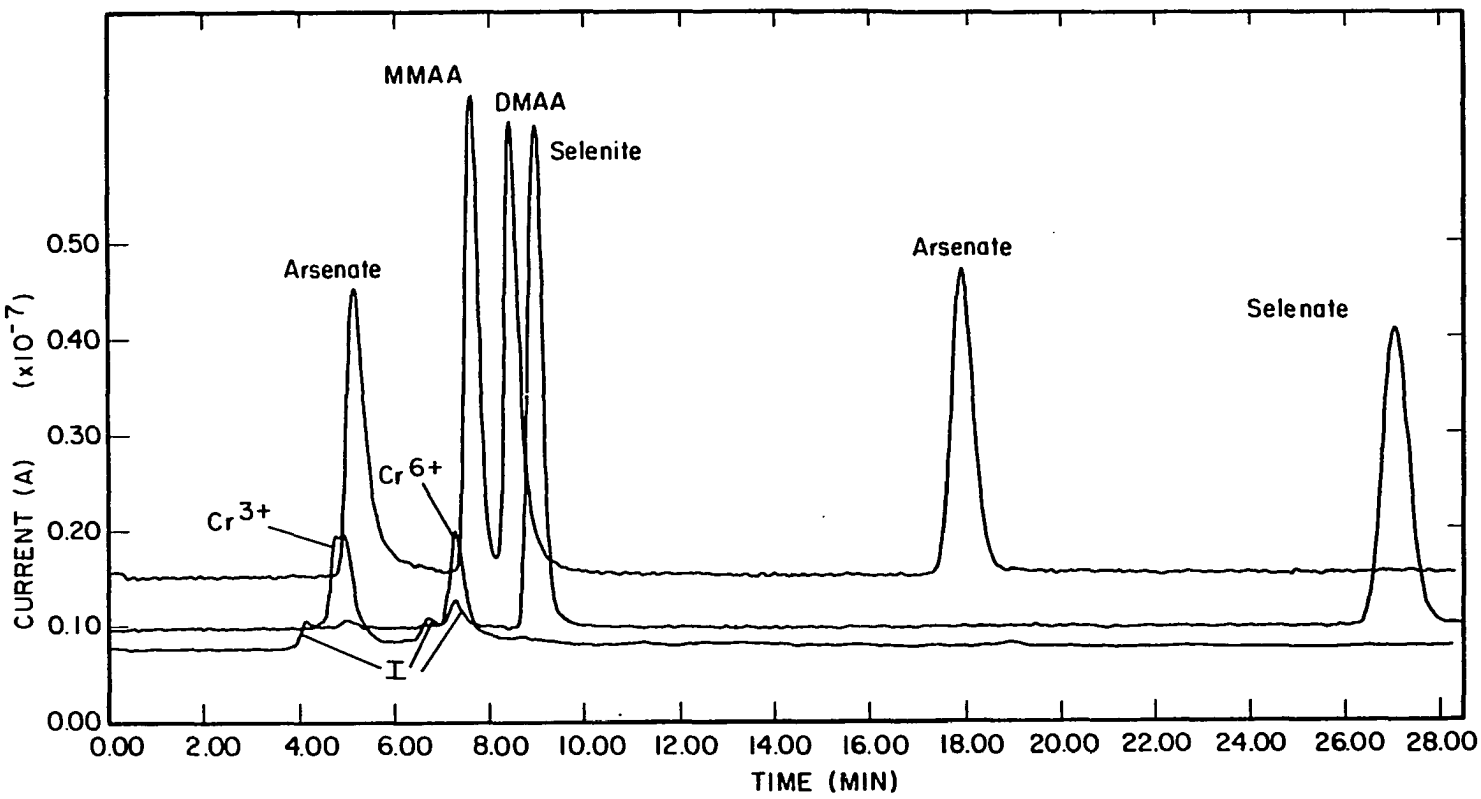

Figure 20. Ion-pairing, reverse-phase, simultaneous, multielement chromatogram of several As, Se, and Cr containing ions; 10 μg/mL each as As, Se, or Cr
Mobile phase: 5 mM tetrabutylammonium phosphate in (95/5) water/methanol; column: Whatman Partisil 5 ODS 3 (4.2 mm i.d. x 250 mm L); flow rate: 0.70 mL/min (~15% to plasma); sample size: 200 μL; wavelength: As, 193.7 nm; Se, 196.0 nm; Cr, 205.6 nm; I = impurity peak

Bourbon Vanilla Extract Analyses

Recently, the importation of Bourbon vanilla extracts that have been adulterated with synthetic vanillin has posed a problem in the food industry. In this study, FIA-DIN-ICP-AES and HPLC-DIN-ICP-AES were utilized for the indirect detection of synthetic vanillin in natural Bourbon vanilla extracts. The extracts studied consisted of a natural Bourbon vanilla extract that was concentrated 3 1/2-fold in (30/70) ethanol/water and the same extract, adulterated with synthetic vanillin (McCormick and Co., Inc.)

Elemental analysis

Reference solutions containing 100, 30, 10, 3, 1, and 0 μg/mL of As, Se, Cr, Zn, Pb, Cd, Co, Ni, Fe, Cu, Mn, Ca, and Sr were prepared in a (30/70) ethanol/water matrix. The "standard addition" method of analysis was used to quantitate the various elemental concentrations in the two vanilla extracts, whereby exactly 50 μL of a given reference solution was added to 450 μL of each vanilla extract sample. The spiked vanilla extracts were subjected to FIA-DIN-ICP-AES analysis under operating conditions described in Chapter II. The results of this study are given in Table XII. As no element provided a good "marker" for the differentiation of the two vanilla extracts, further analysis was required.

HPLC-DIN-ICP-AES analysis

As a starting point, the ultraviolet (UV) absorption chromatogram (254 nm) of the pure and adulterated Bourbon vanilla extracts were obtained as shown in Figure 21. As can be seen, the chromatograms were

Table XII. Elemental concentrations in two Bourbon vanilla extracts (μg/mL)

Element	Pure	Adulterated
As	1.6	1.6
Se	0.91	0.92
Cr	0.064	0.069
Zn	2.9	2.9
Pb	1.3	0.83
Cd	0.053	0.008
Co	0.076	0.058
Ni	0.28	0.20
Fe	0.96	1.0
Cu	0.34	0.34
Mn	26	26
Ca	263	147
Sr	3.2	3.5

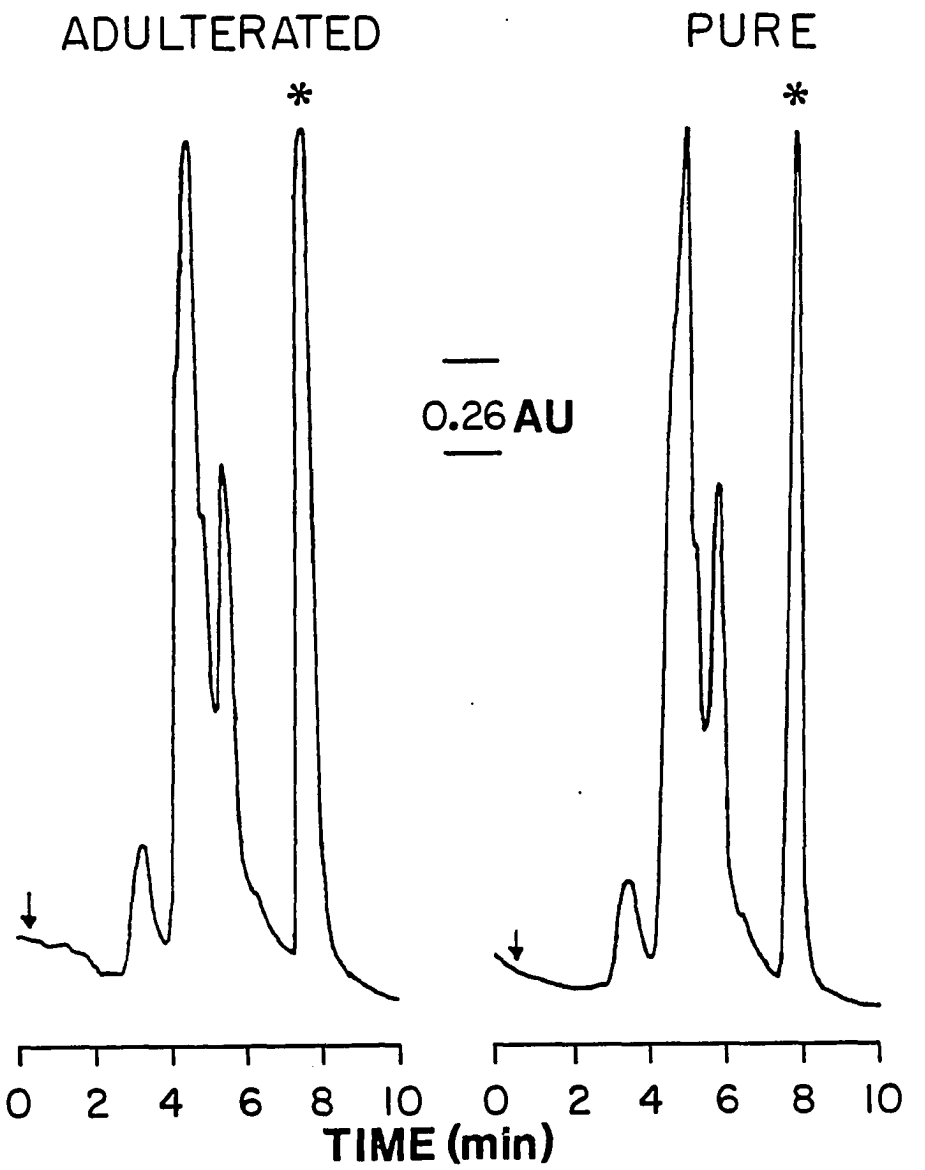

Figure 21. UV absorption (254 nm) chromatograms of an adulterated and pure natural Bourbon vanilla extract
Mobile phase: (30/70) ethanol/water; column: Whatman Partisil 5 ODS-3 (4.2 mm i.d. x 250 mm L); flow rate: 0.7 mL/min; sample size: 5 μL (Asterisk indicates vanillin peak)

virtually identical. The vanillin peak was identified by spiking the sample with synthetic vanillin (McCormick and Co., Inc.).

Element-specific, multielement chromatograms were recorded for each of the two vanilla extracts under identical spectroscopic and chromatographic conditions, employing the HPLC-DIN-ICP-AES system. The most interesting results are shown in Figure 22 where it can be seen that the vanillin present in the adulterated sample appears to form a relatively strong complex with Cu and Fe. In addition, the peak eluting at a retention time of about 3 minutes was present in the chromatogram of the adulterated vanilla extract for several metals (Cu, Fe, Ni, and Co), but was absent in the chromatogram of the pure vanilla extract. The presence of the Cu-, and Fe-vanillin complex appears to be a definite means of verifying the presence of synthetic vanillin in the natural vanilla extracts.

Energy-related Materials

The speciation of organically bound metals in energy-related materials presents a real challenge. Although detectable levels of known and suspected carcinogens have been identified in a variety of energy-related materials, little attention has been focused on inorganic contaminants that may also pose health hazards. Many elements such as As, Cu, Fe, and Se, can exist in environmental matrices in more than one valence state. As the biological activity of such elements is highly dependent on their chemical form, speciation is an important issue. For example, epidemologic data appear to indicate that inorganic As(III) compounds represent a greater carcinogenic hazard than As(V) (174,175). Clearly, however, the speciation of organometallic compounds is not only

Figure 22. HPLC-DIN-ICP-AES element-specific chromatograms of an adulterated and pure natural Bourbon vanilla extract
Mobile phase: (30/70) ethanol/water; column: Whatman Partisil 5 ODS-3 (4.2 mm i.d. x 250 mm L); flow rate: 0.7 mL/min; sample size: 100 μL (asterisk indicates metallo-vanillin complex)

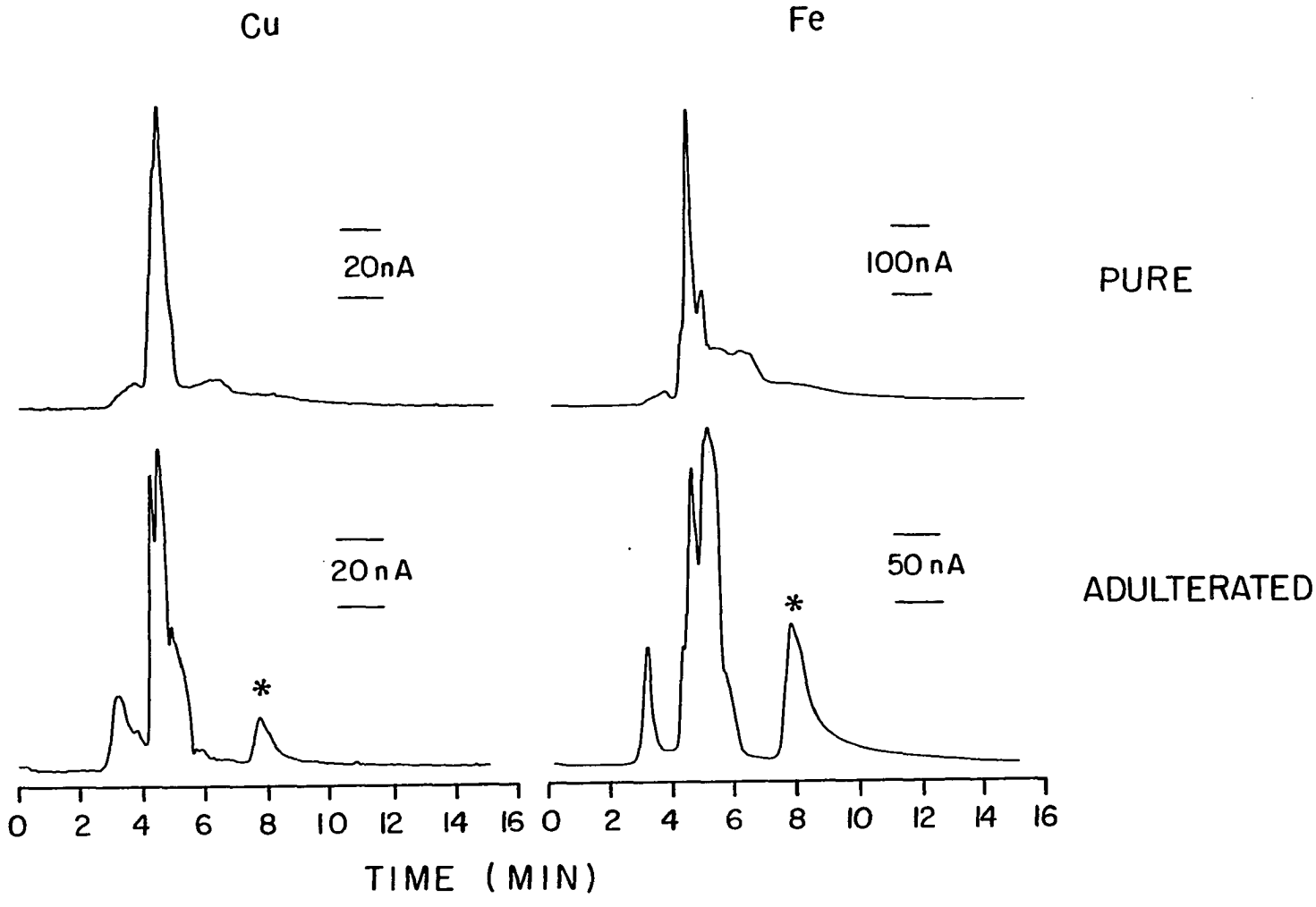
Cu
Fe
20nA
100nA
PURE
20nA
50nA
ADULTERATED
*
*
0 2 4 6 8 10 12 14 16
0 2 4 6 8 10 12 14 16
TIME (MIN)

relevant with regard to our health and environment. The nature of the metals and their abundance reveals important information as to the origin, migration, and maturation of the energy-related material, and provides a basis for geochemical prospecting (176). In addition, metal containing compounds hold the key to industrial processing because: 1) metals can exhibit catalytic effects; and 2) refining and upgrading must involve the use of catalysts that can be poisoned by the metals (177).

Fossil fuels are produced by the gradual decomposition of organic materials and residues over millions of years (178). Although petroleum has been the predominant energy resource, recent speculation as to its future availability has led to the investigation of alternative energy sources such as shale oil, coal liquifaction products, and oil products from tar sands. These materials are predominantly composed of hydrocarbon compounds contaminated with S, N, and O heterocyclic compounds, high molecular weight asphaltic molecules, minerals such as silica, and metal containing compounds (177) and are invariably complex. Very little data have been reported for the speciation of metals in energy-related materials, presumably because of the lack of suitable metal-specific detectors for liquid chromatography. In addition, the separation of chelated or complexed metals is complicated because the ligands are often completely compatible with the oil matrix.

The applicability of the ICP as a multielement, element-specific detector for HPLC effluents from energy-related materials such as shale oil, shale oil process water, crude oil, and SRC II was investigated. The results of this study were very encouraging and are presented in the following sections.

Shale oil process waters

Shale oil is recovered from oil shale kerogen during a controlled pyrolysis at 500°C employing both surface and in situ technologies. Shale oil process water typically originates from mineral dehydration, combustion products, ground water seepage, and from steam or vapor condensates that accumulate during the recovery of shale oil (179). Because the waters are intimately associated with the shale oil, the process waters contain a variety of trace metals, some of which are potentially toxic in certain forms (180). In this investigation, a shale oil process water from a simulated in situ process (Run #17,Oak Ridge National Laboratory) and a Paraho shale oil process water (Green River Formation, CO) were examined. These samples were warmed to room temperature, filtered (0.45 μm, Spartan-3) and directly subjected to FIA-DIN and HPLC-DIN analysis with ICP-AES detection.

Elemental analysis The elemental concentrations in the two shale oil process waters were first determined by FIA-DIN-ICP-AES using the "standard addition" method. Exactly 900 μL of the filtered process water was spiked with 100 μL of the appropriate reference solutions. The signals produced by three, 20 μL injections were recorded for each spiked sample and the elemental concentrations determined by extrapolation of the peak area measurements to zero. The elemental concentrations are summarized in Table XIII for the two process waters, and compared to one set of literature values (181). In view of the variability of shale oil process water from different sites and the differing characteristics of different retort processes, meaningful comparisons cannot be drawn. The

Table XIII. Elemental concentrations in two shale oil process waters (μg/mL)

Element	Paraho	ORNL	Literature[a]
As	4.7	3.9	5.00±0.04
Se	0.43	0.37	0.86±0.22
Cr	0.27	0.10	<0.02
Fe	1.5	0.64	<1
Cd	<0.004	0.033	—
Co	0.23	0.93	0.65±(0.004)
Cu	0.13	0.059	—
Ni	1.9	1.9	—
Zn	0.38	0.37	2.70±0.08
Hg	0.10	0.09	0.2±0.03

[a]Reference 181, Piceance Creek basin

values simply provide an insight on the range of concentrations normally encountered.

HPLC-DIN-ICP-AES analysis Simultaneous multielement chromatograms on the ORNL and Paraho shale oil process waters are shown in Figures 23 and 24 for the ten elements studied. The separations were obtained on a Whatman Partisil 5 ODS-3 column. Two-hundred microliters of the filtered shale oil process water was injected directly on the column. The mobile phase contained 5 mM TBAP in water. As verified by Figure 23, arsenite, monomethylarsonic acid (MMAA), arsenate, selenite, and Cr(III) were identified in the ORNL shale oil process water. The Se species that eluted at a retention time of about 10 minutes was not identified, but is likely to be neutral, or anionic in nature. All other metallic elements detected have very similar retention times. It is speculated that these metallic elements are cationic in nature, presumably paired with anions such as sulfate or chloride. In the Paraho shale oil process water, arsenite, arsenate, selenite, and Cr(III) were identified. The Se (~11 min) and Cr (~17.5 min) species were not identified, but are likely neutral or anionic in nature. Again, because of similar retention times, it is speculated that the other metallic elements are cationic in nature, presumably paired with anions such as sulfate or chloride. In both process waters, arsenate comprised about 72% of the total arsenic. The results agree well with Fish et al. (179) who clearly demonstrated that each process water had a distinctive As "fingerprint" and that substantial but variable quantities of arsenate, MMAA, and phenylarsonic acid were present. The speciation of elements other than As in shale oil process waters has not been reported in the literature.

Figure 23. HPLC-DIN-ICP-AES element-specific chromatograms of an ORNL shale oil process water (Simulated in situ Process Run: #17) Mobile phase: 5 mM tetrabutylammonium phosphate in (95/5) water/methanol; column: Whatman Partisil 5 ODS-3 (4.2 mm i.d. x 250 mm L); flow rate: 0.7 mL/min (~15% to plasma); sample size: 200 μL; (1) arsenite, (2) MMAA, (3) arsenate, (4) selenite, (5) unknown, and (6) Cr(III)

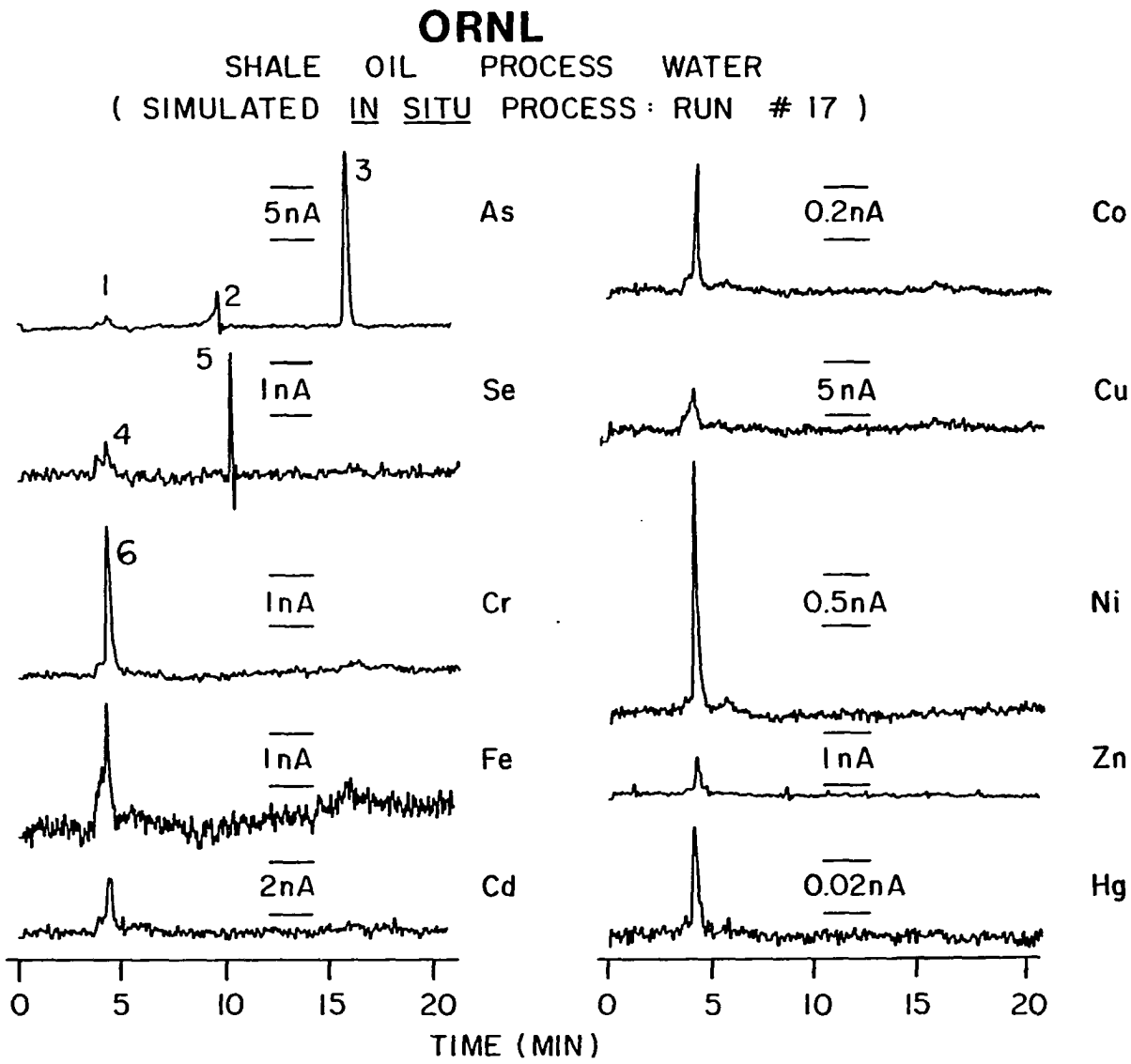
ORNL
SHALE OIL PROCESS WATER
(SIMULATED IN SITU PROCESS : RUN # 17)
1
2
3
4
5
6
5nA
As
0.2nA
Co
1nA
Se
5nA
Cu
1nA
Cr
0.5nA
Ni
1nA
Fe
1nA
Zn
2nA
Cd
0.02nA
Hg
0
5
10
15
20
TIME (MIN)

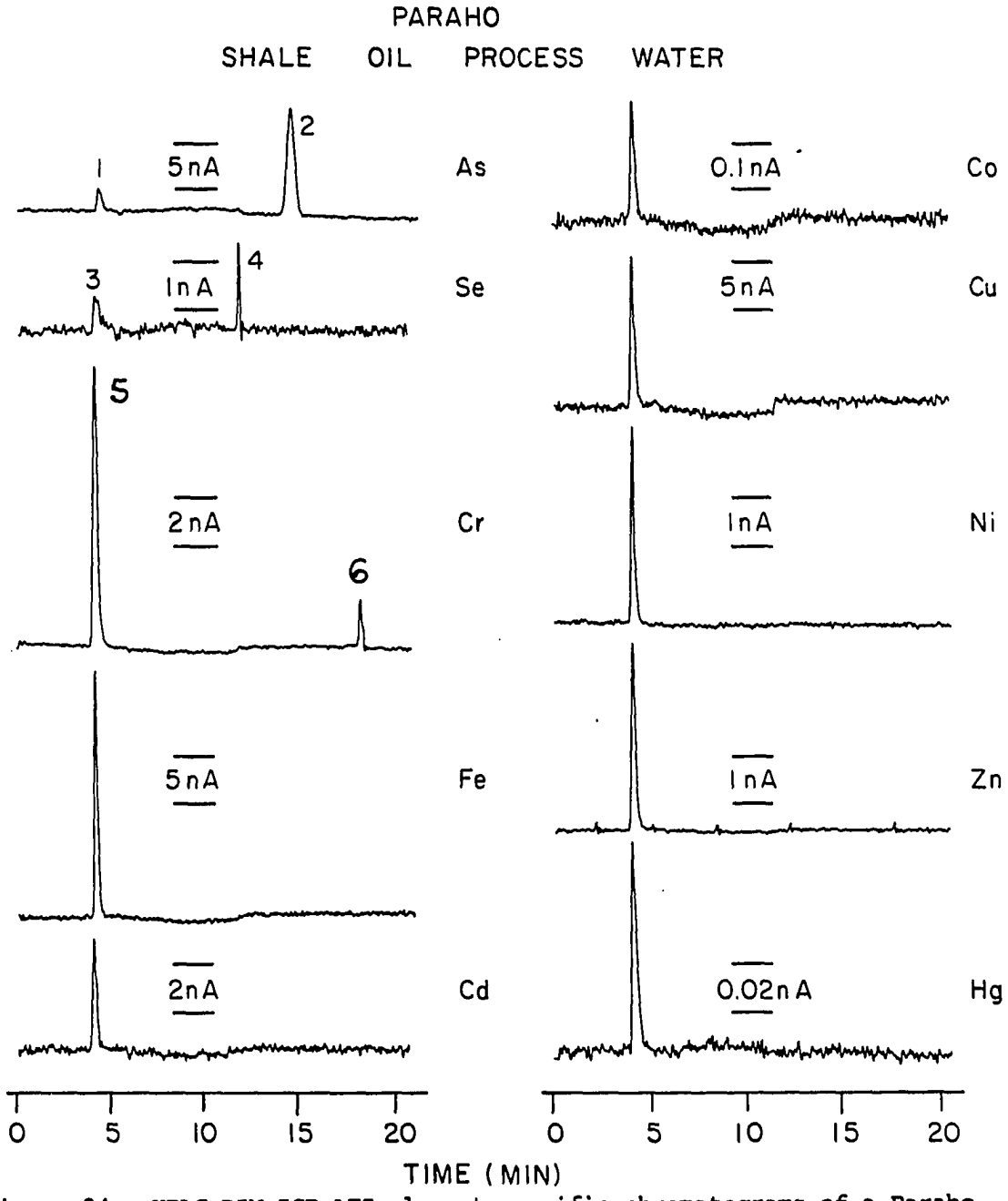

Figure 24. HPLC-DIN-ICP-AES element-specific chromatograms of a Paraho shale oil process water
Mobile phase: 5 mM tetrabutylammonium phosphate in (95/5) water/methanol; column: Whatman Partisil 5 ODS-3 (4.2 mm i.d. x 250 mm L); flow rate: 0.7 mL/min (~15% to plasma); sample size: 200 μL; (1) arsenite, (2) arsenate, (3) selenite, (4) unknown, (5) Cr(III), and (6) unknown

Coal liquifaction products

Coal describes a large range of fossil fuels derived from partial degradation of plants. Although coal has provided a steady source of energy for decades, there has been much concern over pollution caused by its combustion products. Emissions from coal combustion include sulfur oxides, carbon monoxide, hydrocarbons, nitrogen oxides, and aldehydes, as well as trace elements (e.g., Pb, Cd, and Se) that are emitted with particulate matter or fly ash. As a significant fraction of sulfur is converted to SO_2 during combustion, it is desirable to remove the sulfur from the coal. In high sulfur coal (3 to 6%) a large fraction of the sulfur may be present as mineral sulfides. As the sulfides are much more dense that the coal, they can be removed by mechanical means. In most coals, however, approximately half of the sulfur is in organic form and is an integral part of the coal matrix. The removal of organic sulfur is more difficult and requires chemical conversion processes such as the Gravimelt process (182-184).

For the present investigation, a sample of coal (Charming Creek, New Zealand) was cleaned by the Gravimelt process to yield a low ash, low sulfur product, plus three process streams that contained the materials removed from the coal. These process streams consisted of a spent caustic that was separated from the cleaned coal (PS-1), water washings of the separated coal (PS-2), and acid washings of the water washed, cleaned coal (PS-3). Methanol soluble and acid soluble fractions isolated from the PS-1 process stream were subjected to HPLC-DIN-ICP-AES analysis.

The procedures used for the isolation of the methanol and acid soluble fractions from the PS-1 process stream are summarized in Figure 25. The PS-1 process stream was acidified the pH 1.2 with HCl and a precipitate formed. The precipitate (arbitrarily designated humic-like materials) was separated by filtration through a Whatman #40 filter paper and the filtrate was removed for further separation. The precipitate collected on the filter paper was washed with methanol yielding the methanol soluble fraction. The filtrate from the precipitation of the humic-like organic materials was extracted with n-butanol to recover the phenolic-like materials. This extract was concentrated by evaporation and back-extracted to yield the acid (HCl) soluble fraction. The acid soluble fraction was evaporated to dryness on a hot plate under a stream of nitrogen. For HPLC studies, approximately 0.1 g of each the acid soluble or methanol soluble fraction was dissolved in the (90/10) methanol/water mobile phase.

The UV absorption (254 nm) and ICP-AES sulfur-specific (182.0 nm) chromatograms of the acid soluble and methanol soluble fractions of the Charming Creek coal are compared in Figures 26 and 27, respectively. Specific chromatographic conditions are given with each figure. Comparison of the UV and S-specific chromatograms revealed that the chromatograms were structurally very similar, however, the UV absorption chromatogram was far less specific. Peaks 1 through 4 in the S-specific chromatograms were reproducible. In Figure 26, the shoulders on the right and left side of peak 2 were reproducible. Peak 4 exhibited little absorption in the UV (254 nm), but was apparently rich in sulfur.

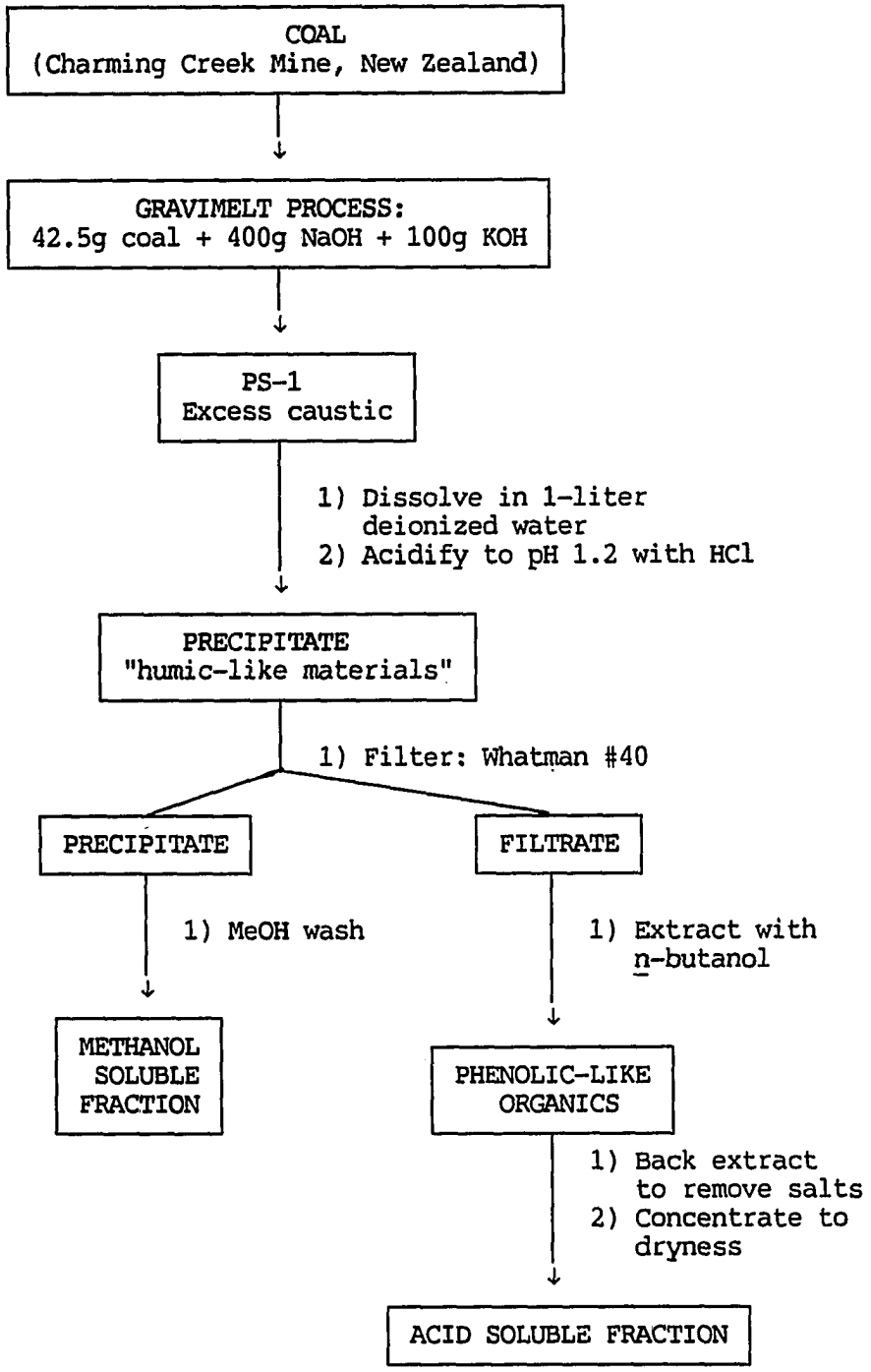

Figure 25. Separation scheme for Charming Creek coal samples

Figure 26. Chromatograms of the acid soluble fraction of a Charming Creek coal
[A] UV absorption (254 nm) and [B] ICP, sulfur-specific (182.0 nm)
Mobile phase: (90/10) methanol/water; column: Whatman Partisil 5 ODS-3 (4.2 mm i.d. x 250 mm L); flow rate: 0.75 mL/min (for [B], ~15% to plasma); sample size: 5 μL for [A], 100 μL for [B]

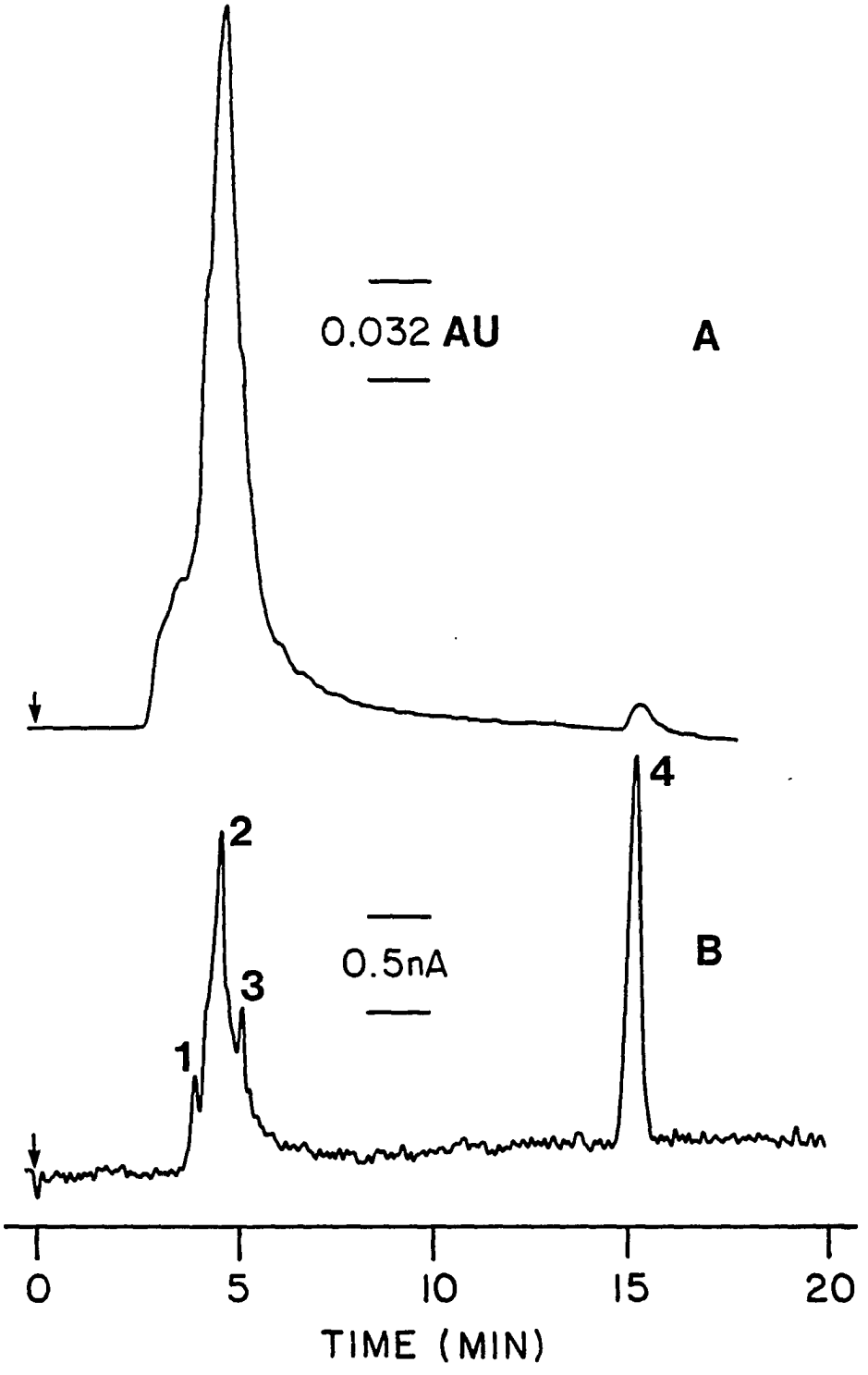
0.032 AU
A
4
2
0.5nA
B
3
1
0
5
10
15
20
TIME (MIN)

Figure 27. Chromatograms of the methanol soluble fraction of a Charming Creek coal
[A] UV absorption (254 nm) and [B] ICP, sulfur-specific (182.0 nm)
Mobile phase: (90/10) methanol/water; column: Whatman Partisil 5 ODS-3 (4.2 mm i.d. x 250 mm L); flow rate: 0.75 mL/min (for [B], ~15% to plasma); sample size: 5 μL for [A], 100 μL for [B]

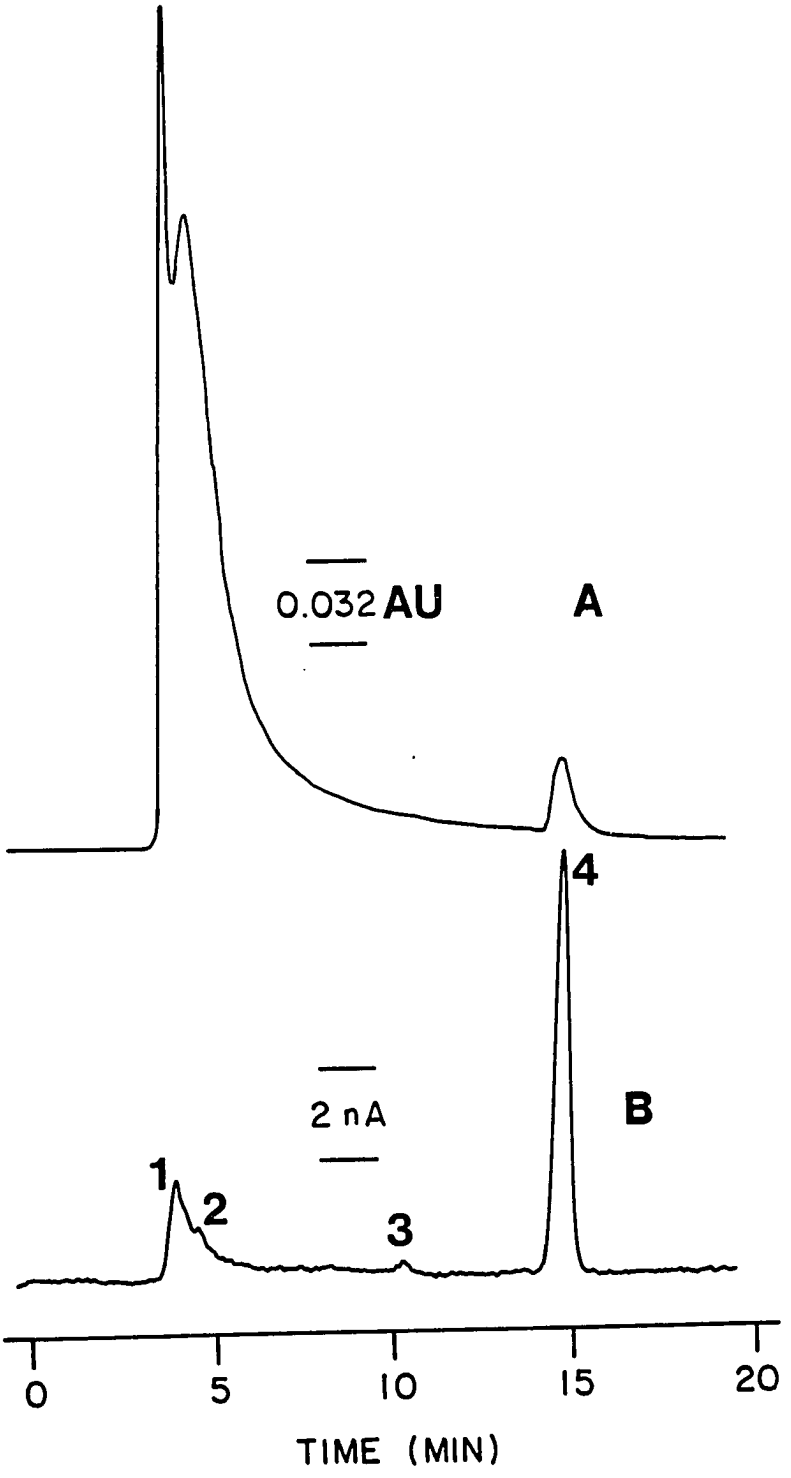
0.032 AU
A
4
2 nA
B
1
2
3
0
5
10
15
20
TIME (MIN)

The ICP-AES multielement, element-specific chromatograms of the acid soluble and methanol soluble fractions of the Charming Creek coal are illustrated in Figures 28 and 29, respectively. Specific chromatographic conditions are given with each figure. Neither As nor Se were detected in the acid soluble or methanol soluble fractions; V was not detected in the methanol soluble fraction. In Figure 28, the "satellite" peaks observed for Cr, Zn, Cd, Ni, Fe, V, and Cu were reproducible; the "satellite" peak was predominant in the Fe-specific chromatogram. In Figure 29, the "satellite" peaks that were observed for Cr, Zn, and Fe, were also reprodcible. The negative deflection in the background that was prominent for Cd was an anomally that resulted from the 3^{rd} order Butterworth filter routine that was used to smooth the data. The anomally occurred when there was an abrupt change in the slope of the acquired data points (e.g., a sharp peak) and was analogous to the oscillations observed for a heavily damped inductance-resistance-capacitance (LRC) circuit.

The relative Cu and Fe concentrations in the acid soluble fraction were found to be 10-fold greater than in the methanol soluble fraction. The methanol fraction contained about 4 times more sulfur as compared to the acid soluble fraction. In Figures 28 and 29, the chromatographic peaks that occurred at retention times of 3.5 to 6 min in the S-specific chromatograms were likely comprised of inorganic S (predominantly sulfide), aliphatic sulfur, thiophenols, and complex thiophenes, whereas the peak at a retention time of 15 min may have been higher molecular weight polycyclic compounds (185). This hypothesis seems reasonable in view of a recent study completed at the Ames Laboratory of the Charming Creek coal (186), in which sulfide (2132 ppm), thiophenes (425 ppm),

Figure 28. HPLC-DIN-ICP-AES element-specific chromatograms of the acid soluble fraction of a Charming Creek coal
Mobile phase: (90/10) methanol/water; column: Whatman Partisil 5 ODS-3 (4.2 mm i.d. x 250 mm L); flow rate: 0.75 mL/min (~15% to plasma); sample size: 100 μL

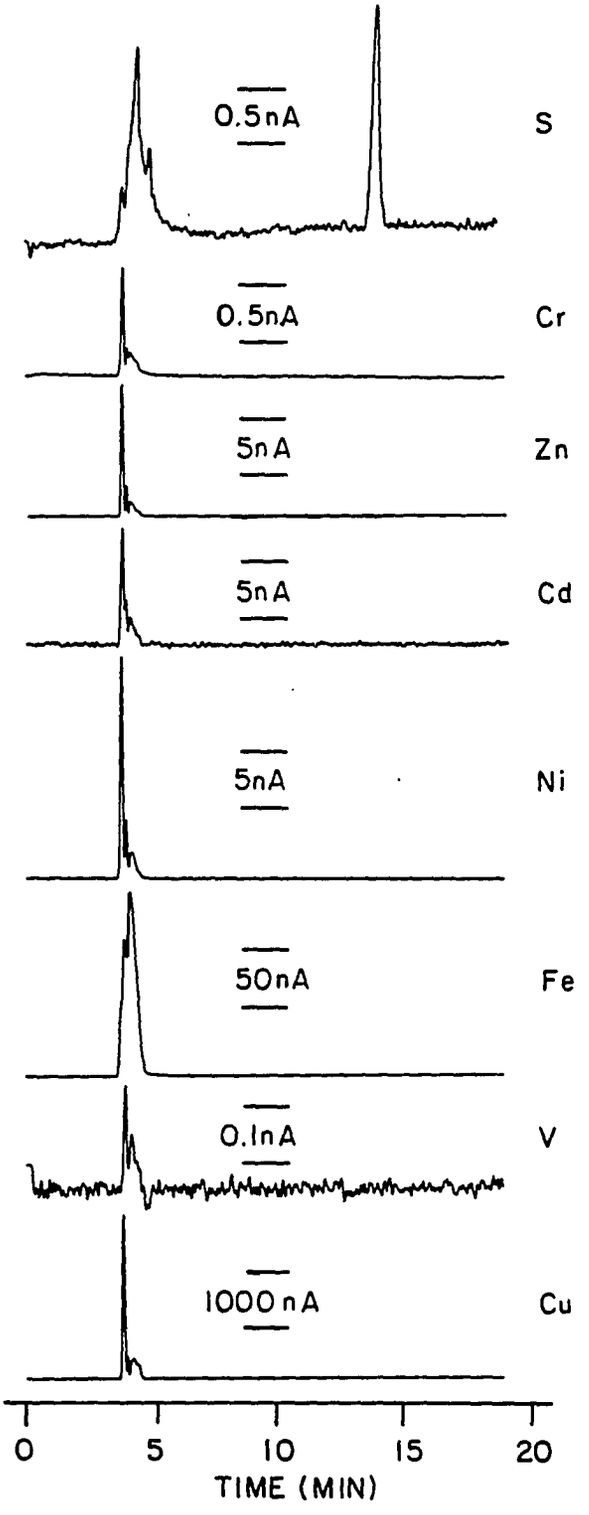
0.5nA
S
0.5nA
Cr
5nA
Zn
5nA
Cd
5nA
Ni
50nA
Fe
0.1nA
V
1000nA
Cu
0
5
10
15
20
TIME (MIN)

Figure 29. HPLC-DIN-ICP-AES element-specific chromatograms of the methanol soluble fraction of a Charming Creek coal Mobile phase: (90/10) methanol/water; column: Whatman Partisil 5 ODS-3 (4.2 mm i.d. x 250 mm L); flow rate: 0.75 mL/min (~15% to plasma); sample size: 100 μL

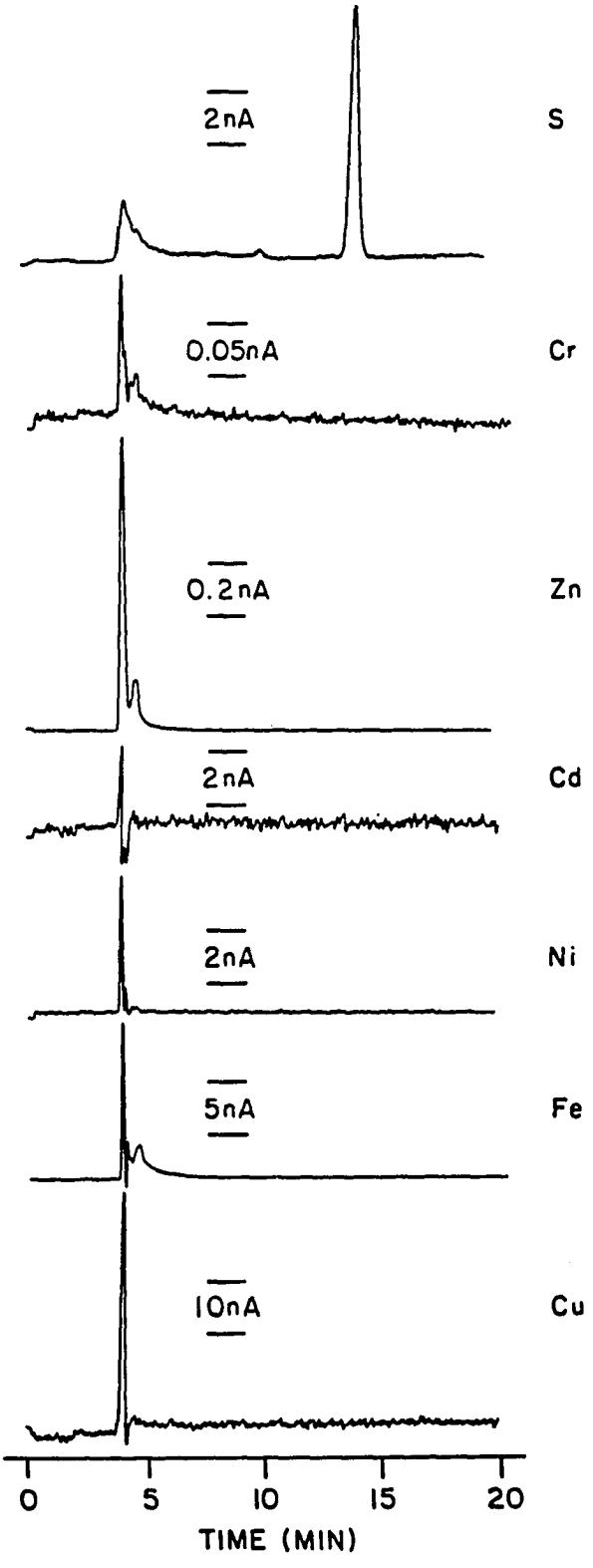
2nA
S
0.05nA
Cr
0.2nA
Zn
2nA
Cd
2nA
Ni
5nA
Fe
10nA
Cu
0
5
10
15
20
TIME (MIN)

thiols (591 ppm), and complex thiophenes (4.95%) were quantitated by H_2S evolution. Although some of the metals are likely cationic in nature (perhaps with S^{2-}, SO_4^{2-}, Cl^- as counterions), the presence of the "satellite" peaks indicate that many of the metals may be complexed with low molecular weight sulfur and oxygen containing compounds.

Unfortunately, individual species separation has not been achieved with the HPLC approach, as there are likely hundreds of compounds present in each of the fractions. A better approach to the solution of the speciation problem may be gas or supercritical fluid chromatographic separation followed by element-specific detection, e.g., with the helium afterglow detector(187).

Shale oil, crude oil, and SRC II analyses

Acidic fraction of a crude shale oil Shale oil is known to contain relatively large amounts of arsenic (>40 $\mu g/g$), as inorganic and acidic organoarsenicals (38,39,188). During the initial stages of shale oil refinement, arsenic acts as a poison to nickel, tungsten, or cobalt catalysts that facilitate the removal of nitrogen, and also increases the hydrogen content of the oil from 11% (wt) to the 13% (wt) necessary for fuels used in internal-combustion engines (189). Thus, the speciation of As in shale oil may provide insight towards the development of de-arsenation processes.

For the present As speciation study, crude Paraho Shale Oil A (CRM-2, DOE Fossil Fuels Research Material Facility, Oak Ridge National Laboratory) was subjected to the extraction procedure summarized in Figure 30. A 40 mL aliquot of the shale oil was transferred to a 500 mL separatory funnel and diluted with 200 mL of methylisobutylketone (MIBK).

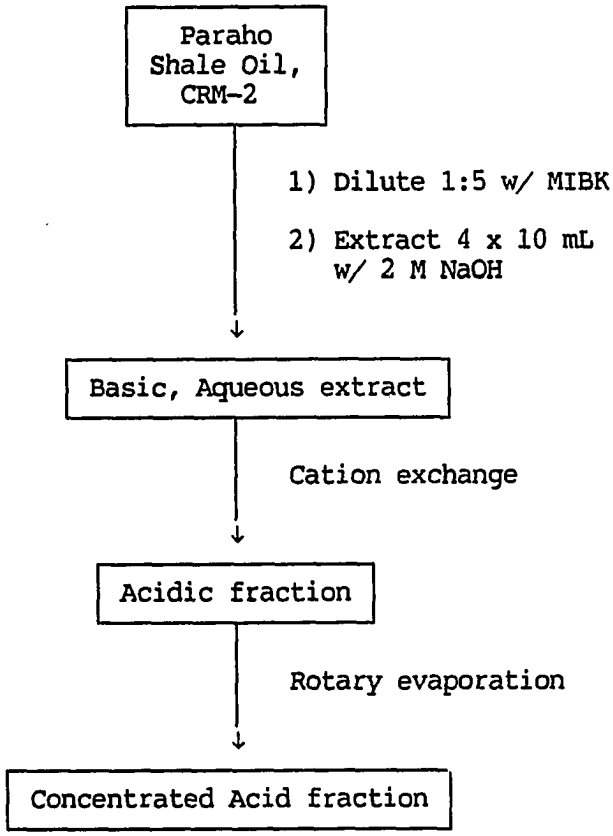

Figure 30. Separation scheme for crude Paraho shale oil

The shale oil/MIBK solution was extracted four times with 10 mL of 2 M NaOH and the aqueous extracts combined (37 mLs recovered). To effect the removal of sodium, the aqueous extract was allowed to pass over a 60 mL bed of cation exchange resin (Bio-Rad, AG 50W-X8, 100-200 mesh) that had been converted to the acid form. Excess water was drawn off on a rotary evaporator until approximately 1 mL remained. The volume of the aqueous extract was brought up to 3 mL and filtered (0.45 μm, Spartan-3). This extract yielded the arsenic-specific chromatograms shown in Figures 31b and 31c. For comparison purposes, a chromatogram of a reference solution containing 3 μg/mL each as As of arsenite, MMAA, DMAA, arsenate, and benzenearsonic acid (BAA) is illustrated in Figure 31a. Arsenite, MMAA, DMAA, and arsenate were systematically identified in the extract by spiking the extract with standard solutions that contained known compounds. The two species observed at retention times of approximately 9.5 and 10.5 min were not identified. The peak observed at approximately 15 min in Figure 31c was as anomally. Peak area comparisons among the six As species indicated that approximately 82% of the total arsenic in the concentrated, aqueous shale oil extract was contributed by arsenate. This result cannot be related to the original shale oil sample, as the extraction efficiencies of each of the species was not known.

Application of Farcasiu fractionation procedure to shale and crude oil, and a coal liquifaction products The fractionation procedure described by Farcasiu (190) was utilized to perform a compound class separation on crude, Paraho Shale Oil A (CRM-2, DOE Fossil Fuels Research Material Facility, Oak Ridge National Laboratory), Wilmington crude oil (CRM-3, DOE Fossil Fuels Research Material Facility, Oak Ridge National

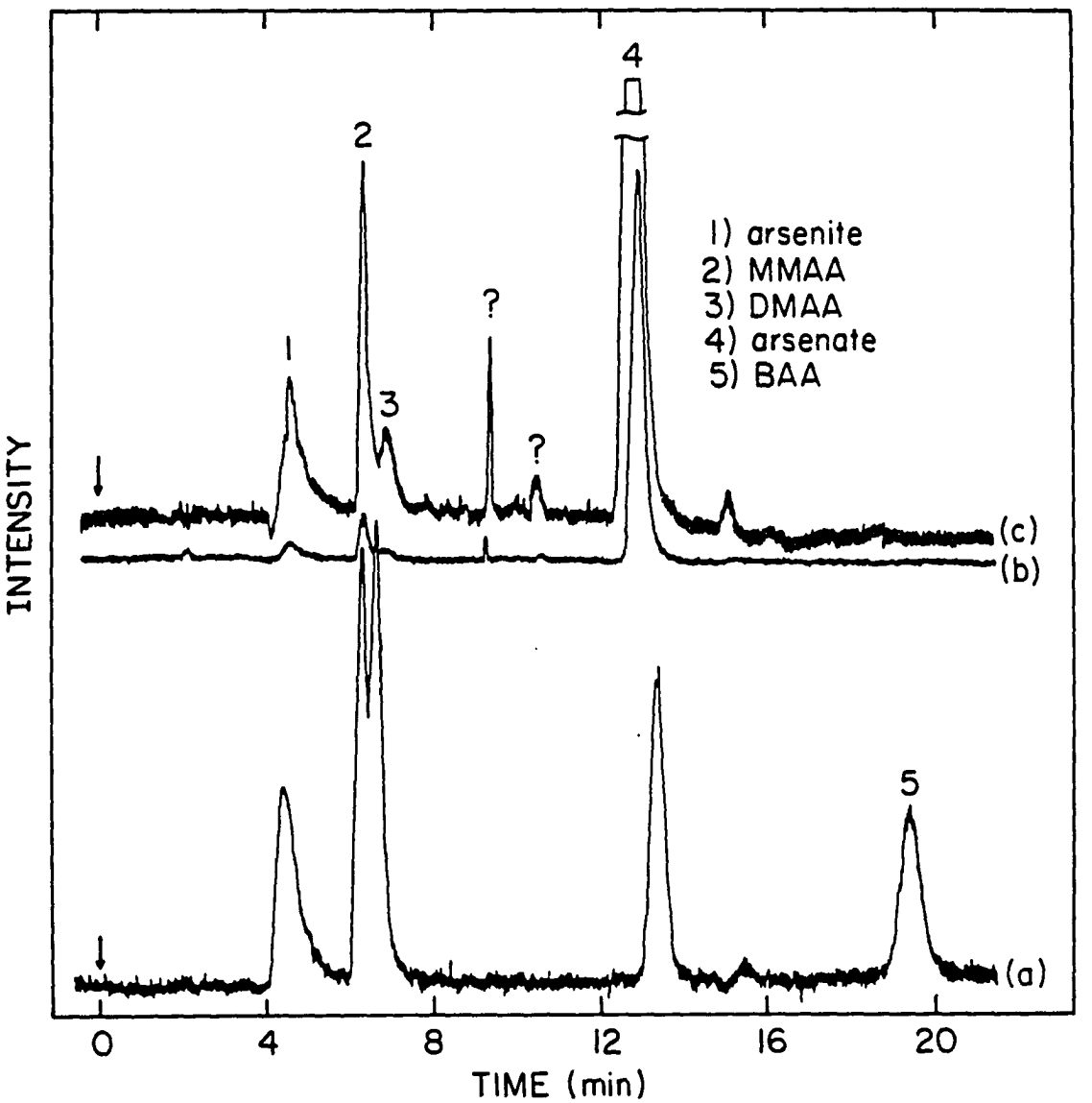

Figure 31. Ion-pairing, reverse-phase separation of [A] arsenite (1), monometylarsonic acid (2), dimetylarsinic acid (3), arsenate (4), and benzenearsonic acid (5), 600 ng (3 μg/mL) each as As, 3 x 10^{-8} A; [B] Acidic fraction of crude Paraho Shale Oil A, 3 x 10^{-7} A; [C] Acidic fraction of crude Paraho Shale Oil A, 3 x 10^{-8} A
Mobile phase: 5 mM tetrabutylammonium phosphate in (90/10) water/methanol; column: Whatman Partisil 5 ODS-3 (4.2 mm i.d. x 250 mm L); flow rate: 0.75 mL/min (~15% to plasma); sample size: 200 μL; wavelength: 193.7 nm

Laboratory), and an SRC II (National Bureau of Standards, Surrogate Reference Material). The fractionation procedure was designed to separate each of the materials into nine fractions that ranged from aliphatic hydrocarbons to highly functional, polar molecules.

The fractionation was performed via sequential elution by solvents chromatography (SESC) on a silica gel column. The ratio of sample to silica gel was 1:25 (by weight). The silica gel (60-200 mesh) was washed with methanol and dried overnight at 120°C. The water content was adjusted to 4% (by weight) before the column was packed. Approximately 2 g of the energy-related material was transferred to the column. The fractions were eluted successively with HPLC grade solvents as described in Figure 32. The fractions were collected in round bottom flasks and excess solvent was removed using a rotary evaporator. The residues were diluted to 2 mL with pyridine and stored in the refrigerator.

At the time of analysis, each of the fractions was filtered (0.45 μm, Spartan-3) and chromatographed using pyridine as the mobile phase on a Whatman Partisil 5 ODS-3 column with subsequent DIN-ICP-AES detection. This work yielded over 210 element-specific chromatograms for the elements S, As, Se, Cr, Zn, Cd, Ni, Fe, V, and Cu that were under study. The elemental distributions of each of these elements in the nine fractions for each material studied are summarized in Figure 33. The general distribution of the elements in each of the materials was quite similar. Sulfur was detected in all 9 fractions; As and Se only in Fraction 6. Fraction 6 was found to contain the highest relative concentrations of the elements studied. A trace of Cd was found only in Fraction 9 of the SRC II material.

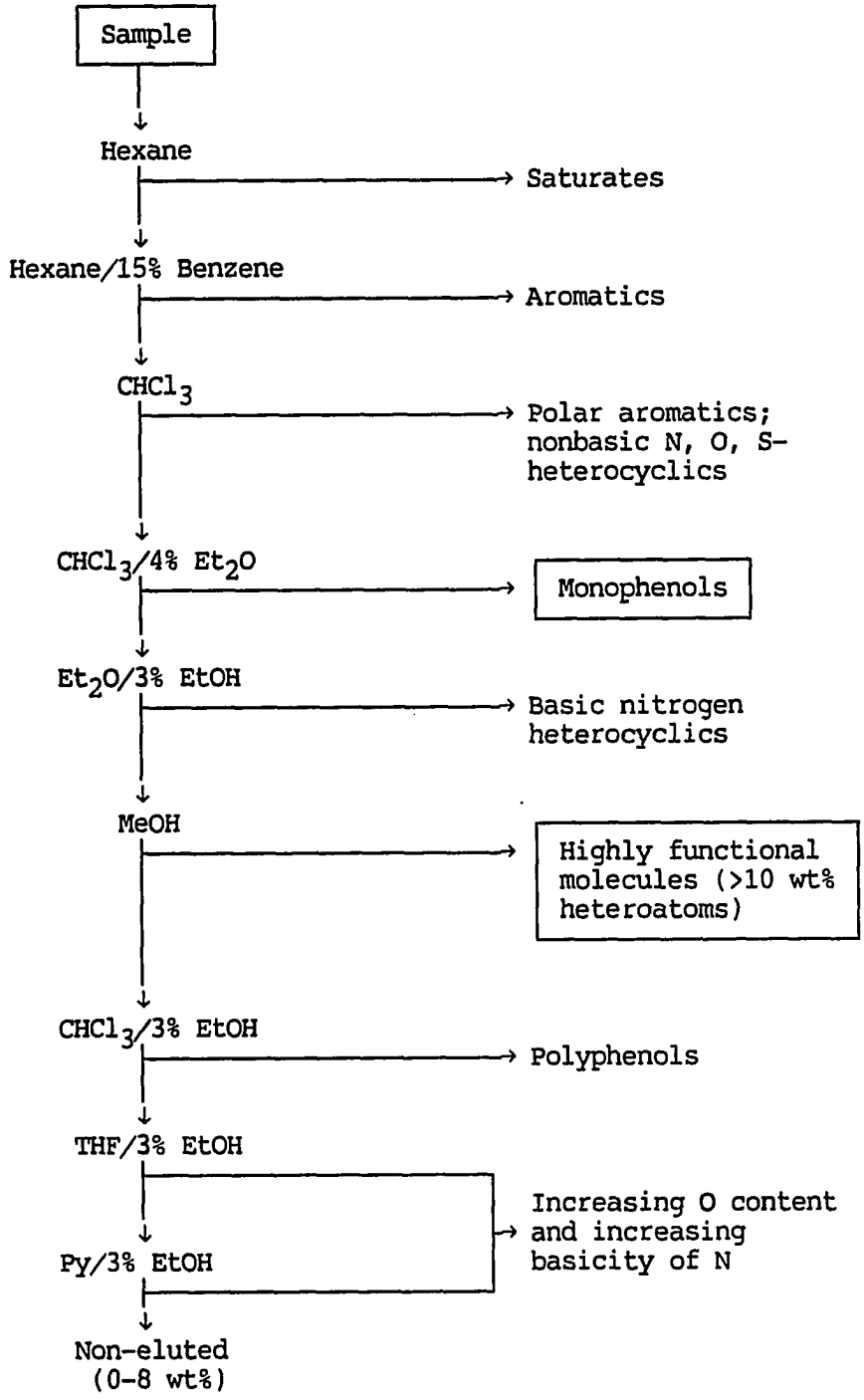

Figure 32. Separation scheme used for crude Paraho Shale Oil A, Wilmington crude oil, and SRC II (Farcasiu procedure)

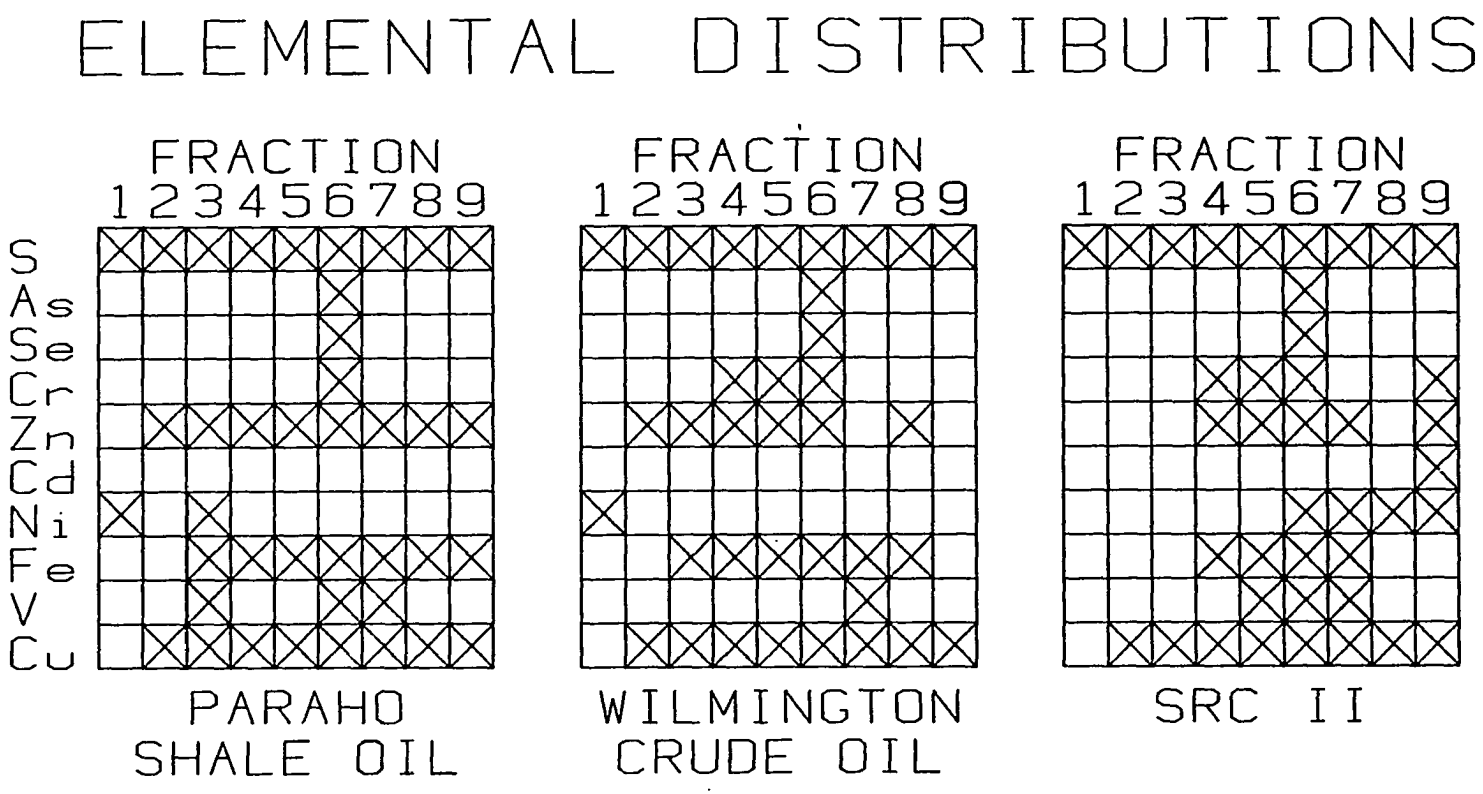

Figure 33. Distribution of elements found in the various fractions that were obtained for crude Paraho Shale Oil A, Wilmington crude oil, and SRC II (Farcasiu procedure)

Representative HPLC-DIN-ICP-AES element-specific chromatograms for Fractions 4 and 6 of the crude shale oil, Wilmington crude oil, and SRC II are illustrated in Figures 34 through 37. The S-specific chromatograms shown in Figure 34 illustrated that there was a broad variety of sulfur compounds present in the energy-related materials; especially Fraction 6 of the Wilmington crude oil sample. The Fe- and Cu-specific chromatograms also showed a wide variety of compounds present. Because the retention times of the Fe and Cu species were similar to those observed for S, much of the Fe and Cu may be complexed with low molecular weight, heteratomic (S, O, and N) organic compounds. The relative Fe concentrations in Fractions 4 and 6 were similar; Cu was found to be present in Fraction 6 at concentrations that ranged from about 2 to 10-fold higher than in Fraction 4. Although the absolute concentrations of the metals were not determined, the relative concentrations in each energy-related material can be compared from intensity measurements. There was a sharp contrast in the distribution of Zn-containing species between Fractions 4 and 6 (Figure 37); the chromatogram for Fraction 4 indicated that a range of Zn compounds was present, whereas a singular species was indicated by the Fraction 6 chromatograms. It is also interesting to note that there existed a sharp peak in all of the element-specific chromatograms of Fraction 6 that corresponded to the singular Zn species that eluted at a retention time of about 5 minutes.

Unfortunately, individual elemental species separation was not demonstrated in the present work, nor has it been demonstrated by any other authors to date. This is not too surprising in view of the complexity of the oil matrices. Efforts should now focus on the

Figure 34. HPLC-DIN-ICP-AES sulfur-specific chromatograms for fractions 4 and 6 from crude Paraho Shale Oil A, Wilmington crude oil, and SRC II
Mobile phase: 100% pyridine; column: Whatman Partisil 5 ODS-3 (4.2 mm i.d. x 250 mm L); flow rate: 0.75 mL/min (~15% to plasma); sample size: 200 μL; wavelength: 182.0 nm

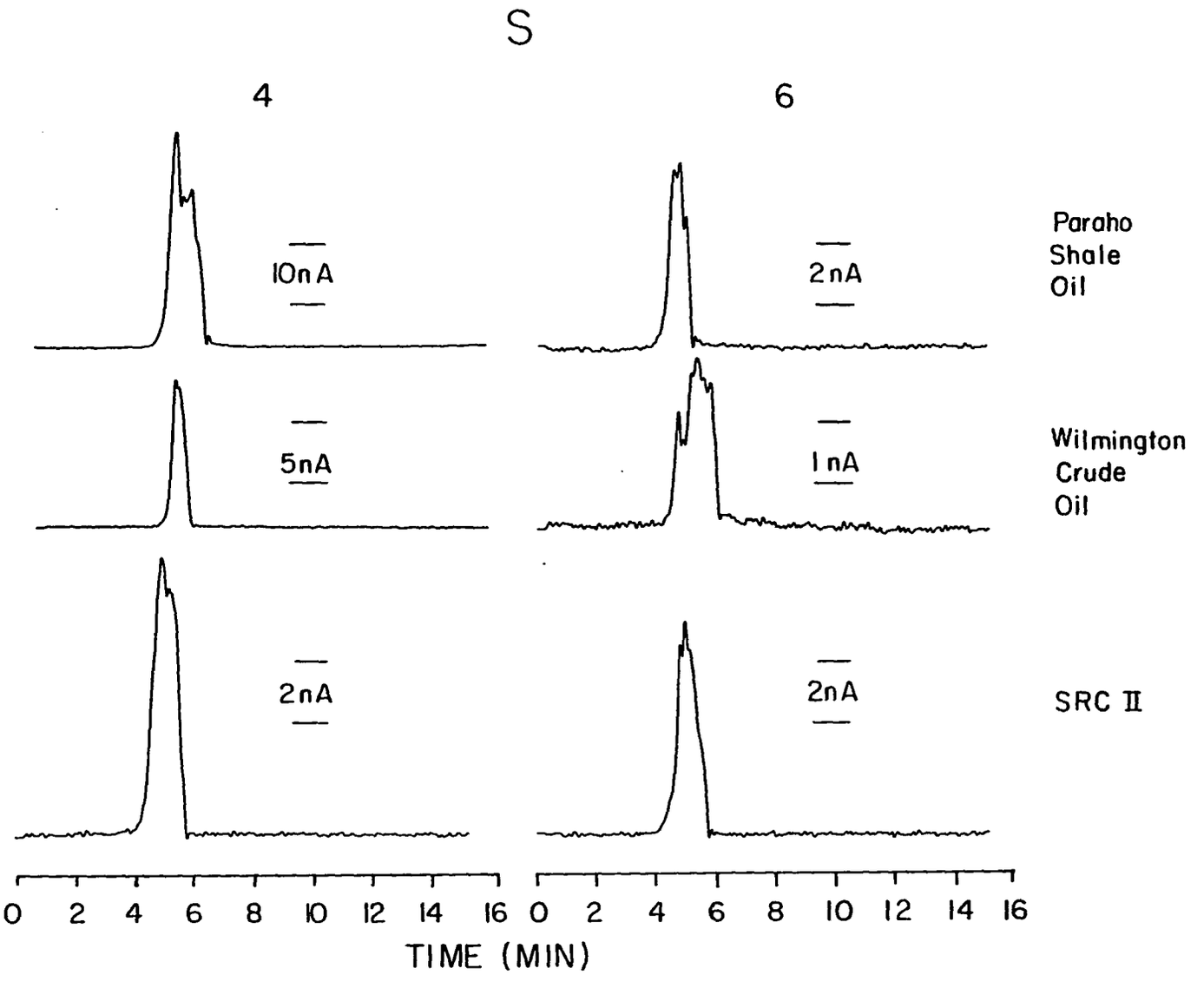
S
4
6
10nA
2nA
5nA
1nA
2nA
2nA
Paraho
Shale
Oil
Wilmington
Crude
Oil
SRC II
0 2 4 6 8 10 12 14 16
0 2 4 6 8 10 12 14 16
TIME (MIN)

Figure 35. HPLC-DIN-ICP-AES iron-specific chromatograms for fractions 4 and 6 from crude Paraho Shale Oil A, Wilmington crude oil, and SRC II
Mobile phase: 100% pyridine; column: Whatman Partisil 5 ODS-3 (4.2 mm i.d. x 250 mm L); flow rate: 0.75 mL/min (~15% to plasma); sample size: 200 μL; wavelength: 261.2 nm

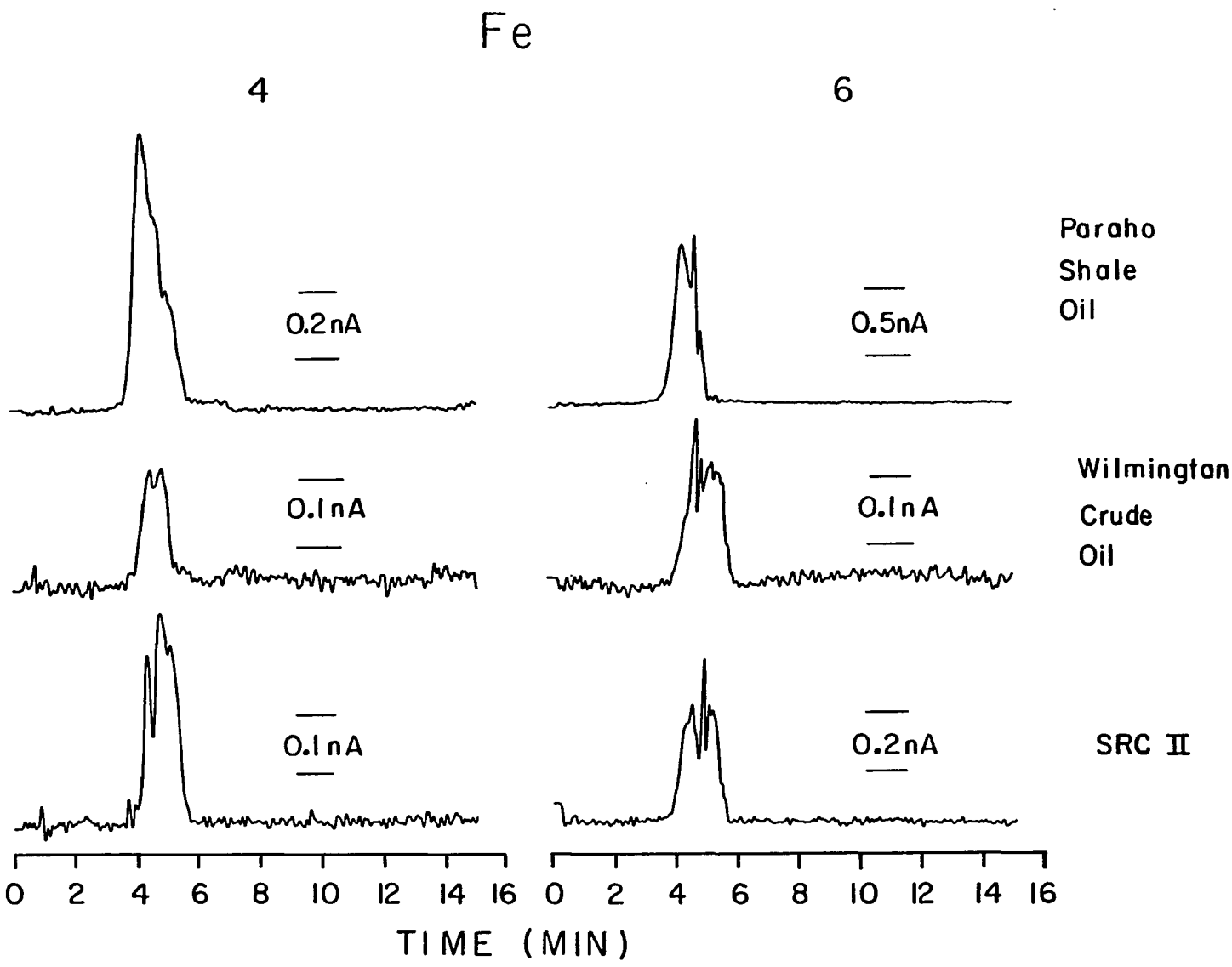
Fe
4
6
0.2nA
0.5nA
0.1nA
0.1nA
0.1nA
0.2nA
Paraho
Shale
Oil
Wilmington
Crude
Oil
SRC II
0 2 4 6 8 10 12 14 16
0 2 4 6 8 10 12 14 16
TIME (MIN)

Figure 36. HPLC-DIN-ICP-AES copper-specific chromatograms for fractions 4 and 6 from crude Paraho Shale Oil A, Wilmington crude oil, and SRC II
Mobile phase: 100% pyridine; column: Whatman Partisil 5 ODS-3 (4.2 mm i.d. x 250 mm L); flow rate: 0.75 mL/min (~15% to plasma); sample size: 200 μL; wavelength: 324.8 nm

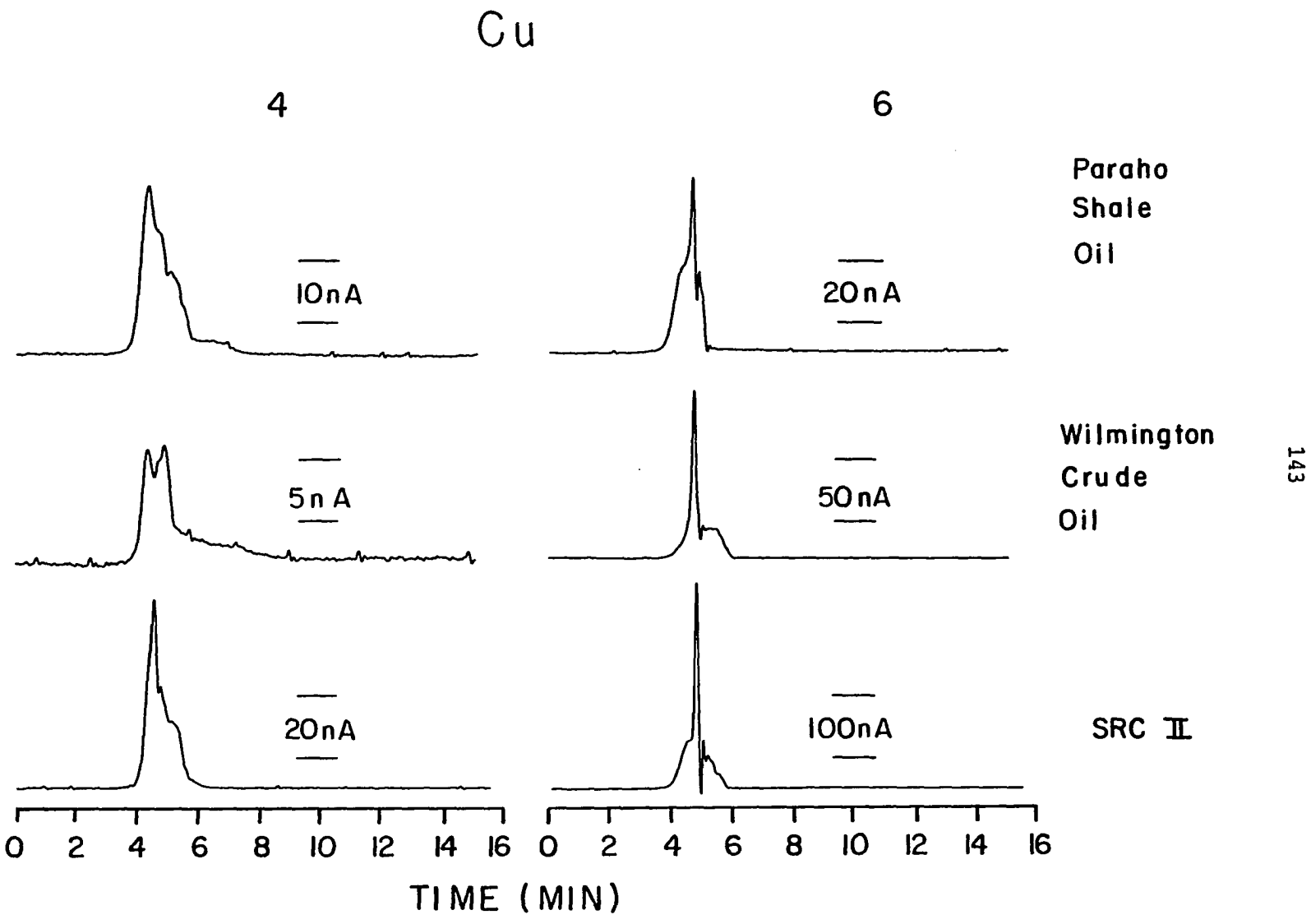
Cu
4
6
Paraho
Shale
Oil
10nA
20nA
Wilmington
Crude
Oil
5nA
50nA
SRC II
20nA
100nA
0 2 4 6 8 10 12 14 16
0 2 4 6 8 10 12 14 16
TIME (MIN)

Figure 37. HPLC-DIN-ICP-AES zinc-specific chromatograms for fractions 4 and 6 from crude Paraho Shale Oil A, Wilmington crude oil, and SRC II
Mobile phase: 100% pyridine; column: Whatman Partisil 5 ODS-3 (4.2 mm i.d. x 250 mm L); flow rate: 0.75 mL/min (~15% to plasma); sample size: 200 μL; wavelength: 213.9 nm

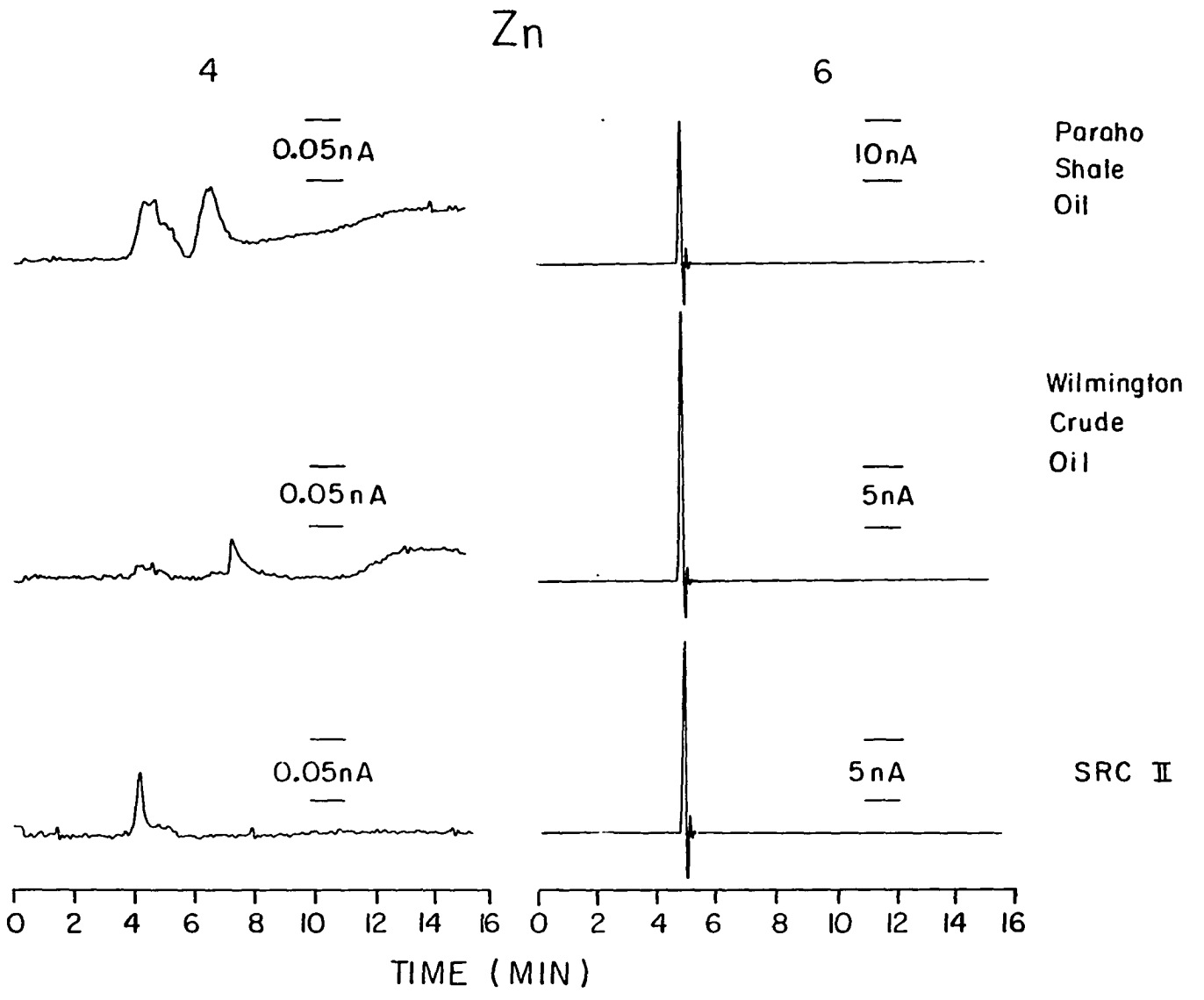
Zn
4
6
0.05nA
10nA
Paraho
Shale
Oil
Wilmington
Crude
Oil
0.05nA
5nA
0.05nA
5nA
SRC II
0 2 4 6 8 10 12 14 16
0 2 4 6 8 10 12 14 16
TIME (MIN)

optimization of the HPLC technology such that individual elemental species separation can be achieved in the highly complex oil matrices. Without a doubt, the results presented in this section represent only the "tip of an iceberg". Four points, however, should be evident; 1) the speciation of materials contained in complex matrices such as crude oils does indeed pose a real challenge, 2) there is a wealth of information contained in each of the 200+ element-specific chromatograms obtained in this study, 3) the ICP holds great potential as a "probe" of HPLC effluents from energy-related materials, and finally 4) organic mobile phases pose no threat to plasma stability when the DIN interface in employed. The next section will discuss further attempts toward improvement in chromatographic resolution and will concentrate on the speciation of a synthetic mixture of sulfur heterocyclic compunds and the compounds contained in the crude, Paraho Shale Oil A sample.

Attempts toward improvement of chromatographic resolution

Speciation of sulfur heterocyclic compounds A synthetic mixture of approximately 100 μg/mL each as S of 1-benzothiophene, dibenzothiophene, benzo[b]naphtho[2,3-d]thiophene, benzo[b]naphtho[2,1-d]thiophene, and benzo[2,3]phenanthro[4,5-bcd]thiophene was prepared so that the retention times of several sulfur heterocyclic compounds could be ascertained. As mentioned in Chapter II, when predominantly organic mobile phases are required for compound separation, the formation and optical emission of the CO fourth positive molecular band system imposes a serious limitation on the detection of S-containing species at the 182.0 nm wavelength. This limitation is illustrated in Figure 38, which shows the spectral interference of the CO fourth positive molecular band system

Figure 38. Spectral interference of the CO fourth positive molecular band system on the (1) 180.7 nm, (2) 182.0 nm, and (3) 182.6 nm wavelengths of sulfur in the presence of [A] distilled-deionized water; [B] 1 μg/mL as S of SO_4^{2-} in distilled-deionized water; [C] 1 μg/mL as S of SO_4^{2-} in 0.1 % acetonitrile; [D] 1 μg/mL as S of SO_4^{2-} in 0.5 % acetonitrile; and [E] 1 μg/mL as S of SO_4^{2-} in 1.0 % acetonitrile

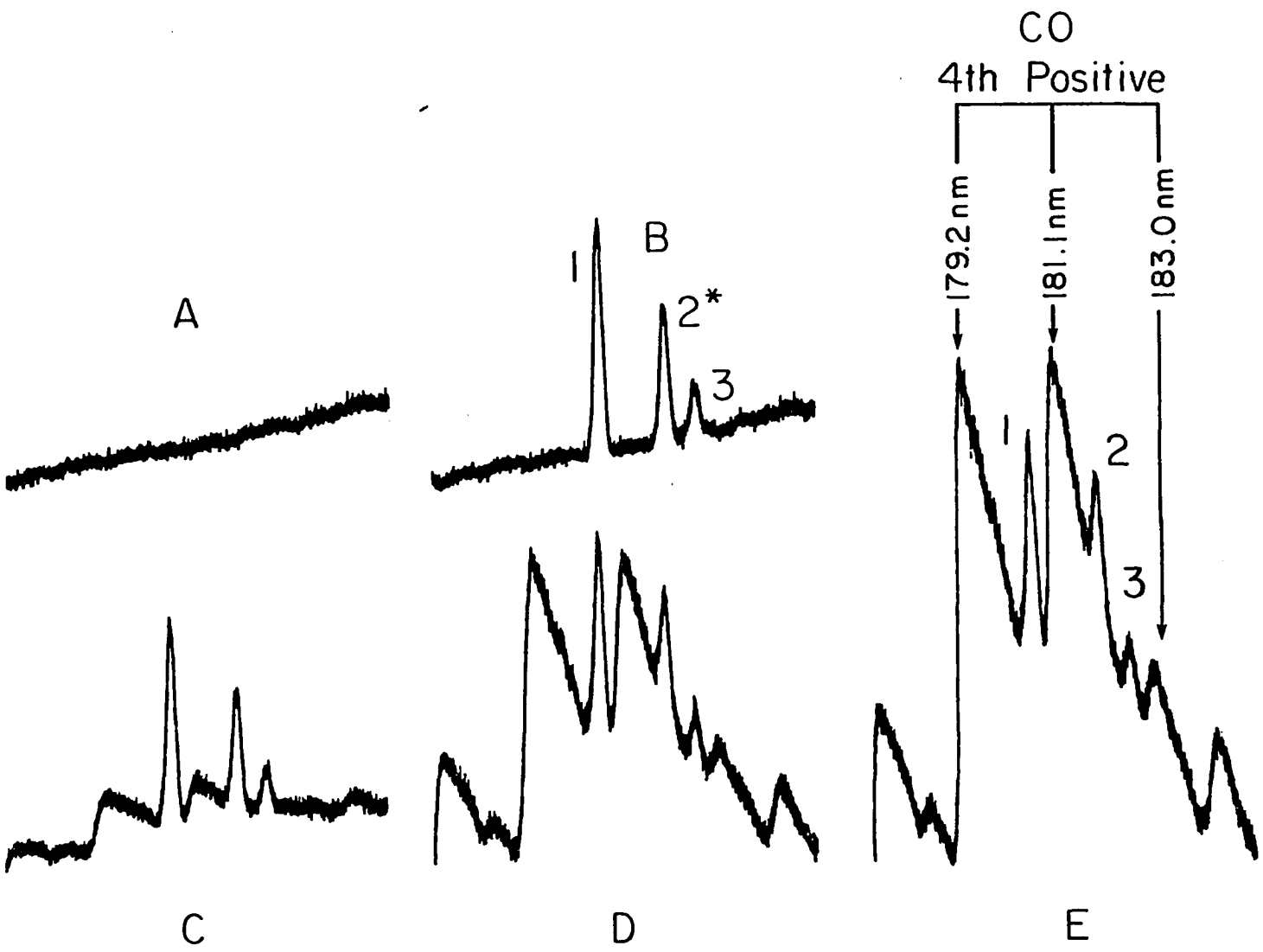
CO
4th Positive
179.2nm
181.1nm
183.0nm
A
B
1
2*
3
1
2
3
C
D
E

on the 180.7 nm, 182.0 nm, and 182.6 nm wavelengths of sulfur in the presence of variable concentrations of acetonitrile in water. The CO fourth positive molecular band system was also detected for the introduction of methanol and pyridine. It is important to note that Figure 38e represents the introduction of 1% acetonitrile in water; the interference would be greatly enhanced in 90% acetonitrile, as was the condition for the chromatogram shown in Figure 39b that illustrates the separation of the synthetic mixture of sulfur heterocyclic compounds. These compounds were separated by reverse phase HPLC. The mobile phase consisted of (90/10) acetonitrile/water and the effluent was monitored by UV absorption (254 nm) and ICP-AES, S-specific (182.0 nm) detectors. The ICP detector response for sulfur when the 182.0 nm line is used is even worse that it first appears, because the mixture of sulfur heterocyclic compounds used to obtain the UV absorption chromatogram in Figure 39a was concentrated by a factor of 10 before the S-specific chromatogram shown in Figure 39b could be obtained. The detectability of sulfur should improve if the polychromator were re-programmed to measure the 180.7 nm S line, as this line falls in the valley between the molecular bands at 179.2 nm and 181.1 nm.

To determine the extent of the apparent spectral interferences caused by the introduction of organic solvents into the plasma, the limits of detection for several elements of interest in matrices of varying methanol concentration were determined by FIA-DIN-ICP-AES. The results of this study are given in Table XIV. Only the limits of detection obtained for sulfur were significantly affected by the presence of increased organic solvent. Detection limits for As and Se were only degraded by a factor of

Figure 39. Chromatograms of several heterocyclic, sulfur compounds [A] UV absorption (254 nm) and [B] ICP, sulfur-specific (182.0 nm)
Mobile phase: (90/10) acetonitrile/water; column: Whatman Partisil 5 ODS-3 (4.2 mm i.d. x 250 mm L); flow rate: 0.75 mL/min (for [B], ~15% to plasma); sample size: 5 μL for [A], 100 μL for [B]; (1) 1-benzothiophene, (2) dibenzothiophene, (3) benzo[b]naphtho[2,3-d]thiophene, (4) benzo[b]naphtho[2,1-d]thiophene, (5) benzo[2,3]phenanthro[4,5-bcd]thiophene (S conc. in B= 10 x A)

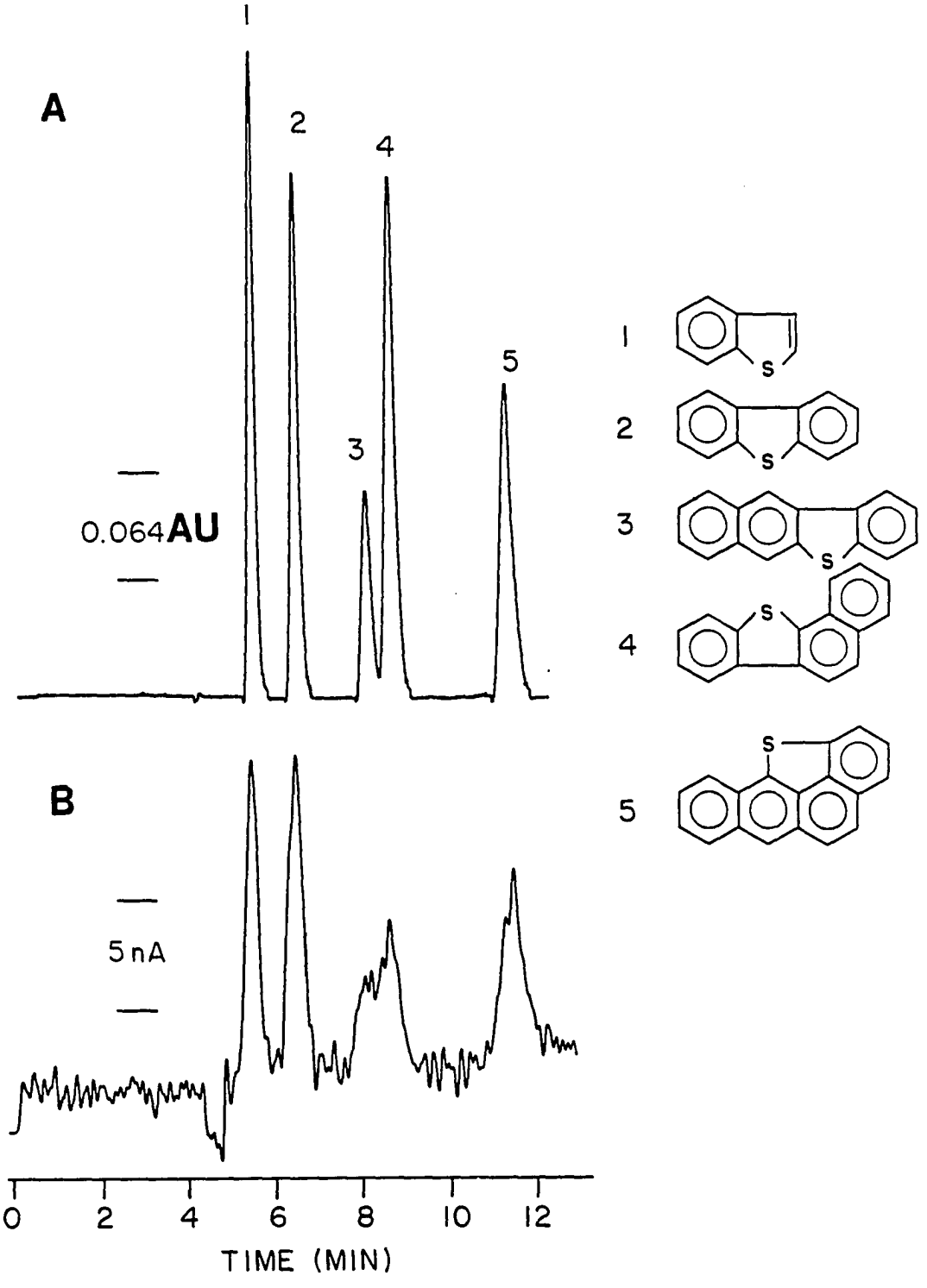
A
1
2
3
4
5
0.064AU
B
5nA
0
2
4
6
8
10
12
TIME (MIN)
1
2
3
4
5
S

Table XIV. LODs for several elements in matrices of varying methanol (MeOH) concentration (ng/mL)

Element	H_2O	20% MeOH	40% MeOH	60% MeOH	80%MeOH	MeOH
S	100	2600	>10,000	>10,000	>10,000	>10,000
As	42	66	84	100	120	90
Se	38	43	58	100	120	70
Cr	5	6	6	5	4	9
Zn	2	4	3	2	1	2
Co	7	5	3	5	3	3
Ni	15	13	7	11	11	10
Fe	14	11	11	12	11	8
Cd	3	3	2	3	2	2
Cu	6	3	5	5	3	3

2 to 3 in the organic solvent as compared to water. The detection limits obtained for the metals of interest were not affected by methanol concentration.

Application of the Lee fractionation procedure to crude Paraho Shale Oil A The procedure developed by Later and coworkers (191) was used to fractionate the crude, Paraho Shale Oil A (CRM-2, DOE Fossil Fuels Research Material Facility, Oak Ridge National Laboratory). A schematic diagram of the fractionation method is given in Figure 40. Neutral aluminum oxide (Brockman Activity I, 80-20 mesh) was used to separate the raw material into four fractions; A-1, aliphatic hydrocarbons; A-2, neutral polycyclic aromatic compounds (PAH, PASH, PAOH); A-3, nitrogen containing polycyclic aromatic compounds (N-PAC); and A-4, hydroxyl polycyclic aromatic hydrocarbons (HPAH). Approximately 5 g of the crude, Paraho Shale Oil A was dissolved in 10 mL of chloroform and adsorbed onto 30 g of neutral alumina. The solvent was slowly removed from the alumina by vigorously stirring the mixture under a gentle stream of dry N_2 gas. The alumina with adsorbed sample was packed on top of a 22 mm i.d. column that already contained 60 g of the neutral alumina. The sample was then eluted with the following chromatographic grade solvent: Fraction A-1, approximately 200 mL of hexane; Fraction A-2, approximately 400 mL of benzene; Fraction A-3, approximately 370 mL of chloroform (contained 0.75% ethanol preservative); and Fraction A-4, approximately 200 mL of 10% ethanol in tetrahydrofuran (THF). Excess solvent was removed on a rotary evaporator. The final volume of each of the four fractions was diluted to 4 mL with (90/10) acetonitrile/water.

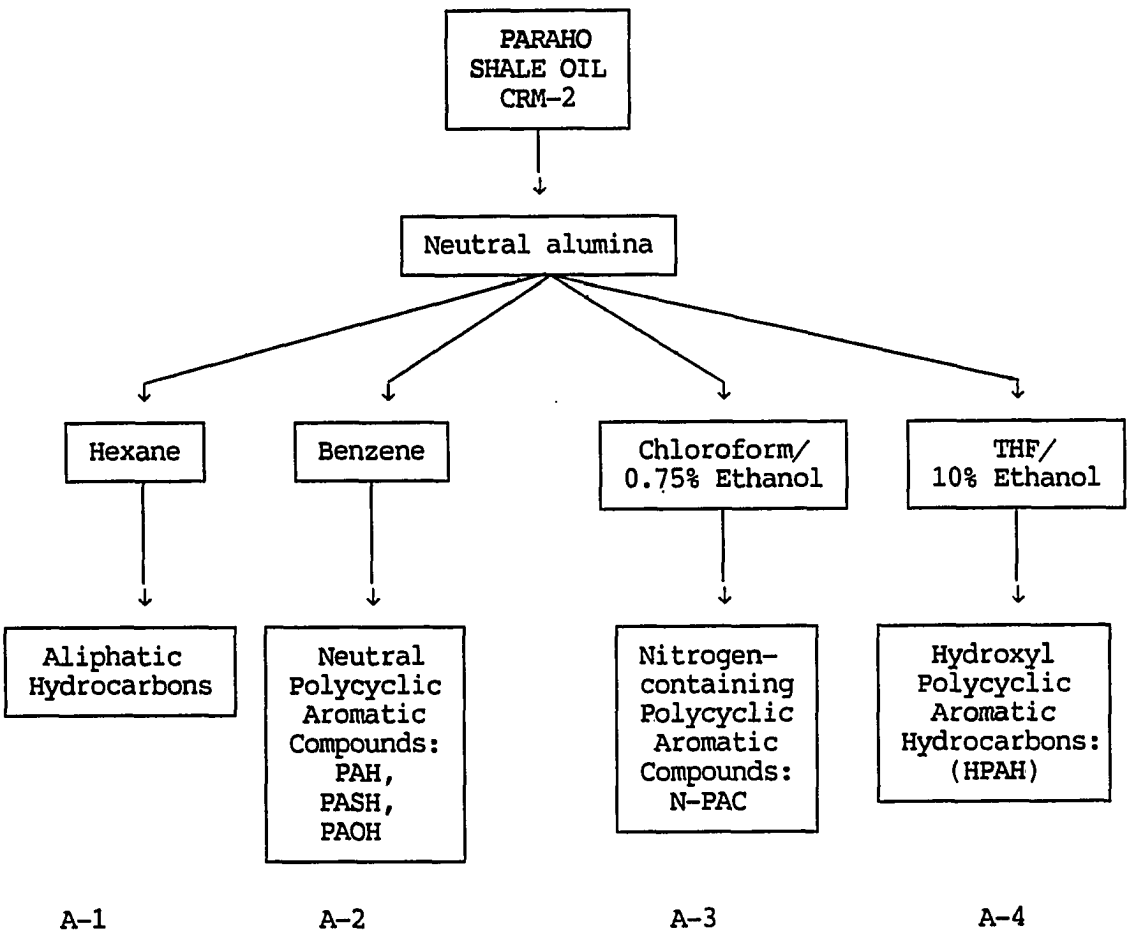

Figure 40. Separation scheme used for crude Paraho Shale Oil A (Lee procedure)

One-hundred to two-hundred microliter aliquots of fractions A-2, A-3, and A-4 were filtered (0.45 μm, Spartan-3) and subjected to reverse phase, HPLC analysis under conditions similar to those used for the speciation of the sulfur heterocyclic compounds. The UV absorption (254 nm) chromatograms are shown in Figure 41. Based upon retention time comparisons with the sulfur heterocyclic compounds (Figure 39), these chromatograms illustrate that the shale oil is rich in polycyclic materials. The chromatographic resolution obtained in this study was reasonable in view of the wide variety of compounds present in the shale oil.

The three fractions were next subjected to HPLC-DIN-ICP-AES analysis and S, As, Se, Cr, Zn, Co, Ni, Fe, V, and Cu wavelengths were monitored. The chromatographic conditions were identical to those given in Figure 41, except that the sample size injected was 100 μL. Little sulfur and virtually no metals were detected. Similar results were observed when THF of methanol were used as the mobile phase. It would appear that neither THF, methanol, nor acetonitrile appreciably solubilized the organometallic complexes that should be present in the shale oil fractions. After removal of the acetonitrile in each fraction and dissolution of the residues in 3 to 4 mL of pyridine, the fractions were again subjected to HPLC-DIN-ICP-AES analysis and the multielement, element-specific chromatograms shown in Figures 42 through 44 were obtained. The chromatographic conditions are given with each figure. It was quite evident that all three fractions were rich in S and Cu and that Fraction A-3 and A-4 contained a variety of other metals (Zn, Co, Ni, and Fe), yet these were not detected using acetonitrile as the mobile phase.

Figure 41. UV absorption (254 nm) chromatograms of three fractions of crude Paraho Shale Oil A
Column: Whatman Partisil 5 ODS-3 (4.2 mm i.d. x 250 mm L); flow rate: 0.7 mL/min; sample size: 5 μL; [A] Fraction A-2, (90/10) AcN/water; [B] Fraction A-3, (60/40) AcN/water; [C] Fraction A-4, (60/40) AcN/water

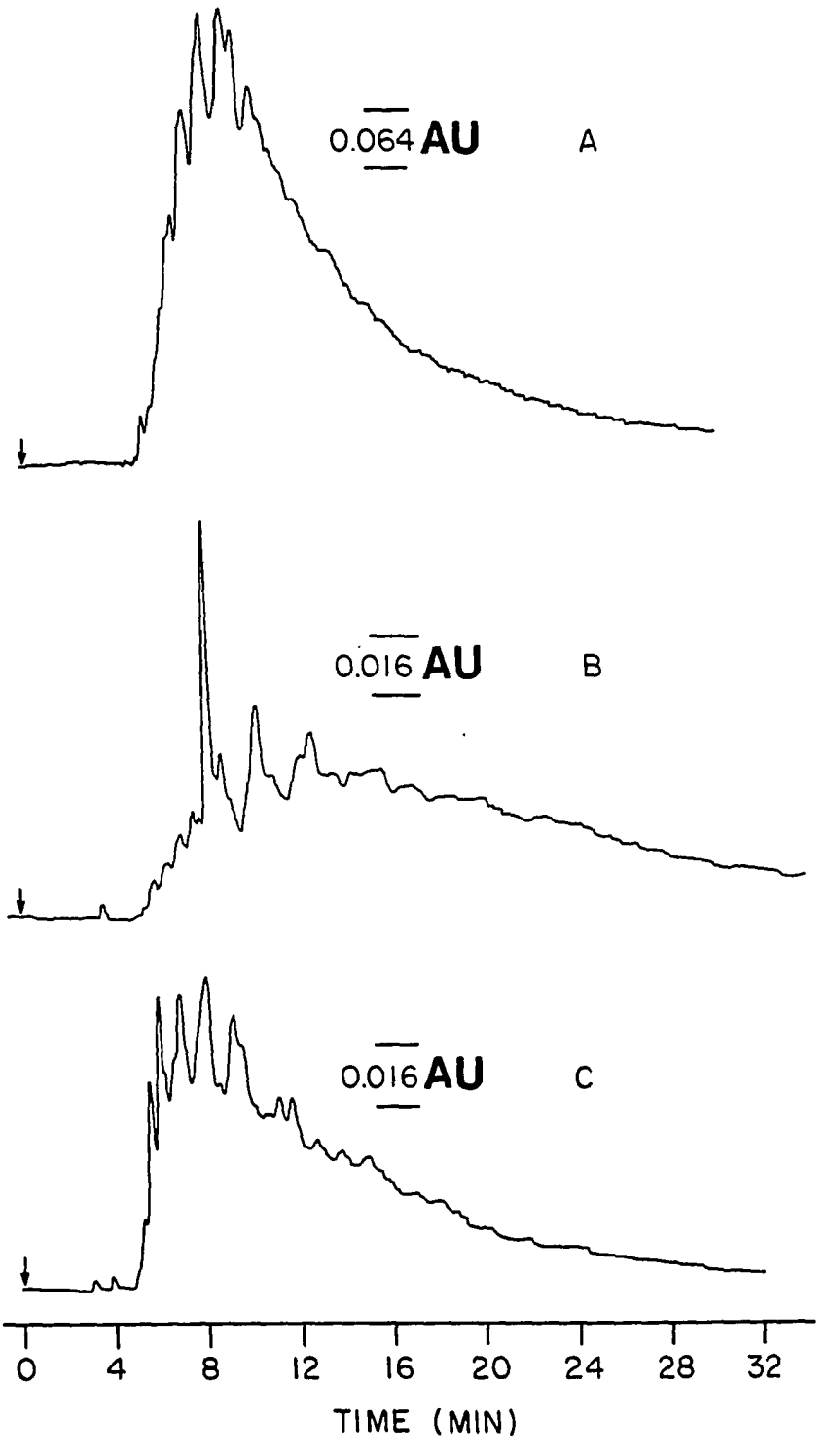
0.064 AU
A
0.016 AU
B
0.016 AU
C
0
4
8
12
16
20
24
28
32
TIME (MIN)

Figure 42. HPLC-DIN-ICP-AES element-specific chromatograms for Fraction A-2 from crude Paraho Shale Oil A
Mobile phase: (95/5) pyridine/water; column: Whatman Partisil 5 ODS-3 (4.2 mm i.d. x 250 mm L); flow rate: 0.7 mL/min (~15% to plasma); sample size: 100 μL

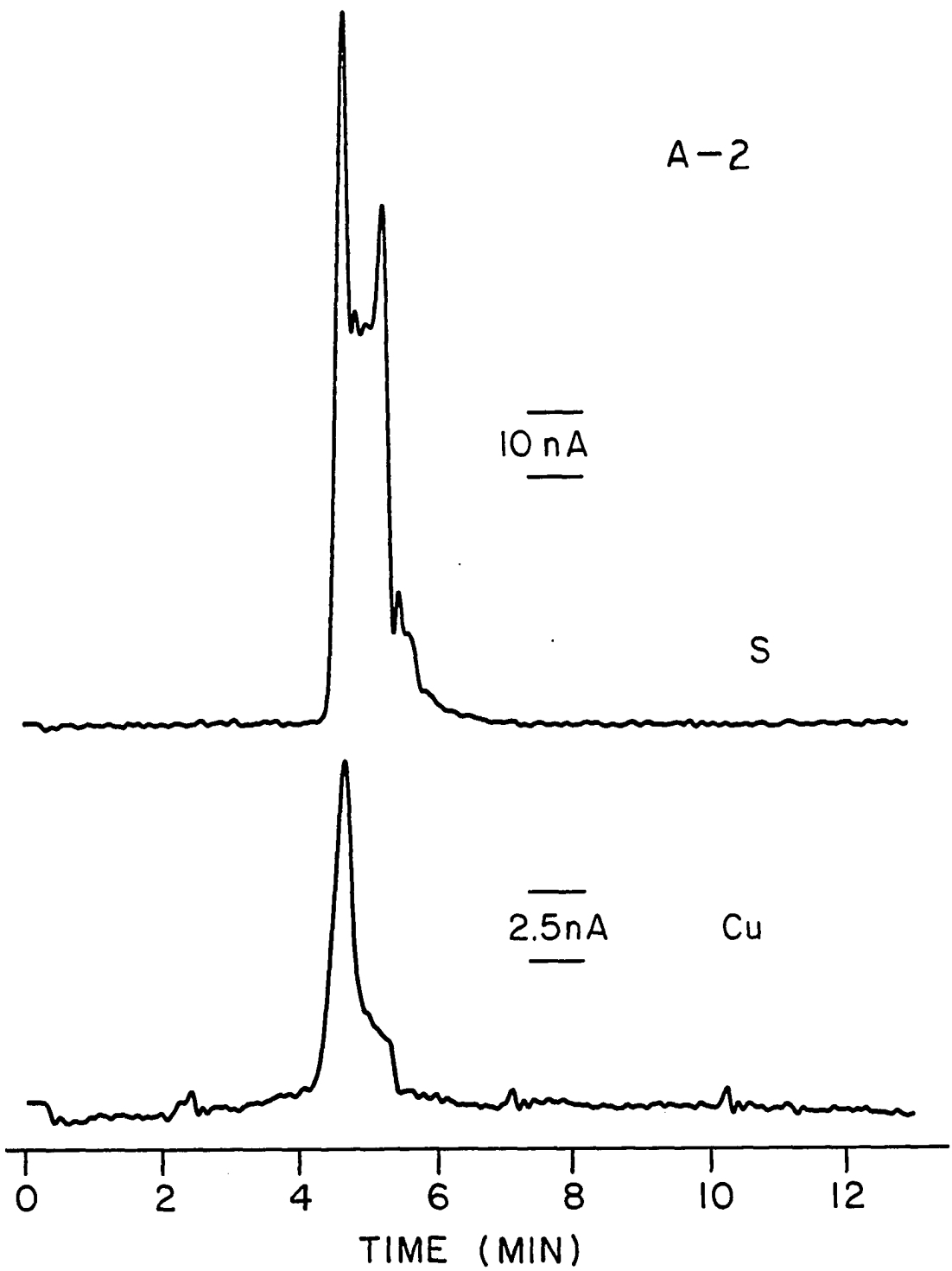
A-2
10 nA
S
2.5nA
Cu
0
2
4
6
8
10
12
TIME (MIN)

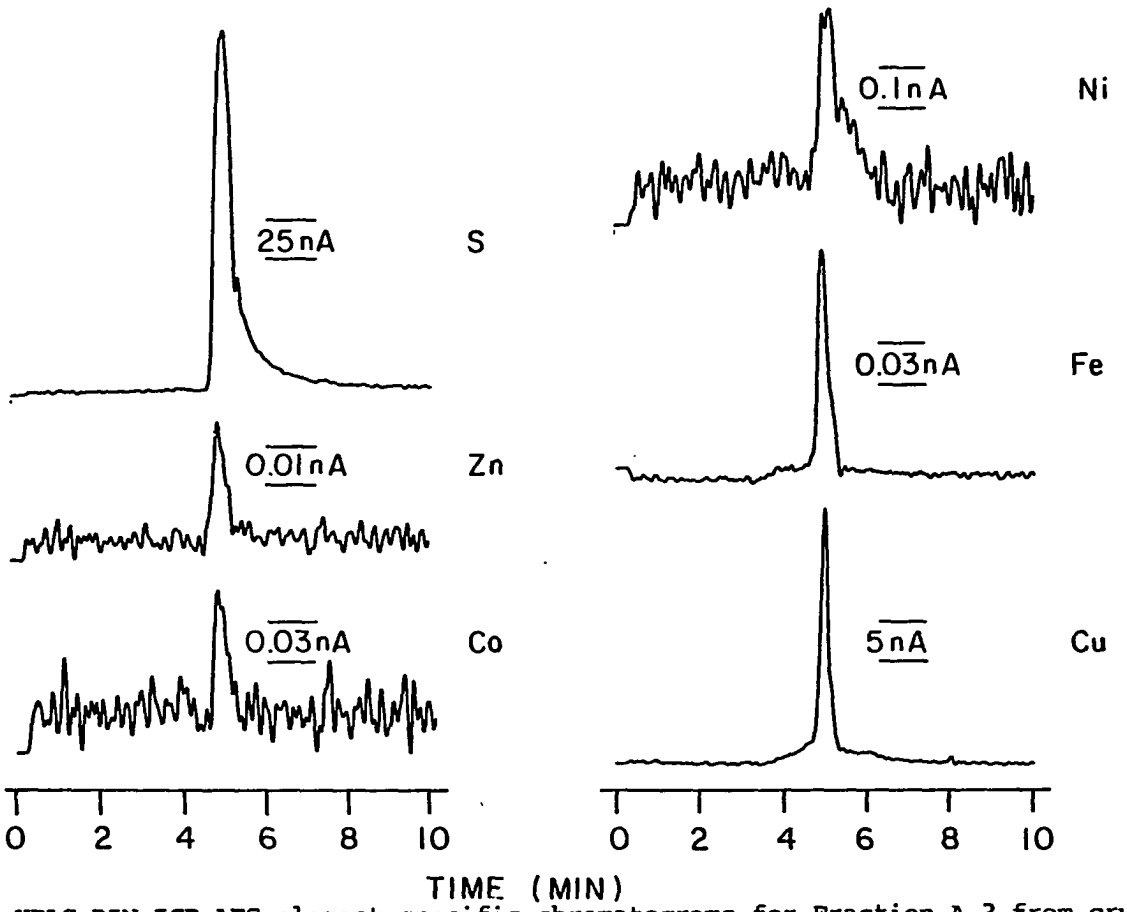

Figure 43. HPLC-DIN-ICP-AES element-specific chromatograms for Fraction A-3 from crude Paraho Shale Oil A
Mobile phase: (90/10) pyridine/water; column: Whatman Partisil 5 ODS-3 (4.2 mm i.d. x 250 mm L); flow rate: 0.7 mL/min (~15% to plasma); sample size: 100 μL

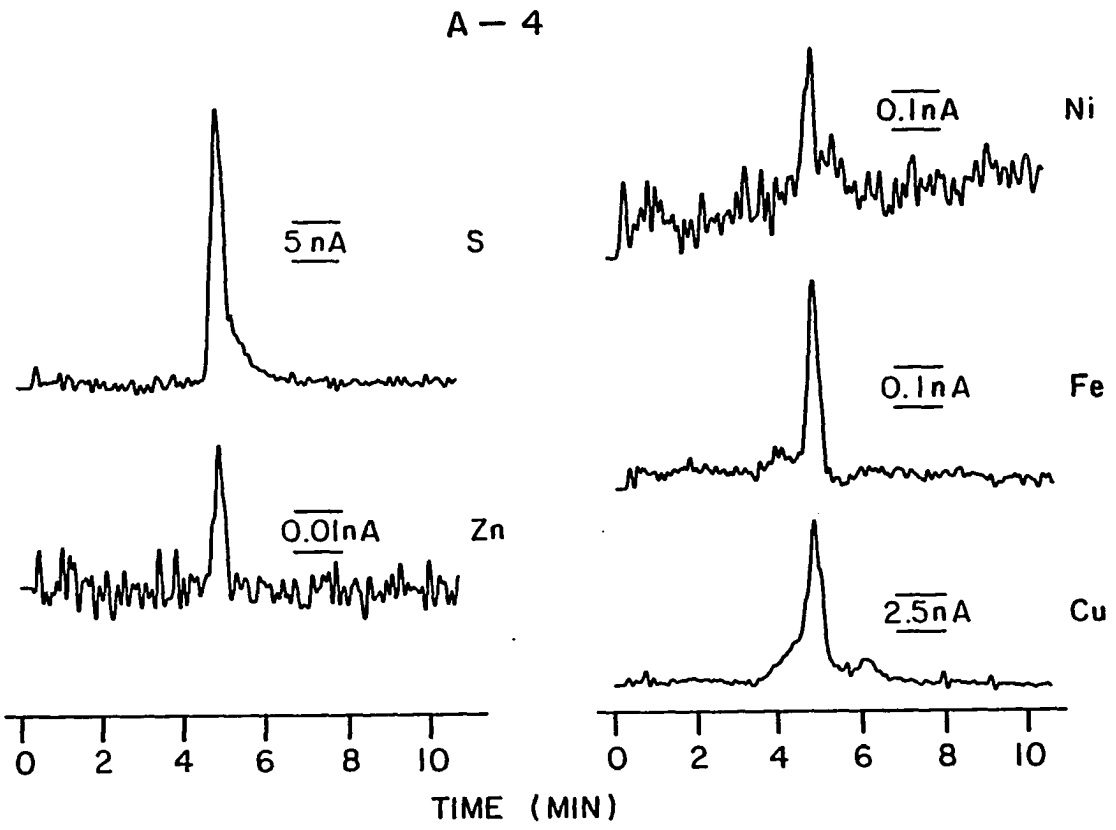

Figure 44. HPLC-DIN-ICP-AES element-specific chromatograms for Fraction A-4 from crude Paraho Shale Oil A
Mobile phase: (90/10) pyridine/water; column: Whatman Partisil 5 ODS-3 (4.2 mm i.d. x 250 mm L); flow rate: 0.7 mL/min (~15% to plasma); sample size: 100 μL

Unfortunately, pyridine yields relatively poor chromatographic resolution, even when modified with water. At water concentrations of greater than 10%, a visual precipitate forms in the fractions. Indeed, the separation of crude oils for the simultaneous detection of individual sulfur and organometallic species poses an intriguing problem whose solution would require endeavors beyond the intent of this investigation. Nevertheless, it has been clearly demonstrated that the ICP holds potential for the simultaneous multielement analysis of HPLC effluents when the DIN is used as an interface.

CHAPTER V. CONCLUSIONS AND SUMMARY

The analytical utility of the direct injection nebulizer as an interface for FIA and HPLC coupled with ICP-AES detection has been successfully demonstrated. The analytical figures of merit for the DIN when used as an interface for FIA-ICP-AES may be summarized as follows: 1) The limits of detection obtained by FIA with the DIN (30 μL) were comparable to those obtained by either FIA introduction of 200 μL or continuous sample introduction into a cross-flow pneumatic nebulizer; 2) the direct nebulization of 30 μL volumes provided overall reproducibility values comparable to those measured for cross-flow pneumatic (200 μL) and ultrasonic (500 μL) nebulization; 3) the absolute and relative LODs were comparable to or within the range of values reported for most microliter sample introduction techniques; 4) a linear response over 3 to 4 orders of magnitude was observed; and 5) the interelement effects were comparable in magnitude to conventional cross-flow pneumatic nebulization. However, two important questions remain to be addressed; 1) whether the DIN offers improvement in the HPLC-ICP-AES interface arrangement as compared to documented HPLC-ICP-AES approaches, and 2) whether the HPLC-DIN-ICP-AES approach offers improvement over other HPLC-atomic spectroscopic techniques.

In Table XV, the relative LODs for continuous flow- and HPLC-DIN-ICP-AES are compared to literature values reported for the various HPLC-atomic spectroscopic techniques. In this Table, LODs obtained by either preparatory-scale HPLC (64) or HPLC with subsequent hydride generation (29,36,88) interfaced to atomic spectroscopic detectors were omitted so

Table XV. Relative limits of detection (ng/mL) for FIA- and HPLC-DIN-ICP-AES as compared to literature values reported for several HPLC-atomic spectroscopic techniques

Element	Continuous-flow-DIN-ICP-AES	HPLC-DIN-ICP-AES	HPLC-FAAS	HPLC-GFAAS	HPLC-DCP-AES	HPLC-ICP-AES
S	100	164	—	—	—	1000 to 3000[a]
As	40	61 to 100	—	240[b] 2[d] 10[f] 250[h] 500[i]	—	130[c] 2600 to 2850[e] 1500 to 3100[g]
Se	52	42 to 71	—	—	—	280[j] 4550 to 7000[e]
Cr	12	20	—	—	5 to 15[k] 10,000 to 100,000[l]	20[j] 220,000 to 450,000[m]
Zn	2	4	30[n]	—	—	19[j]
Co	7	3	—	—	—	21[j]
Ni	15	5	—	—	—	43[j]
Cd	1	4	—	—	—	89[j] 120 to 350[g]

Cu	6	7	100 to 200[o]	—	—	6.8[j] 0.6[p] 3300[q]

[a]Reference 82.
[b]Reference 34.
[c]Reference 80.
[d]Reference 35.
[e]Reference 83.
[f]Reference 37.
[g]Reference 90.
[h]Reference 52.
[i]Reference 53.
[j]Reference 68.
[k]Reference 59.
[l]Reference 61.
[m]Reference 87.
[n]Reference 26.
[o]References 19, 20.
[p]Reference 69.
[q]Reference 96.

that comparisons could be made between various approaches in which analytical-scale HPLC was directly interfaced to the atomic spectroscopic detector. Many comparisons and conclusions can be drawn from Table XV. First, for the DIN interface, the LODs obtained in the HPLC-DIN-ICP-AES mode were either comparable to those obtained by continuous-flow sample introduction into the ICP, or inferior by up to only a factor of 4 (As). As stated in Chapter I, the use of conventional pneumatic nebulizers as an interface for HPLC-ICP-AES has led to deterioration in LODs of one or more orders of magnitude as compared to continuous sample introduction of unlimited sample volumes. Thus, the low dead volume (1.5 μL) associated with the DIN interface resulted in low or negligible extracolumn analyte dispersion. The analyte dispersion observed with the DIN interface is likely inherent in the HPLC methodology and is primarily attributed to retention of the analyte by the HPLC column. Second, the LODs obtained by HPLC-DIN-ICP-AES were generally superior to those values reported in the literature. As discussed in Chapter I, Gast et al. (69) reported very good LODs for HPLC-ICP-AES, but they cannot be reconciled. Irgolic et al. (80) reported a competitive value for As (130 μL), but it was obtained at the more intense 189.0 nm line of As and was found to be inferior by a factor of 8.7 as compared to continuous sample introduction of unlimited sample volumes. Although Fraley et al. (68) have reported reasonable LODs for several elements, these were obtained with a "dummy" column and do not adequately represent LODs that would have been obtained under actual HPLC separation conditions. It should also be noted that for half of the HPLC-ICP-AES publications, the authors have not even reported LODs for the species that were under investigation. Although the ICP has a

relatively low tolerance to common HPLC solvents, the DIN interface allows for the direct injection into the ICP of a variety of common HPLC solvents (up to 100% methanol, acetonitrile, MIBK, pyridine, and water) at variable flow rates (10 to 200 μL/min). Overall, therefore, it may be concluded that the DIN interface offers significant improvement in the HPLC-ICP-AES interface arrangement as compared to the conventional pneumatic nebulizer.

From Table XV, it can be seen that as compared to ICP-AES, the LODs reported for other HPLC-atomic spectroscopic techniques are limited. The LODs reported for HPLC-FAAS are inferior by greater than an order of magnitude as compared the the HPLC-DIN-ICP-AES approach. The LOD obtained for As (40 μL/mL) for the HPLC-DIN-ICP-AES approach was within the range of values reported for HPLC-GFAAS, but two very good HPLC-GFAAS values (35,37) were reported. As discussed in Chapter I, HPLC-GFAAS has yielded some of the most impressive LODs for metal speciation studies. Unfortunately, conventional GFAAS requires that the analytical process be executed "off-line", in a batch mode and results in a loss of chromatographic resolution. For HPLC-DCP-AES, there was one good entry (59); other LODs have either not been reported or are very poor. Therefore, it may be concluded that the HPLC-DIN-ICP-AES approach offers substantial improvement over other on-line, HPLC atomic spectroscopic techniques. However, the one exceptionally good value for Cr (59) suggests that the HPLC-DCP-AES approach should be critically evaluated.

CHAPTER VI. SUGGESTIONS FOR FUTURE RESEARCH

A significant potential exists for the investigation of other applications of the HPLC-DIN-ICP-AES facility. Metal speciation capabilities would no doubt be attractive to a host of researchers with environmental, industrial, pharmaceutical, toxicological, or biological interests. The identification of organometallics in many, if not all "real world" sample matrices has been a difficult task. The future should prove HPLC coupled with ICP-AES a useful tool in the identification of these compounds.

Several researches have shown that for pure solvents, the evaporation rate from pure solvent droplets is dependent on droplet size, diffusion coefficient of the solvent vapor, molecular weight, surface tension, solvent density, saturation vapor pressure, and temperature (192,193). An enhancement in analyte signals has been observed for relatively volatile compounds due to volatilization and enrichment of the solute during aerosol generation and transport processes associated with conventional sample introduction methods. Emission intensities increase strongly, with decreasing boiling point (increased volatility). For example, the quantitation of a mixture of several sulfur-containing compounds of varying volatility would be difficult, because the ICP detector response would be different for each compound. This should not happen with the direct injection nebulizer, as there is no chance of vapor enrichment during the nebulization process, because the analyte is directly injected into the axial channel of the plasma. This hypothesis is supported by the observation that the ICP detector response was approximately equal for the

peak area measurement of several species that contained a common element (e.g., As, Chapter IV). In fact, the DIN should yield the opportunity to devise a scheme for the determination of S, P, B, Br, Cl, and I (and possibly N and O) in organic compounds. The possibilities are exciting in that the potential would then exist for the determination of empirical formulae under high resolution, chromatographic conditions.

LITERATURE CITED

1. Manahan,S.E. "Environmental Chemistry", 3rd ed.; Willard Grant Press: Boston, MA, 1979.

2. Krull, I.S. In "Liquid Chromatography in Environmental Analysis", Lawrence, J.K., Ed.; Humana Press, Inc.: Clifton, N.J., 1983; Chapter 5.

3. Krull, I.S. Trends Anal. Chem. (1984) 3, 76-80.

4. Krull, I.S.; Jordan, S. Am. Lab. (1980) 12(10), 21-33.

5. Carnahan, J.W.; Mulligan, K.J.; Caruso, J.A. Anal. Chim. Acta (1981) 130, 227-241.

6. Jewett, K.L.; Brinckman, F.E. In "Detectors in Liquid Chromatography" Vickrey, T.M., Ed.; Marcel Dekker Publishers: New York, 1983.

7. Van Loon, J.C. Am. Lab. (1981) 13(5), 47-53.

8. Veening, H.; Willeford, B.R. Reviews in Inorganic Chemistry (1979) 1, 281-302.

9. Randall, L.G. Sep. Sci. Technol. (1982) 17, 1-118.

10. Gast, C.H.; Krask, J.C. J. Liq. Chromatogr. (1981) 4, 765-783.

11. Cassidy, R.M. In "Trace Analysis", Lawrence, J.F., Ed.; Academic Press, Inc.: New York, 1981.

12. Schwedt, G. Chromatographia (1978) 11, 145-148.

13. Schwedt, G. Chromatographia (1979) 12, 613-619.

14. Ettre, L.S. J. Chromatogr. Sci. (1978) 16, 396-417.

15. White, P.C. Analyst (1984) 109, 677-697.

16. Yoza, N.; Ohashi, S. Anal. Lett. (1973) 6, 595-601.

17. Manahan, S.E.; Jones, D.R.,IV Anal. Lett. (1973) 6, 745-753.

18. Botre, C.; Cacace, F.; Cozzani, R. Anal. Lett. (1976) 9, 825-830.

19. Jones, D.R., IV; Manahan, S.E. Anal. Chem. (1976) 48, 502-505.

20. Jones, D.R., IV; Manahan, S.E. Anal. Chem. (1976) 48, 1897-1899.

21. Koizumi, H.; Hadeishi, T.; McLaughlin, R. Anal. Chem. (1978) 50, 1700-1701.

22. Naranjit, D.; Thomassen, Y.; Van Loon, J.C. Anal. Chim. Acta (1979) 110, 307-312.

23. Renoe, B.W.; Shideler, C.E.; Savory, J. Clin. Chem. (1981) 27, 1546-1550.

24. Burns, D.T.; Glockling, F.; Harriott, M. Analyst (1981) 106, 921-930.

25. Messman, J.D.; Rains, T.C. Anal. Chem. (1981) 53, 1632-1636.

26. Ishii, M.; Kaji, K.; Yoko, A.O.; Ogino, T. Bunseki Kagaku (1984) 33, E335-E341.

27. Robinson, J.W.; Boothe, E.D. Spectrosc. Lett. (1984) 17, 673-688.

28. Robinson, J.W.; Boothe, E.D. Spectrosc. Lett. (1984) 17, 689-712.

29. Tye, C.T.; Haswell, S.J.; O'Neill, P.O.; Bancroft, K.C.C. Anal. Chim. Acta (1985) 169, 195-200.

30. Hill, S.J.; Ebdon, L. Eur. Spectrosc. News (1985) 58, 20-24.

31. Ebdon, L.; Hill, S.J.; Jones, P. Analyst (1985) 10, 515-517.

32. Van Loon, T.C.; Lichwa, J.; Radziuk, B. J. Chromatogr. (1977) 136, 301-305.

33. Siemer, D.D.; Koteel, P.; Haworth, D.T.; Taraszewski, W.J.; Lawson, S.R. Anal. Chem. (1971) 51, 575-579.

34. Brinckman, F.E.; Blair, W.R.; Jewett, K.L.; Iverson, W.P. J. Chromatogr. Sci. (1977) 15, 493-503.

35. Iverson, D.G.; Anderson, M.A.; Holm, T.R.; Stanforth, R.R. Environ. Sci. Technol. (1979) 13, 1491-1494.

36. Ricci, G.R.; Shepard, L.S.; Colovos, G.; Hester, N.E. Anal. Chem. (1981) 53, 610-613.

37. Gabinski, A.A. Anal. Chem. (1981) 53, 966-968.

38. Brinckman, F.E.; Jewett, K.L.; Iverson, W.P.; Irgolic, K.J.; Ehrhardt, K.C.; Stockton, R.A. J. Chromatogr. (1980) 191, 31-46.

39. Weiss, C.S.; Jewett, K.L.; Brinckman, F.E.; Fish, R.H. NBS Publication 618. NBS, Gaithersburg, MD, May 18-20, 1981 (Issued November 1981).

40. Fish, R.H.; Brinckman, F.E.; Jewett, K.L. Environ. Sci. Technol. (1982) 16, 174-179.

41. Weiss, C.S.; Parks, E.J.; Brinckman, F.E. In "Arsenic: Industrial, Biomedical, and Environmental Perspectives", Lederer, W.H.; Fensterheim, R.J., Eds.; Van Nostrand-Reinhold Co.: New York, 1982.

42. Brinckman, F.E.; Weiss, C.S.; Fish, R.H. In "Chemical and Geochemical Aspects of Fossil Fuel Extraction", Yen, T.F., Ed.; Ann Arbor Science Publishers: Ann Arbor, MI, 1983.

43. Brinckman, F.E.; Blair, W.R. NBS Publication 556. NBS, Gaithersburg, MD, November 29-30, 1977 (Issued September 1979).

44. Parks, E.J.; Brinckman, F.E.; Blair, W.R. J. Chromatogr. (1979) 185, 563-572.

45. Parks, E.J.; Brinckman, F.E.; Mullin, C.E.; Andersen, D.M.; Castelli, V.J. J. Appl. Polym. Sci. (1981) 26, 2967-2974.

46. Parks, E.J.; Brinckman, F.E. In "Controlled Release of Pesticides and Pharmaceuticals", Lewis, D.H., Ed.; Plenum Publishing Corp.: New York, 1981.

47. Jewett, K.L.; Brinckman, F.E. J. Chromatogr. Sci. (1981) 19, 583-593.

48. Chang, Y.; Sternson, L.A.; Repta, A.J. Anal. Lett. (1978) B11, 449-459.

49. Vickrey, T.M.; Buren, M.S.; Howell, H.E. Anal. Lett. (1978) A11, 1075-1095.

50. Kahn, N.; Van Loon, J.C. J. Liq. Chromatogr. (1979) 2, 23-36.

51. Koizumi, H.; McLaughlin, R.D.; Hadeishi, T. Anal. Chem. (1979) 51, 387-392.

52. Woolson, E.A.; Aharonson, N. J. Assoc. Off. Anal. Chem. (1980) 63, 523-528.

53. Iradevaia, R.; Aharonson, N.; Woolson, E.A. J. Assoc. Off. Anal. Chem. (1980) 63, 742-746.

54. Tittarelli, P.; Mascherpa, A. Anal. Chem. (1981) 53, 1466-1469.

55. Fish, R.H.; Komlenic, J.J. Anal. Chem. (1984) 56, 510-517.

56. Fish, R.H.; Komlenic, J.J.; Wines, B.K. Anal. Chem. (1984) 56, 2452-2460.

57. Billiet, H.A.H.; van Dalen, J.P.J.; Schoenmaker, P.J.; De Galen, L. Anal. Chem. (1983) 55, 847-851.

58. Ibrahim, M.; Nisamaneepong, W.; Caruso, J. J. Chromatogr. Sci. (1985) 23, 144-150.

59. Krull, I.S.; Panaro, K.W.; Gershman, L.L. J. Chromatogr. Sci. (1983) 21, 460-472.

60. Uden, P.C.; Bigley, I.E. Anal. Chim. Acta (1977) 94, 29-34.

61. Uden, P.C.; Quimby, B.D.; Barnes, R.M.; Elliott, W.G. Anal. Chim. Acta (1978) 101, 99-109.

62. Uden, P.C.; Bigley, I.E.; Walters, F.H. Anal. Chim. Acta (1978) 100, 555-561.

63. Koropchak, J.A.; Coleman, G.N. In "Developments in Atomic Plasma Spectrochemical Analysis", Barnes, R.M., Ed.; Heyden and Sons, Inc.: New York, 1982.

64. Gardiner, P.E.; Bratter, P.; Negretti, V.E.; Schulze, G. Spectrochim. Acta, Part B (1983) 38B, 427-436.

65. Mazzo, D.J.; Elliott, W.G.; Uden, P.C.; Barnes, R.M. Appl. Spectrosc. (1984) 38, 585-590.

66. Biggs, W.R.; Gano, J.T.; Brown, R.J. Anal. Chem. (1984) 56, 2653-2657.

67. Kirkman, G.M.; Zu-Ben, C.; Uden, P.C.; Stratton, W.J.; Henderson, D.E. J. Chromatogr. (1984) 317, 569-578.

68. Fraley, D.M.; Yates, D.; Manahan, S.E. Anal. Chem. (1979) 51, 2225-2229.

69. Gast, C.H.; Kraak, J.C.; Poppe, H.; Maessen, F.J.M.J. J. Chromatogr. (1979) 185, 549-561.

70. Morita, M.; Uehiro, T.; Fuwa, K. Anal. Chem. (1980) 52, 349-351.

71. Hausler, D.W.; Talyor, L.T. Anal. Chem. (1981) 53, 1223-1227.

72. Taylor, L.T.; Hausler, D.W.; Squires, A.M. Science (1981) 213, 644-646.

73. Hausler, D.W.; Taylor, L.T. Anal. Chem. (1981) 53, 1227-1231.

74. Morita, M.; Uehiro, T.; Fuwa, K. Anal. Chem. (1981) 53, 1806-1808.

75. Morita, M.; Uehiro, T. Anal. Chem. (1981) 53, 1997-2000.

76. Fraley, D.M.; Yates, D.A.; Manahan, S.E.; Stalling, D.; Petty, J. Appl. Spectrosc. (1981) 35, 525-531.

77. Heine, D.R.; Denton, M.B.; Schlabach, T.D. Anal. Chem. (1982) 54, 81-84.

78. Whaley, B.S.; Snable, K.R.; Browner, R.F. Anal. Chem. (1982) 54, 162-165.

79. Gardner, W.S.; Landrum, P.F.; Yates, D.A. Anal. Chem. (1982) 54, 1198-1200.

80. Irgolic, K.J.; Stocton, R.A.; Chakraborti, D.; Beyer, W. Spectrochim. Acta, Part B (1983) 38B, 437-445.

81. Jinno, K.; Tsuchida, H.; Nakanishi, S.; Hirata, Y.; Fujimoto, C. Appl. Spectrosc. (1983) 37, 258-261.

82. Yoshida, K.; Hasegawa, T.; Haraguchi, H. Anal. Chem. (1983) 55, 2106-2108.

83. McCarthy, J.P.; Caruso, J.A.; Fricke, F.L. J. Chromatogr. Sci. (1983) 21, 389-393.

84. Ibrahim, M.; Gilbert, T.W.; Caruso, J.A. J. Chromatogr. Sci. (1984) 22, 111-115.

85. Bushee, D.; Krull, I.S.; Savage, R.N.; Smith, S.B., Jr. J. Liq. Chromatogr. (1982) 5, 463-478.

86. Bushee, D.; Young, D.; Krull, I.S.; Savage, R.N.; Smith, S.B., Jr. J. Liq. Chromatogr. (1982) 5, 693-706.

87. Krull, I.S.; Bushee, D.; Savage, R.N.; Schleicher, R.G.; Smith, S.B., Jr. Anal. Lett. (1982) 15, 267-281.

88. Bushee, D.S.; Krull, I.S.; Demko, P.R.; Smith, S.B., Jr. J. Liq. Chromatogr. (1984) 7, 861-876.

89. Jinno, K.; Nakanishi, S.; Nagoshi, T. Anal. Chem. (1984) 56, 1977-1979.

90. Nisamaneepong, W.; Ibrahim, M.; Gilbert, T.W.; Caruso, J.A. J. Chromatogr. Sci. (1984) 22, 473-477.

91. Jinno, K.; Nakanishi, S.; Nagoshi, T. Chromatographia (1984) 18, 437-440.

92. Yoshida, K.; Haraguchi, H. Anal. Chem. (1984) 56, 2580-2585.

93. Hausler, D.W. Spectrochim. Acta, Part B (1985) 40B, 389-396.

94. Ibrahim, M.; Nisamaneepong, W.; Haas, D.L.; Caruso, J.A. Spectrochim. Acta, Part B (1985) 40B, 367-376.

95. Aulis, R.; Bolton, A.; Doherty, W.; Vret, A.V.; Wong, P. Spectrochim. Acta, Part B (1985) 40B, 377-387.

96. Jinno, K.; Nakanishi, S.; Fujimoto, C. Anal. Chem. (1985) 57, 2229-2235.

97. Olsen, E.D. "Modern Optical Methods of Analysis", McGraw-Hill Book Co.: New York, 1975.

98. Horvath, J.J. Master's Thesis, University of Florida, 1980.

99. Sturgeon, R.E.; Chakrabarti, C.L. Spectrochim. Acta, Part B (1977) 32B, 231-255.

100. Sturgeon, R.E.; Chakrabarti, C.L. Anal. Chem. (1977) 49, 1100-1106.

101. Skogerboe, R.K.; Coleman, G.N. Anal. Chem. (1976) 48, 611A-620A.

102. Greenfield, S.; McGeachin, H. McD.; Smith, P.B. Talanta 22, 553-562.

103. Fassel, V.A. XVI Colloquium Spectroscopicum Internationale, Heidelburg, Adam Hilger Ltd.: London, England, 1971 (Plenary Lectures).

104. McCormack, A.J.; Tong, S.C.; Cooke, W.D. Anal. Chem. (1965) 37, 1470-1476.

105. Quimby, B.D.; Uden, P.C.; Barnes, R.M. Anal. Chem. (1978) 50, 2112-2118.

106. Quimby, B.D.; Delaney, M.F.; Uden, P.C.; Barnes, R.M. Anal. Chem. (1979) 51, 875-880.

107. Quimby, B.D.; Delaney, M.F.; Uden, P.C.; Barnes, R.M. Anal. Chem. (1980) 52, 259-263.

108. Lichte, F.E.; Skogerboe, R.K. Anal. Chem. (1973) 45, 399-401.

109. Skogerboe, R.K.; Coleman, G.W. Appl. Spectrosc. (1976) 30, 504-507.

110. Beenakker, C.I.M. Spectrochim. Acta, Part B (1976) 31B, 483-486.

111. Beenakker, C.I.M.; Bosman, B.; Boumans, P.W.J.M. Spectrochim. Acta, Part B (1978) 33B, 373-381.

112. Haas, D.L.; Carnahan, J.W.; Caruso, J.A. Appl. Spectrosc. (1983) 37B, 82-85.

113. Winge, R.K.; Peterson, V.J.; Fassel, V.A. Appl. Spectrosc. (1979) 33, 206-219.

114. Bollo-Kamara, A.; Codding, E.G. Spectrochim. Acta, Part B (1981) 36B, 973-982.

115. Kollotzek, D.; Tschopel, P.; Tolg, G. Spectrochim. Acta, Part B (1982) 37B, 91-96.

116. Kollotzek, D.; Tschopel, P.; Tolg, G. Spectrochim. Acta, Part B (1984) 39B, 625-636.

117. Panaro, K.W.; Krull, I.S. Anal. Lett. (1984) 17, 157-172.

118. Mazzo, D.J.; Elliott, W.G.; Uden, P.C.; Barnes, R.M. Appl. Spectrosc. (1984) 38, 585-589.

119. Greenfield, S.; McGeachin, H. McD.; Smith, P.B. Talanta (1976) 23, 1-14.

120. Fassel, V.A. Science (1978) 202, 183-191.

121. Fassel, V.A. Anal. Chem. (1979) 51, 1290A-1308A.

122. Browner, R.F.; Boorn, A.W. Anal. Chem. (1984) 56, 786A-798A.

123. Browner, R.F.; Boorn, A.W. Anal. Chem (1984) 56, 875A-888A.

124. Browner, R.F. Trends Anal. Chem. (1983) 2, 121-124.

125. Boorn, A.W.; Browner, R.F. Anal. Chem (1982) 54, 1402-1410.

126. Nisamaneepong, W.; Haas, D.L.; Caruso, J.A. Spectrochim. Acta, Part B (1985) 40B, 3-10.

127. Vestal, M.L. Mass Spectrom. Rev. (1983) 2, 447-480.

128. Blakley, C.R.; Vestal, M.L. Anal. Chem. (1983) 50, 750-754.

129. Blakley, C.R.; Carmody, J.J.; Vestal, M.L. Anal. Chem. (1980) 52, 1636-1641.

130. Meyer, G.A.; Roeck, J.S.; Vestal, M.L. ICP Inform. Newsl. (1985) 10, 955-963.

131. Doherty, M.P.; Hieftje, G.M. Appl. Spectrosc. (1984) 38, 405-412.

132. Hulmston, P. Analyst (1983) 108, 166-170.

133. Hulmston, P.; McKillop, S. Analyst (1985) 110, 559-562.

134. Zhuang, H.Z.; Barnes, R.M. Spectrochim. Acta, Part B (1985) 40B, 11-19.

135. Ibrahim, M.; Nisamaneepong, W.; Caruso, J.A. J. Chromatogr. Sci. (1985) 23, 144-150.

136. Greenfield, S. Ind. Res. Dev. (1981) 21(8), 140-145.

137. Greenfield, S. Spectrochim. Acta, Part B (1983) 38B, 93-105.

138. Eckels, D.E. (Ames Laboratory, Iowa State University, Ames, IA).

139. Kniseley, R.N.; Amenson, H.; Butler, C.C.; Fassel, V.A. Appl. Spectrosc. (1974) 28, 285-286.

140. Scott, R.H.; Fassel, V.A.; Kniseley, R.N.; Nixon, D.E. Anal. Chem. (1974) 46, 75-80.

141. Bear, B.R., M.S. Thesis, Iowa State University, Ames, Iowa, 1983.

142. Olsen, K.W.; Haas, W.J., Jr.; Fassel, V.A. Anal. Chem. (1977) 49, 632-637.

143. Butterworth, S. Wireless Engineer (1930) 7, 536-541.

144. Oppenheim, A.V.; Schafer, R.W. "Digital Signal Processing", Prentice-Hall Inc.: Englewood Cliffs, NJ, 1975.

145. Larson, G.F.; Fassel, V.A.; Scott, R.H.; Kniseley, R.N. Anal. Chem. (1975) 47, 238-243.

146. Ruzicka, J.; Hansen, E.H. "Flow Injection Analysis", Wiley-Interscience: New York, 1981.

147. Broekaert, J.A.C.; Leis, F. Anal. Chim. Acta (1979) 109, 73-83.

148. Broekaert,J.A.C.; Leis, F.; Laqua, K. Fresenius Z. Anal. Chem. (1980) 301, 105-106.

149. Sobel, C.B. Appl. Spectrosc. (1984) 38, 444-447.

150. Faske, A.J.; Snable, K.R.; Boorn, A.W.; Browner, R.F. Appl. Spectrosc. (1985) 39, 542-545.

151. Swaidan, H.M.; Christian, G.C. Anal. Chem. (1984) 56, 120-122.

152. Aziz, A.; Broekaert, J.A.; Leis, F. Spectrochim. Acta, Part B (1982) 37B, 369-379.

153. Crabi, G.; Cavalli, P.; Achilli, M.; Rossi, G.; Omenetto, M. At. Spectrosc. (1982) 3, 81-88.

154. Gunn, A.M.; Millard, D.L.; Kirkbright, G.F. Analyst (1978) 103, 1066-1073.

155. Ng, K.C.; Caruso, J.A. Anal. Chim. Acta (1982) 143, 209-222.

156. Long, S.E.; Snook, R.D.; Browner, R.F. Spectrochim. Acta, Part B (1985) 40B, 553-568.

157. Matusiewitz, H.; Horvath, Z.; Barnes, R.M. Appl. Spectrosc. (1985) 39, 558-560.

158. Matusiewitz, H.; Barnes, R.M. Appl. Spectrosc. (1985) 39, 715-718.

159. Dahlquist, R.L.; Knoll, J.W.; Hojt, R.E. (Paper presented at the Twenty-first Canadian Spectroscopy Symposium Ottawa, ONT., Canada, October 7-9, 1974).

160. Nixon, D.E.; Fassel, V.A.; Kniseley, R.N. Anal. Chem. (1974) 46, 210-213.

161. Tikkanen, M.W.; Niemczyk, T.M. Anal. Chem. (1984) 56, 1997-2000.

162. Abdullah, M.; Fuwa, K.; Haraguchi, H Spectrochim. Acta, Part B (1984) 39B, 1129-1139.

163. Kirkbright, G.F.; Walton, S.J. Analyst (1982) 107 276-281.

164. Kirkbright, G.F.; Li-Xing, Z. Analyst (1982) 107, 617-622.

165. Salin, E.D.; Sing, R.L.A. Anal. Chem. (1984) 56, 2596-2598.

166. Hermann, R.; Alkemade, C.Th.J.; Gilbert, P.T. "Chemical Analysis by Flame Photometry", Interscience: New York, 1963.

167. Fassel, V.A.; Becker, D.A. Anal. Chem. (1969) 41, 1522-1526.

168. Fukushima, S. Mikrochim. Acta (1959) 596-618.

169. Alkemade, C.Th.J. Anal. Chem. (1966) 38, 1252-1253.

170. Browner, R.F.; Boorn, A.W.; Smith, D.D. Anal. Chem. (1982) 54, 1411-1419.

171. Nukiyama, S.; Tanasawa, Y. "Experiments on the Atomization of Liquids in an Air Stream", E. Hope, Transl.; Defense Research Board, Department of National Defense: Ottawa, Canada, 1950.

172. May, K.R. J. Sci. Instrum. (1950) 27, 128-130.

173. Hieftje, G.M.; Malmstadt, H.V. Anal. Chem. (1968) 40, 1860-1867.

174. "Medical and Biological Effects of Environmental Pollutants: Arsenic", National Academy of Sciences, Washington, D.C., 1977, pp. 195-215.

175. Pershagen, G. Environ. Health Persp. (1981) 40, 93-100.

176. Filby, R.H. In "The Role of Trace Metals in Petroleum", Yen, T.F., Ed.; Ann Arbor Science Publishers, Inc.: Ann Arbor, MI, 1974, pp. 31-58.

177. Yen, T.F. In "The Role of Trace Metals in Petroleum", Yen, T.F., Ed.; Ann Arbor Science Publishers, Inc.: Ann Arbor, MI, 1974, pp. 1-29.

178. Whitehurst,D.D.; Mitchell, T.O.; and Farcasiu, M. In "Coal Liquifaction. The Chemistry and Technology of Thermal Processes", Academic Press: New York, 1980.

179. Fish, R.H.; Brinckman, F.E.; Jewett, K.L. Environ. Sci. Technol. (1982) 16, 174-179.

180. Yen, T.F.; Chilingarian, G.V., Eds. "Developments in Petroleum Science", Elsevier: Amsterdam, 1976; Vol. 5.

181. Fruchter, J.S.; Laul, J.C.; Petersen, M.R.; Ryan, P.W., Meeting of the American Chemical Society, New Orleans, March 20-25, 1977.

182. Masciantonio, P.X. Fuel (1965) 44, 269-275.

183. Markuszewski, D.R.; Mroch, G.A.; Norton, G.A.; Straszheim, W.E. Am. Chem. Soc. Div. of Fuel Chem. Preprints (1985) 30(2), 41-48.

184. Chiotti, P.; Markuszewski, R. Ind. Eng. Chem., Process Des. and Dev. (in press).

185. Chriswell, C., Ames Laboratory-USDOE, Ames, IA 50011, (Private Communication).

186. Fossil Energy Group, Ames Laboratory-USDOE, Ames, IA 50011 (Unpublished Results).

187. Rice, G.W.,; D'Silva, A.P.; Fassel, V.A. Spectrochim. Acta, Part B (1985) 40B, 1573-1584.

188. Brinckman, F.E.; Weiss, C.S.; Fish, R.H. In "Chemical and Geochemical Aspects of Fossil Fuel Extraction", Yen, T.F., Ed.; Ann Arbor Science Publ.: Ann Arbor, MI, 1983.

189. Ind. Res. Dev. (1983) 25(3), 77-78.

190. Farcasiu, M. Fuel (1977) 56, 9-14.

191. Later, D.W.; Lee, M.L.; Bartle, K.D.; Kong, R.C.; Vassilaros, D.L. Anal. Chem. (1981) 53, 1612-1620.

192. Boorn, A.W.; Cresser, M.S.; Browner, R.F. Spectrochim. Acta, Part B (1980) 35B, 823-832.

193. Cresser, M.S. Prog. Analyst. At. Spectrosc. (1982) 5, 35-62.

194. Boumans, P.W.J.M.; DeBoer, F.J. Spectrochim. Acta, Part B (1976) 31B, 355-375.

195. Kalnicky, D.J.; Kniseley, R.N.; Fassel, V.A. Spectrochim. Acta, Part B (1975) 30B, 511-525.

196. Alder, J.F.; Bombelka, R.M.; Kirkbright, G.F. Spectrochim. Acta, Part B (1980) 35B, 163-175.

197. Kirkbright, G.F. In "Developments in Atomic Plasma Spectrochemical Analysis", Barnes, R.M., Ed.; Heyden and Sons, Inc.: New York, 1982.

198. Jarosz, J.; Mermet, J.M.; Robin, J.P. Spectrochim. Acta, Part B (1978) 33B, 55-78.

199. Kornblum, G.R.; deGalen, L. Spectrochim. Acta, Part B (1977) 32B, 71-96.

200. Kalnicky, D.J.; Fassel, V.A.; Kniseley, R.N. Appl. Spectrosc. (1977) 31, 137-150.

201. Blades, M.W. Spectrochim. Acta, Part B (1982) 37B, 869-879.

202. Mermet, J.M. Spectrochim. Acta, Part B (1975) 30B, 383-396.

203. Mermet, J.M.; Jarosz, J.; Robin, J.P. Preprints 17th Coll. Spectrosc. Int., Florence (1973), 1, p. 101.

204. Mermet, J.M. Ph.D. Dissertation, University of Lyon (1974).

205. Alder, F.; Mermet, J.M. Spectrochim. Acta, Part B (1973) 28B, 421-433.

206. Jarosz, J.; Mermet, J.M., Robin, J.P. C. R. Acad. Sci. Paris B (1974) 278, p. 885.

207. Kornblum, G.R.; deGalen, L. Spectrochim. Acta, Part B (1974) 29B, 249-261.

208. Visser, K.; Hamm, F.H.; Zeeman, P.B. Appl. Spectrosc. (1976) 30, 34-38.

209. Eckert, H.U.; Pridmore-Brown, D.C. J. Appl. Phys. (1971) 42, 5051-5054.

210. Scholz, P.D.; Anderson, T.P. J. Quant. Spectrosc. Radiative Transfer (1968) 8, 1411-1418.

211. Stokes, A.D. J. Phys. D: Appl. Phys. (1971) 4, 916-929.

212. Miller, R.C.; Ayen, R.J. J. Appl. Phys. (1969) 40, 5260-5273.

213. "Radiation of Hot Gases (thermal and non-thermal)", In Plasma Diagnostics Lochte-Holtgreven, W., Ed.; North-Holland, Amsterdam (1968).

214. Faires, L.M., Palmer, B.A.; Engleman, R., Jr.; Niemczyk, T.M. Spectrochim. Acta, Part B (1984) 39B, 819-828.

215. Fuhr, J.R.; Martin, G.A.; Wiese, W.L.; Younger, S.M. J. Phys. Chem. Ref. Data (1981) 10, 305-387.

216. Bridges, J.M.; Kornblith, R.L. Astrophys. J. (1974) 192, 793-812.

217. Banfield, F.P.; Huber, M.C.E. Astrophys. J. (1973) 186, 335-346.

218. Blackwell, D.E.; Ibbetson, P.A.; Petford, A.D.; Shallis, M.J. Mon. Not. R. Astr. Soc. (1979) 186, 633-650.

219. Blackwell, D.E.; Petford, A.D.; Shallis, M.J. Mon. Not. R. Astr. Soc. (1979) 186, 657-668.

220. Blackwell, D.E.; Collins, B.S. Mon. Not. R. Astr. Soc. (1972) 157, 255-271.

221. Blackwell, D.E.; Ibbetson, P.A.; Petford, A.D. Mon. Not. R. Astr. Soc. (1975) 177, 195-208.

222. Blackwell, D.E.; Ibbetson, P.A.; Petford, A.D. Mon. Not. R. Astr. Soc. (1976) 177, 219-226.

223. Blackwell, D.E.; Shallis, M.J. Mon. Not. R. Astr. Soc. (1979) 186, 669-672.

224. Blackwell, D.E.; Petford, A.D.; Shallis, M.J.; Simmons, G.J. Mon. Not. R. Astr. Soc. (1980) 191, 445-450.

225. Reif, I.; Fassel, V.A.; Kniseley, R.N.; Kalnicky, D.J. Spectrochim. Acta, Part B (1978) 33B, 807-815.

226. Reif, I.; Fassel, V.A.; Kniseley, R.N. Spectrochim. Acta, Part B (1976) 31B, 377-384.

227. Reif, I.; Fassel, V.A.; Kniseley, R.N. Spectrochim. Acta, Part B (1973) 28B, 105-123.

ACKNOWLEDGEMENTS

I would like to gratefully acknowledge the support and encouragement extended by Dr. Velmer Fassel during the course of the study. His critical review of my work is greatly appreciated.

I would especially like to acknowledge the contributions of three colleagues: Gary Rice, for his involvement in the conception and design of the DIN; Dave Eckels, for the design and development of the simultaneous multielement data aquisition system; and Colin Chriswell, for his guidance in the HPLC separation of the energy-related materials.

The contributions of Harold Hall, Harry Amenson, and Gary Wells are acknowledged.

Tammy Eick's patience in the preparation of the figures for this dissertation is also gratefully acknowledged.

Warm thoughts are extended to all of the many friends I have met during the course of this study; those that have moved on and those that remain in the Ames area. Special thanks are extended to Laura and her pigs.

Special thanks are extended to my parents, Billie and Dean Lawrence, for their support and encouragement throughout all of my endeavors.

Warm thoughts are also extended to my grandparents, William and Frances Hejnosz.

Finally, I wish to thank my husband, Bryant LaFreniere, for the support, friendship, and love that he has given me throughout this arduous task. I will never forget all of the time he spent quizzing me before

prelims and the unselfish effort that he put into typing this dissertation. Thank you.

APPENDIX A. COMPILATION OF ACRONYMS

AcN	acetonitrile
ADP	adenosine diphosphate
AES	atomic emission spectroscopy
AFS	atomic fluorescence spectroscopy
AMP	adenosine monophosphate
ATP	adenosine triphosphate
CMP	cytidine monophosphate
DCP	direct current plasma
DIN	direct injection nebulizer
DMA	dimethylarsonate
DMAA	dimethylarsinic acid
DMDEL	dimethyldiethyllead
EC	electrochemical
EDTA	(ethylenedinitrilo)tetraacetate
EtOH	ethanol
FAAS	flame atomic absorption spectroscopy
FI	flame ionization
FIA	flow injection analysis
FL	fluorescence
GC	gas chromatography
GFAAS	graphite furnace atomic absorption spectroscopy
HPLC	high performance liquid chromatography
IC	ion chromatography
ICP	inductively coupled plasma
IP	ion pair

IR	infrared
LC	liquid chromatography
LOD	limit of detection
MeOH	methanol
METL	methyltriethyllead
MIBK	methylisobutyl ketone
MIP	microwave induced plasma
MMA	monomethylarsenate
MMAA	monomethylarsonic acid
MMDD	mass median droplet diameter
NH_4OAc	ammonium acetate
NP	normal phase
NTA	nitrilotriacetate
ODS	octadecylsilyl
PY	pyridine
RI	refractive index
RP	reverse phase
SEC	size exclusion chromatography
SEP	single electrode plasma
SESC	sequential elution by solvents chromatography
SMDD	Sauter median droplet diameter
SRC	solvent refined coal
TBAP	tetrabutylammonium phosphate
TBT	tributyltin
TCA	trichloroacetic acid
TEL	tetraethyllead

TMEL	trimethylethyllead
TML	tetramethyllead
UMP	uridine monophosphate
USN	ultrasonic nebulizer
UV	ultraviolet

APPENDIX B. PLASMA EXCITATION TEMPERATURE MEASUREMENTS

Introduction

As discussed in Chapter I, the inductively coupled plasma (ICP) has proven to be a valuable excitation source for atomic emission spectroscopy, although current methods of sample introduction severely constrain the ultimate relative limits of detection achievable, due to inefficient participation of the original sample in the total analytical process. The direct injection nebulizer (DIN) has been shown to exhibit analytical merit as an alternative method of sample introduction for flow injection into an ICP (Chapter III). In a comparison of the limits of detection realized with conventional pneumatic, direct injection, and ultrasonic nebulization into an ICP (Chapter III), the DIN yielded limits of detection (LODs) comparable to those obtained with the pneumatic nebulizer, but fell short of the expected improvement when evaluated on the following basis.

The differences in the mass flow rates into an ICP among the conventional pneumatic nebulizer, DIN, and ultrasonic nebulizers (USN) with and without subsequent aerosol desolvation are summarized in Table B-I. These rates were based upon the indicated uptake rates and overall efficiencies for aerosol formation, transport, and injection. The considerably greater overall efficiency of aerosol formation and transport for the DIN as compared to the conventional pneumatic nebulizer suggests that an approximate 10 to 15-fold improvement in the LODs should be realized with the DIN. These expectations, however, were not realized. An analogous situation prevails for the USN without subsequent aerosol

Table B-I. Rates of aerosol injection into an ICP for several nebulizers

Nebulizer	Efficiency (%)	Typical solution uptake rates (mL/min)	Nominal rate of mass flow (μL of H_2O/min)
Conventional pneumatic	1 to 2	1 to 2	10 to 40
Direct injection	100	0.1 to 0.15	100 to 150
Ultrasonic without aerosol desolvation	10 to 20	1 to 2	100 to 400
Ultrasonic with aerosol desolvation	10 to 20	1 to 2	0.016 to 0.032[a]

[a]Reference 141.

desolvation when compared with the conventional pneumatic nebulizer. Although the rate of mass flow for the USN without subsequent aerosol desolvation is approximately 10-fold greater as compared to the conventional pneumatic nebulizer, the corresponding improvement in the LODs has not been realized (142, herein Table VII).

The results of several studies have implied that "cooling" of the excitation temperature in the axial channel occurs with increased mass flow rates of water through the plasma (122,123,125,142,194,195). Alder et al. (196) and Kirkbright (197) reported an increase in the excitation temperature experienced by an analyte species in the presence of small quantities of water vapor, but speculated that when ultrasonic nebulization is used without subsequent aerosol desolvation, the higher rates of water transport may result in lower excitation temperatures.

As a part of this thesis investigation, the impact of different rates of mass transport of an aqueous aerosol on the vertical excitation temperatures experienced by an analyte species in the axial channel of an ICP were evaluated. A conventional pneumatic nebulizer, the direct injection nebulizer, and ultrasonic nebulizers with and without subsequent aerosol desolvation were the modes of sample introduction studied. Analyte excitation temperatures were measured as a function of observation height above the load coil, at 1200 W incident power.

Theoretical Considerations

To date the measurement of excitation temperatures experienced by an analyte species in the ICP is considered a difficult task. Invariably, criticism as to the validity of a temperature measurement arises from two

principle points: 1) whether or not local thermodynamic equilibrium (LTE) can be assumed to exist in the ICP, and 2) the questionable reliability of transition probability values. As arguments both for and against the existence of LTE in the plasma have been well-documented (195,196,198-213), the question clearly has not been resolved and spectroscopic methods, combined with Boltzman energy distributions continue to be employed for the measurement of excitation temperature in the ICP. The reliability of transition probability values has been addressed in a recent publication (214), where reference is made to a critical compilation of atomic transition probabilities for iron (215). In this compilation, the measured oscillator strength (f) values from Bridges and Kornblith (216) and Banfield and Huber (217) were considered to be quite good, and those of Blackwell et al. (218-224) were thought to be of outstanding accuracy. Because the oscillator strength of an emitted spectral line is proportional to its transition probability, it follows that the transition probabilities reported by the aforementioned authors (216-224) are also reliable. The transition probability values used in this study are those of Reif et al. (225). One report (198) suggests that the values of Reif et al. (225) appear to give higher and less accurate temperatures. The use of the transition probabilities of Reif et al. (225) can be justified as shown in Table B-II, in which the values of Reif et al. (225) are in good agreement with the highly regarded values of Bridges and Kornblith (216) and Blackwell et al. (218,219).

Neutral iron was selected as the thermometric species for reasons discussed in previous reports (195,214,226). For the present work, the Fe I three-line set recommended by Kalnicky et al. (195) was selected for

Table B-II. Emission line data

Wavelength (nm)	Excitation Energy (cm^{-1})	Statistical Weight (g_q)	Relative Transition Probabilities[a] RFKK[b]	BK[c]	BKWL[d]
382.043	33096	9	0.638	0.685	0.668
382.444	26140	7	0.028	---	0.0283
382.588	33507	7	0.567	0.651	0.598

[a]Relative transition probabilities normalized to the Fe I 371.994 nm line by $A_{371.994}$= 0.163.

[b]Reference 225.

[c]Reference 216.

[d]References 218, 219.

excitation temperature measurements. The wavelengths of the individual lines, their excitation energies, statistical weights of the upper level, and relative transition probabilities are summarized in Table B-II.

The "slope" method, chosen for excitation temperature measurement in this study, is based on the measurement of integrated line intensities for a number of transitions between different energy levels of the thermometric species (Fe) in the absence of self-absorption effects (195,200,227). A plot of $\ln(g_q A_{qp} \nu_0 / B_{(em)})$ vs. E_q using several spectral lines will yield a straight line with slope equal to $1/kT_f$; where g_q is the statistical weight of the emitting level, A_{qp} is the transition probability for spontaneous emission, ν_0 is the frequency of the emission transition, $B_{(em)}$ is the emission intensity of the transition $q \rightarrow p$, E_q is the energy of the emitting level, k is the Boltzman constant, and T_f is the analyte excitation temperature. The "slope" method requires that the assumption that LTE exists in the ICP be valid. Uncertainties in the calculated temperatures should be relatively small (~10%), because small errors in intensity measurement or in the transition probability for one of the lines will not greatly influence the calculated value of the excitation temperature determined by a measurement of slope. Abel inverted (axial radial) temperature calculations were not deemed necessary, as it has been shown that at 1000 to 1200 W incident power and for observation points low in the plasma (20 mm or below), non-inverted (lateral) values provide a reasonably accurate description of excitation temperatures experienced by the analyte species (195,199).

Experimental Apparatus and Procedures

The thermometric species (Fe) was nebulized into the plasma as a 150 μg/mL Fe solution. The spectral region of interest (382.0 nm to 382.7 nm) was scanned (0.5 nm/min) in triplicate for each observation height (14, 16, 18, and 20 mm above the load coil) at 1200 W incident power. The relative intensities (determined as peak heights) represent the average of these three measurements.

The operating conditions and facilities employed for this study are the same as those given in Table IV (Chapter II). Direct injection, pneumatic, and ultrasonic (with and without aerosol desolvation) nebulizers were used as modes of sample presentation to the plasma. The direct injection, pneumatic, and ultrasonic nebulizers and their mode of operation have been discussed in Chapters I and II, as well as elsewhere (139-142). For temperature studies that involved the ultrasonic nebulizer without subsequent aerosol desolvation, the desolvation train was replaced by an approximately 20 inch length of 1/2 inch i.d. Tygon tubing.

Results and Discussion

The variation of Fe I excitation temperatures for the four modes of nebulization studied as a function of observation height above the load coil at a constant incident power (1200 W) is illustrated in Figure B-1. In view of the many variables intrinsic to each mode of nebulization (e.g., rate of mass transport, aerosol partical size distribution, nebulizer gas flow rate, and nebulizer gas velocity) the interpretation of the results presented in Figure B-1 is necessarily conservative. Some insight, however, can be gained as to why the LODs obtained with the DIN

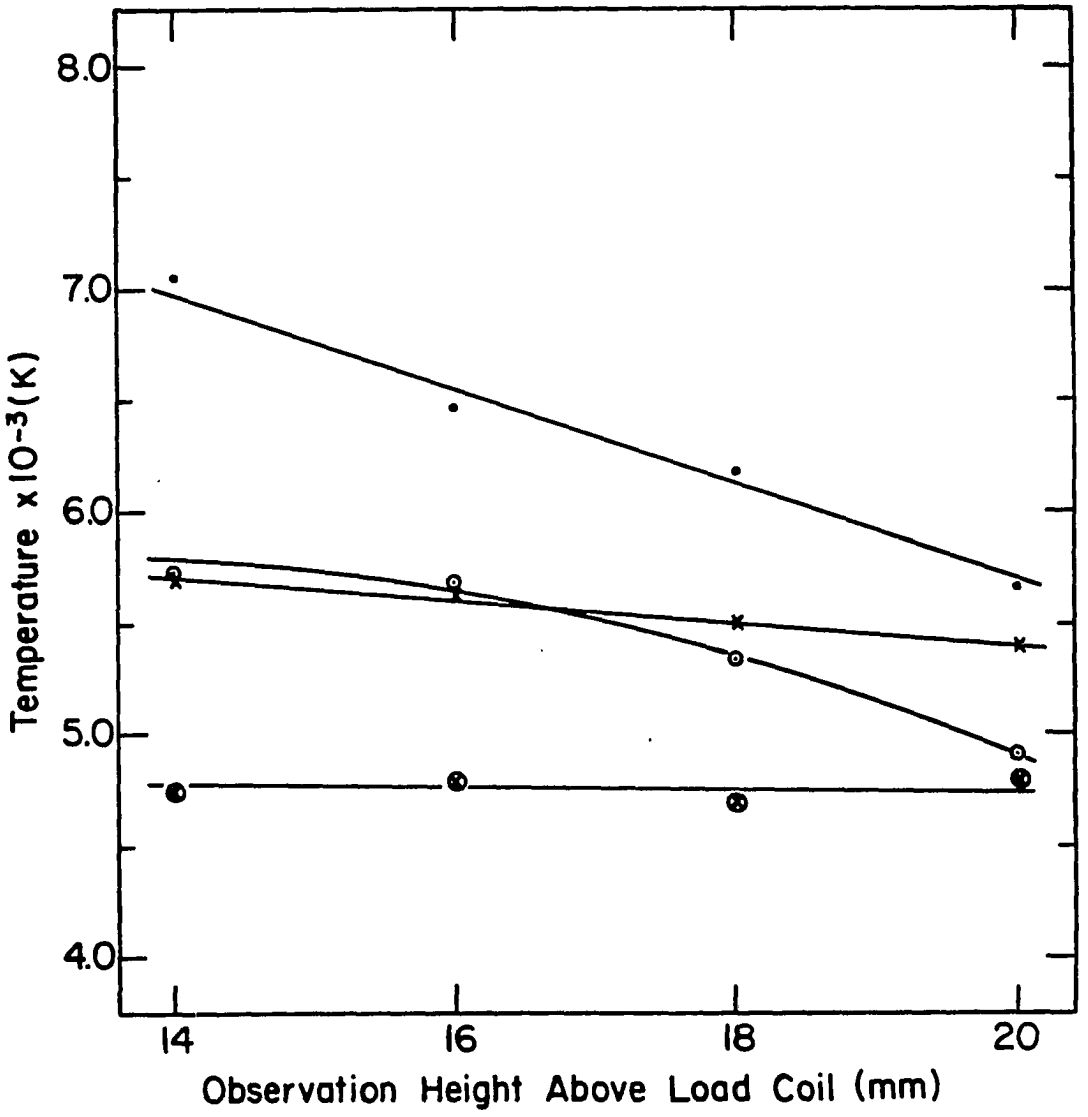

Figure B-1. Three line slope temperature profiles at 1200 W incident power and several observation heights
Direct injection nebulizer (—⊠—); cross-flow pneumatic nebulizer (—⊙—); ultrasonic nebulizer with aerosol desolvation (—●—); ultrasonic nebulizer without aerosol desolvation and desolvation train removed (—✕—)

(or USN without subsequent aerosol desolvation) were not far superior to those obtained by conventional pneumatic nebulization.

For pneumatic nebulization, the Fe I excitation temperatures calculated in this study were in excellent agreement with those obtained by Kalnicky et al. (200). As expected, the USN with subsequent aerosol desolvation exhibited the highest Fe I excitation temperatures at all observation heights above the load coil. At typical analytical observation heights (14 to 18 mm), the excitation temperatures obtained for the USN with subsequent aerosol desolvation were 840 to 1300 K higher than with conventional pneumatic nebulization. The USN technique enhances the analyte mass flow rate to the plasma by a factor of 10, while greatly reducing the total mass flow rate (water + analyte) as compared to the pneumatic nebulizer. Because the aerosol undergoes solvent vaporization and removal prior to injection into the plasma, very little water is transported to the plasma and less energy is required for dissociation of the water molecules, and for the subsequent excitation and ionization of H and O atoms. This implies a higher energy distribution (Boltzmann), thus, a higher population of atoms in the excited state (higher excitation temperatures). The higher population of atoms in the excited state, in effect, increases the analyte mass participation in the analytical process and implies an increase in net signal-to-noise ratios, hence, the predicted approximate 10-fold improvement in the LODs is realized (Table VII).

In the case of the USN without subsequent aerosol desolvation, the Fe I excitation temperatures were found to be comparable to those obtained for conventional pneumatic nebulization at typical analytical observation

heights (14 to 18 mm). This is somewhat surprising in view of the fact that the total mass flow rate (water + analyte) to the plasma from the USN should be about 10-fold greater than the pneumatic nebulizer. As the detection limits obtained for the USN without subsequent aerosol desolvation were found to be comparable to those obtained with conventional pneumatic nebulization (Table VII), it appears that the LODs obtained for the USN without subsequent aerosol desolvation correlate well with the measured analyte excitation temperatures.

For the DIN, the analyte mass flow rate to the plasma is enhanced by a factor of about 10 as compared to the pneumatic nebulizer, thus a 10-fold improvement in the LODs might be predicted. Unfortunately, two factors combine to degrade the predicted LODs to such an extent that the DIN is rendered comparable or slightly superior to the conventional pneumatic nebulizer. First, the analyte is injected into the plasma at a high velocity (~120 m/s) and results in shorter residence times in the analytical observation zone as compared to other nebulizers. Shorter residence times may lead to a lower degree of atomization. The lower degree of atomization, in effect, reduces the analyte mass participation in the analytical process and implies a reduction in net signal-to-noise ratios, hence, a deterioration in LODs. Second, at typical analytical observation heights (14 to 18 mm), the excitation temperatures obtained with the DIN were found to be 990 to 640 K lower than with conventional pneumatic nebulization. In contrast to the USN with subsequent aerosol desolvation, for the DIN, the total mass flow rate (water + analyte) also increases 10-fold and results in a dramatic decrease in the analyte excitation temperatures. The combination of a lower degree of atomization

(due to short residence times) and lower excitation temperature results in a lower degree of excitation. Again, the effective analyte mass participation in the analytical process is diminished and implies a net reduction in signal-to-noise ratios, hence, a deterioration in LODs.